Fabrication of a PDMS microfluidic device for size selective DNA transport and single-stranded DNA generation for SELEX

A DISSERTATION
SUBMITTED TO THE FACULTY OF THE GRADUATE SCHOOL
OF THE UNIVERSITY OF MINNESOTA
BY

Yixiao Sheng

IN PARTIAL FULFILLMENT OF THE REQUIREMENTS
FOR THE DEGREE OF
DOCTOR OF PHILOSOPHY

Michael T. Bowser, Advisor

July, 2012

Acknowledgements

I would like to express my deep and sincere gratitude to many people who made this thesis possible.

Thanks to my advisor, Dr. Michael T. Bowser. I am so grateful I had the opportunity to meet and start working with Mike in the winter five years ago. He always gave me innumerous support and inspirations when I needed help. I owe him lots of gratitude for teaching me to solve the problem patiently, for giving me confidence and helping me out when I was frustrated, for giving me adequate time and space for self-development, and for supporting decisions I made in my life and career.

Thank you to all of the Bowser group members who gave me support and encouragement throughout my education. Especially I want to say thanks to Dr. Christopher R. Harrison who trained me in many fabrication techniques at the beginning of my graduate study. Thanks to Anne Mohns, Eric Castro, Neil Graf, Jing Yang, Ryan Turgeon, Meng Jing, Bryan Fonslow who gave me help and suggestion for this thesis study. They may not realize our scientific interactions inspired me a lot. My experience in the graduate study would be totally different without them.

I am lucky to be advised by numerous people during my graduate study. I would like to acknowledge and thank Professor Ronald Siegel and Professor Victor Barocas who provided me valuable suggestions and critical comments on modeling of the device. Thanks to Professor Edgar Arriaga who taught me what was bioanalytical chemistry. After taking his class, it was getting easier to understand other people's research and his

class was just like a bridge between Analytical chemistry and Biomedical Engineering. I also owe Professor Edgar Arriaga and Professor Victor Barocas gratitude for supporting me in my job hunting process. Thanks to Professor David Odde for accepting to serve on my committee in a short notice.

I wish to extend my thanks to the staff at the nanofabrication center. Mark Fisher gave me valuable advice on mask design. Tony Whipple helped me to solve many problems I met in the fabrication process. I need to say thank you to Mario Costello in the electrical engineering machine shop for guiding me to design instrument parts and substrates needed in my experiments.

Most importantly, I would like to thank my family for being supportive throughout my education. My parents have always provided me with everything I needed to further my education. Their unconditional love is the best thing I have ever got in my life. Special thanks to my husband Xuyong Tu. I could not get through all the difficult times without your companion and support. Thanks to my son William Tu who is always there to distract me from graduate pressures. Thanks to my parents-in-law who gave me support when I needed them.

Finally, I wish to thank my friends Qiqi Deng, Zhihua Su, Linxi Li, Qiang Li, Xiaochuan Chai, Lin Yang, Fengjuan Xu, Yuanting Cheng, Dandan Lai, Tianhui Ding, Zonghao Gao, Jie Xi for all the emotional support and those sunny happy days in my life.

Dedication

To my parents, Shaoer Sheng and Minying Qu

For always supported and encouraged me to further my education.

Abstract

An innovative nanopore based microfluidic device for SELEX has been developed for single-stranded DNA generation and sizing. The objective of my research is to design, fabricate, test and model this device and make this device applicable for SELEX.

The nanopores of the membrane controls fluidic transport between different planes in the device. It adds more functionality and flexibility to the microfluidic device. This device consists of two polydimethylsiloxane (PDMS) channels separated by a polycarbonate membrane. Channels were designed in a CAD software and a master was fabricated using rapid prototyping of PDMS. Multiple PDMS replicas were then cast from this master. The membrane was sandwiched between two channels. Oxygen plasma treatment was applied to bond two PDMS layers and glass substrates were used to support the whole device. Recovery of fluorescein across the membrane was compared with 10 and 80 nucleotide (nt) single stranded DNA(ssDNA) to characterize the device. Recovery of analytes improved with decreasing flow rate. Size selectivity was observed. Two mathematical models which were built based on conservation of mass and constitutive relationships described the process of DNA transportation in the microfluidic device. Trends in recovery measured at various flow rates were consistent with the trends predicted in the two models which support the premise that diffusion dominated the molecular transport in this device. In addition to that, Model 2 demonstrated recovery was affected by the ionic strength of the buffer as well. One application of this device was to automate the process to make double stranded DNA(dsDNA) single stranded which can be integrated into an automatic SELEX system. Streptavidin-coated

polystyrene beads were immobilized with dual-biotin labeled dsDNA and alkaline treatment was adopted to denature dsDNA and release the non-biotinylated ssDNA. 25mM sodium hydroxide (NaOH) was optimized to achieve the best purity. 95.7% of the strands collected across the membrane were the non-biotinylated ssDNA. Capillary Electrophoresis (CE) results confirmed that the non-biotinylated ssDNA was the major component across the membrane.

Table of Contents

List of Tables

List of Figures

Abbreviations

Bi	the Biot number
bp	base pair
CAD	computer aided design
CE	Capillary Electrophoresis
CIEF	capillary isoelectric focusing
dsDNA	double- stranded DNA
EDTA	ethylenediamenetetraacetic acid disodium salt
EOF	electroosmotic flow
FAM	a fluorescence dye
HEGal	hexaethylene glycol
LOC	Lab on a chip
LPA	linear polyacrylamide
MEMS	Microelectromechanical systems
MWCO	molecular weight cut off
NaOH	sodium hydroxide
nt	nucleotide
PAGE	denaturing urea-polyacrylamide gel
PC	polycarbonate
PCTE	polycarbonate track etched membrane
PCR	polymerase chain reaction
PDMS	polydimethylsiloxane
Pe	the Peclet number
PEO	Poly(ethylene oxide)
PE	Polyethylenes

P.M. Acetate	propylene glycol monomethyl ether acetate
PMMA	polymethyl methacrylate
PS	polystyrene
PVC	polyvinylchloride
PVP	polyvinylpyrrolidone
Re	the Reynolds number
R_g	the radius of gyration
rsd	relative standard deviation
SELEX	Systematic Evolution of Ligands by Exponential Enrichment
SNP	single-nucleotide polymorphism
Sh	the Sherwood number
SPR	surface plasmon resonance
SSCP	single-stranded conformation polymorphism
ssDNA	single-stranded DNA
TBE buffer	Tris 89mM, Boric acid 89mM, EDTA 2mM
TE buffer	Tris 10mM, EDTA 1mM
Tg	glass transition temperature
Tris	tris(hydroxymethyl)aminomethane
μ-FFE	micro free flow electrophoresis
μ-TAS	micro total analysis system
VEGF	Vascular endothelial growth factor
UV	ultraviolet

Chapter 1 Introduction

1.1 Aptamer

1.1.1 *Aptamer properties*

Specific sequences of ssDNA or RNA can be selected in vitro that function like biopolymer ligands (aptamers)[3-6]. Aptamers are single stranded RNAs or DNAs that are isolated using the exponential enrichment SELEX process (systematic evolution of ligands by exponential enrichment)[7]. This terms comes from the Latin aptus which means "to fit", stressing "lock-and-key" molecular recognition.

Like all other nucleic acids, aptamers are composed of a linear sequence of nucleotides (A, U, T, C and G). These linear sequences are composed of 15-40 nucleotides. Different from other nucleic acid sequences, aptamers can fold into tertiary structures to interact with targets precisely and specifically(see Figure 1.1). Most aptamers are unstructured in solution. However, once bound to the ligands, the nucleotide chain forms intramolecular interactions that fold the aptamer into a specific three-dimensional shape. The ligand becomes an intrinsic part of the nucleic acid structure. Diverse structural conformations can be formed including hairpin structures[8, 9], pseudoknots[10, 11] and quadruplex structures[12, 13].This structure mostly contributes to the high affinity and specificity of aptamers[7].

Aptamers have high affinity towards a variety of targets from small inorganic molecules to whole cells[10, 14-20]. Anti-protein aptamers have dissociation constants(Kd) in the picomolar (pM) to low nanomolar (nM) range while aptamers for small molecules have a low micromolar dissociation constants(Kd)[14, 21]. Aptamers are so selective that

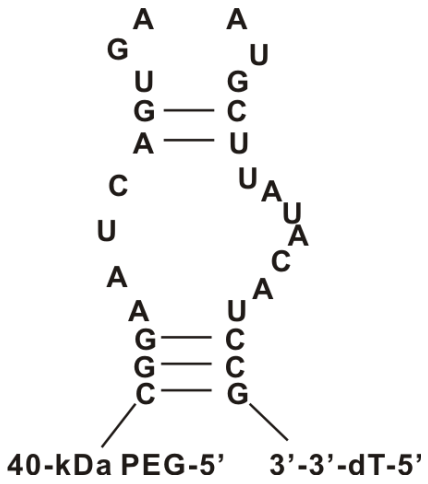

Figure 1.1: An example of aptamer[27]. The unique secondary structure facilitates the interaction between the 55-amino-acid heparin-binding domain of vascular endothelial growth factor$(VEGF)_{165}$ and Mecugen.

even small changes in the target molecule can disrupt aptamer association. Thus, aptamers can distinguish between closely related but non-identical members of a protein family, or between different functional or conformational states of the same protein.

With high affinity and selectivity, aptamers rival antibodies both in therapeutic and diagnostic areas. Compared with antibodies, aptamers have a number of advantages over antibodies. Particularly it is simpler to obtain aptamers. The process does not depend on animals, cells, or even in vivo conditions. Since no animals are used, there is no immune response. Thus, aptamers can be isolated against even highly toxic targets. Furthermore, aptamers are non-toxic and will not induce an immune response. The aptamer can be produced by nucleic acid synthesis with great accuracy and reproducibility while polyclonal antibodies always have lot-to-lot reproducibility issues. Lastly, aptamers can be regenerated easily once denatured so that they are able to be stored for a long term[22].

In addition to that, the aptamer stability and efficacy can be enhanced through chemical modification[23].

With high affinities and excellent specificities, aptamers have broad application ranging from purification[24], detection[25] to diagnostic[26] and therapeutic agents[27] in clinical applications which are based on molecular recognition[21]. Pegaptanib (Macugen) is the first aptamer therapeutic agent for treating age-related macular degeneration in humans, paving the way for developing new aptamer-based agents[28, 29].

1.2 Aptamer Identification-SELEX

Apparently, aptamers have the potential to be applied in broad areas such as therapeutics, diagnostics and biosensors. The most important thing here is not how to apply aptamers but how to obtain aptamers. Although repetitive and time-consuming, SELEX ("Systematic Evolution of Ligands by Exponential Enrichment") is still the only technique to isolate aptamers.

1.2.1 *History of SELEX*

The SELEX process was first introduced in 1990. Tuerk and Gold identified high-affinity RNA for T4 DNA polymerase using SELEX[4]. Ellington and Szostk isolated RNA molecules that bind to organic dyes specifically from a large random RNA library in vitro[3]. However, it is a long and tedious process to isolate aptamers which could be weeks and months. There are several groups trying to automate the SELEX process. Cox, Rudolph and Ellinton have realized automating a typical SELEX using a modified robotic workstation. This device is able to isolate aptamers continuously and automatically in as

little as 2-3 days[30]. Hybarger et al. have developed an automated fluidic SELEX device which is smaller, simpler and relatively inexpensive compared with the robotic workstation[31]. There is also some other groups to use surface plasmon resonance (SPR) to isolate high-affinity aptamers that have the slowest 'off-rates' in the dissociation phase[32].Capillary Electrophoresis (CE) is also used to be as the separation technique to separate the bound DNA from the library. With high efficiency and great separation power, it can dramatically decrease the selection rounds to even a single round[33].

1.2.2 SELEX process

The process begins with a 10^{13}-10^{15} library of DNA or RNA that consists of 20-60 bp randomly generated sequences. DNA or RNA has four types of nucleotides. So the possibility of the sequences generated by n base pairs of DNA or RNA is 4^n. Sequences that do not bind the target are separated by some selection process, usually nitrocellulose filtration or affinity chromatography. The retained sequences are amplified by PCR to prepare for new rounds of selection. After sufficient cycles, high-affinity DNA or RNA for the targets can be isolated (Figure 1.2). Typically, 8-15 rounds are carried out to further enrich the population of high affinity aptamers in the pool.

1.2.3 *CE-SELEX*

In general, SELEX need to run 8-15 cycles to get high-affinity aptamers. And each cycle requires 2 days to complete. Thus, a typical SELEX experiment could take weeks to months from the first selection to the end of cloning and sequencing[22].

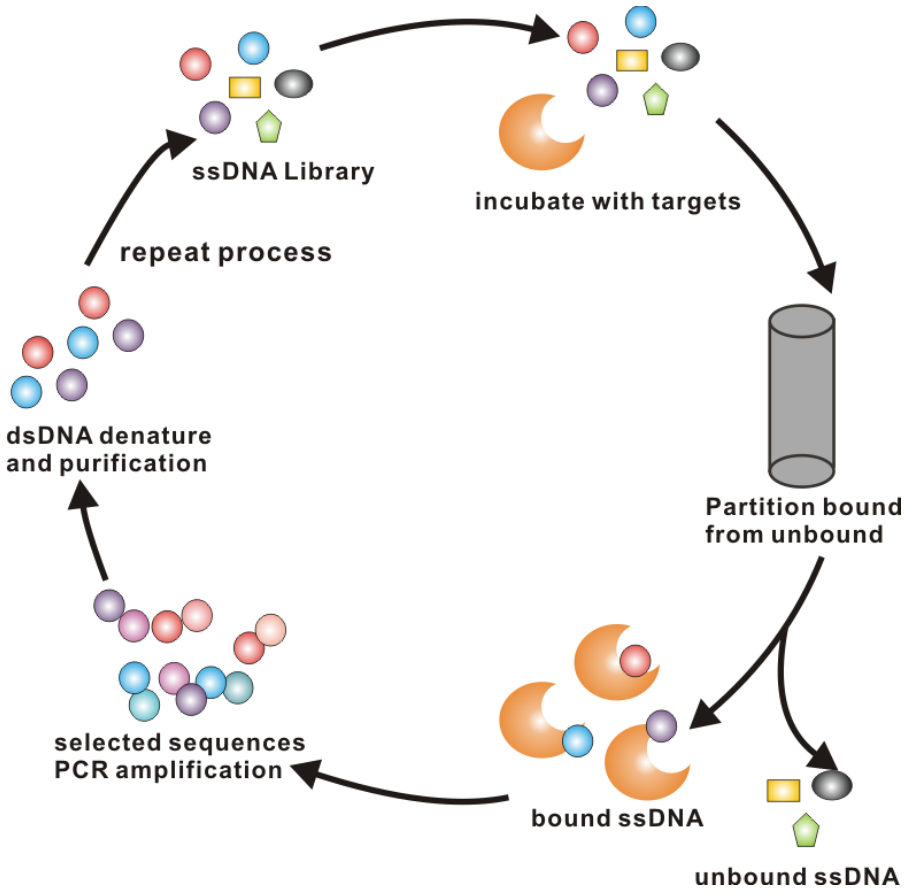

Figure 1.2: Schematic of the SELEX process. A random sequence DNA or RNA library is incubated with the target. Retained sequences are selected using filter or affinity chromatography and amplified by PCR. The resulting PCR products are denatured and one single strand needs to be removed before entering the next selection cycle. 8-15 cycles are carried out before aptamer characterization.

Improving the efficiency of selection (the rate of enrichment) is what most people want to do. In other words, the most important thing is to reduce the number of rounds and the time taken to isolate high-affinity aptamers. The rate of enrichment between SELEX rounds is dependent on the resolution of the separation between binding and nonbinding sequences. The basic principle of SELEX is shown in Figure 1.2. The selection step can be improved to increase the efficiency of selection. That is because the

efficiency of affinity chromatography or filter separation is low although they provide high selectivity.

The higher selectivity and efficiency of CE leads to the higher rates of enrichment compared with affinity chromatography or filter separation. It can be applied in vitro selection (CE-SELEX). The cycles of selection that are needed to obtain high-affinity aptamers can be decreased to 2-4 rounds, which shortens the process significantly (from months to several days)[23, 33, 34]. In addition, selection happens in free solution with no stationary phase and no need of washing. It is simpler[21]!

However, it takes half a year or even a year to train somebody to be able to operate CE-SELEX successfully. Even though it is faster than regular SELEX, it still needs days to complete the selection. SELEX could move into a higher-speed and simpler system if it moved to a chip-based microfluidic environment.

1.3 Single-stranded DNA Generation

1.3.1 *ssDNA Generation Methods*

The SELEX process begins with a DNA or RNA library that consists of 20-60 base pairs (bp) randomly generated sequences. After affinity separation and PCR amplification, single-stranded DNA is generated to enter the next round of selection[34, 35]. DNA sequences after PCR must be carefully purified prior to being introduced into the next round of selection. It is an important step in not only CE-SELEX but also in other sample processing methods such as single-stranded conformation polymorphism (SSCP)[36, 37], single-nucleotide polymorphism (SNP)[38-40], pyrosequencing technology[41-43],

solid phase DNA sequencing[44, 45], and sensing in DNA chips and microarrays[46-49]. The single strands will reanneal with the complementary single strands to prevent the single strands from forming many different structure confirmations which are important in target aptamer binding. Several methods of ssDNA generation following dsDNA production exist, including denaturing urea-polyacrylamide gel (PAGE)[50-53], asymmetrical PCR[54-58], Lambda exonuclease digestion[59-62], and separation with streptavidin-coated beads [20, 48, 63-67].

For denaturing PAGE, extra functional groups need to be conjugated to one of the PCR primers to facilitate selective excision of any of the strands. By doing this, the dsDNA with unequal strands can be separated by denaturing gel electrophoresis[51]. The desired ssDNA has to be eluted from the gel. Several methods are used to generate size difference between two single strands in PCR process. For example, one of PCR primers is synthesized with a spacer as terminater(hexaethylene glycol(HEGal)) and an extension of 20 adenine nucleotides (polyA) to produce strands with different length[51]. The pH-libile base at the 3'-end of the reverse primer can be introduced in the PCR process to break the modified strand of the amplicon upon alkaline treatment[68]. Any ribose residues located between the primer binding region and the randomized region of the SELEX amplicon can be synthesized into one of the PCR primers. Ribonuclease was used to cleave the ribose residue to induce different lengths of the two single strands after denaturation[69]. Urea-PAGE is an expensive and lengthy method[70].

Asymmetrical PCR has become one of the most common forms of generating ssDNA in DNA aptamers production which amplifies one strand more than the other by

adding different concentration of two primers in the PCR process[54].There are two phases of amplification in the asymmetric PCR, the exponentially dsDNA production and the following linearly ssDNA production. Finally, the ssDNA generation will reach a stage whereupon the increase of amplified DNA copies is limited by the amount of enzyme present in the PCR reaction mixture[54]. The most important thing in asymmetrical PCR is the ratio of primer amounts. Most of asymmetric PCR relies on either the forward[55, 56] or reverse primer[71] or dependent on the presence of both primers with different amounts[72-75]. Obtaining higher amount of ssDNA can be realized by increasing the PCR cycles[76]. In addition to that, asymmetrical PCR is the less tedious and the most economic method to generate ssDNA from dsDNA template. It becomes more and more popular. However, not only ssDNA but also dsDNA is contained in the asymmetrical PCR products which necessitates selective ssDNA purification from polyacrylamide gel and following recovery from the gel. Although there are some cases where the final asymmetric PCR products were not purified and the products were incubated with targets directly[77-79]. It is a slow process with a low yield of ssDNA from the gel and not amenable to automation[80, 81].

Lambda exonuclease digestion of undesired strand is an alternative method which selectively digests the 5'-phosphorylated strands of double stranded DNA from the 5' to the 3' end by introducing a 5'-phosphate group into one strand of dsDNA in the PCR process[59, 60]. The phosphorylated strands of dsDNA are digested by an exodeoxyribonuclease which has reduced activity on non-phosphorylated DNA, ssDNA[82]. Phenol-chloroform extraction followed by ethanol precipitation is conducted to

remove the lambda exonuclease enzyme which might be another target in the SELEX experiments. It is a very fast method to generate ssDNA with high quality and yield. The whole process from SELEX to purification by phenol/chloroform extraction lasts only 60-68 min[83]. However, it is a costly method in terms of purchasing the enzyme. What's more, the accumulation of the dsDNA in the reaction mixture may result from the incomplete digestion of the phosphorylated double-stranded PCR product[83] and co-purification of ssDNA and dsDNA from the challenge operation of phenol chloroform extraction. And it is hard to separate ssDNA and dsDNA in denaturing-urea PAGE as they migrate at almost the same rate, not to mention it has smeary appearance of ssDNA on the native PAGE[84, 85].

There is another method which is most common for ssDNA generation, the immobilization of biotinylated dsDNA onto streptavidin-coated beads followed by alkaline denaturation[20]. In this method, one of the PCR primers are biotinylated and the resulting PCR products are immobilized to streptavidin-coated beads. NaOH is used to separate two single strands by weakening the hydrogen bond between two strands. However, NaOH treatment also breaks biotin and streptavidin interaction by fracturing the hydrophobic, van der Waals forces, hydrogen bonds and rupturing the surface streptavidin molecules. As a result, the biotinylated strand would re-hybridize with the complementary strand and streptavidin may be the additional target for SELEX as well. However, many aptamers are still isolated by using this ssDNA generation method[20, 35, 48, 63, 64, 67, 86-89]. In our group, this method is chosen to generate ssDNA. It usually takes three to four hours to generate and purify ssDNA by regular laboratory operation procedures.

The selection will benefit a lot if we can realize it in a microfluidic chip. It consumes fewer reagents and involves little labor. It is going to be a fast, efficient and automatic method with high purity and yield.

1.3.2 *Streptavidin-Biotin Interaction*

All biomolecules are likely to have some specific interactions with other biomolecules or xenobiotic agents (such as therapeutic drugs). There are many examples of these interactions, like biotin and streptavidin, antigen and antibody, Protein A and Fc fragment of antibody, aptamer and target, lectin and carbohydrates, enzyme and substrate, DNA and transcription factor, RNA and proteins and so on. Electrostatic interactions, hydrogen bonding, Van der Waals forces, hydrophobic interactions contribute to these interactions which have their origin at the molecular level[90, 91]. Some interactions are thermodynamically "very strong" so that a stable complex is formed, such as biotin and streptavidin interaction[92].

Streptavidin is a tetrameric protein with a 60kDa molecular weight purified from the bacterium *Streptomyces avidinii*[93]. Biotin is a water soluble B-complex vitamin (vitamin B_7)[94]. The structure of the biotin-streptavidin complex has been described by several groups[95, 96]. The three-dimensional structure of streptavidin demonstrated a pair of subunits is associated tightly with a stable-dimer formation, in which a subunit β-barrel structure of streptavidin binding biotin into its interior. A tetramer is formed by two stable dimers that are result from van der Waals and electrostatics interactions[97]. The biotin-streptavidin system is the strongest noncovalent biological interaction with

extremely high affinity (dissociation constant K_d=10^{-14}-10^{-15} M)[93, 98-101]. And there are many streptavidin and biotin conjugates commercially available. The interaction is stable in wide ranges of pH and temperature[102, 103].

In many applications, streptavidin is attached to a solid phase, such as a bead or a biosensor chip while biotin is attached to the moiety of interest such as nucleic acid, protein and so on. However, after attaching to nanoparticles[104], the streptavidin-biotin stability could decrease dramatically with an approximately million-fold increase of dissociation constant for a biotinylated peptide when streptavidin was attached to beads[105]. Various modifications and analogues of both streptavidin and biotin have been studied by trying to overcome these problems[106-110]. In Uhlen's report, the biotin-streptavidin interaction can be reversibly broken at elevated temperature in nonionic aqueous solutions which demonstrated the biotin-streptavidin interaction is strongly related to ionic strength of the solution and the temperature[98]. In other people's research, it also showed pH played an important role in biotin-streptavidin interaction as well[111]. In this thesis, biotin-streptavidin interaction will play a critical role in the process of ssDNA generation.

1.4 LOC (Lab on a Chip)

1.4.1 *History of LOC*

A Lab on a Chip, or Micro Total Analysis System (μTAS), is a miniaturized analysis system on a single chip conducting many lab functions including sample preparation, separation, detection and so on. LOC devices are a subset of MEMS device

(Microelectromechanical systems). As early as the 70s, Terry *et al.* integrated a miniaturized gas chromatography system on a silicon wafer[112]. However, an exponential growth of this area was triggered by the paper of micro total analysis systems (μTAS) in 1990. There are four labs which is the origination of the microfluidic systems: Manz[113-115], Harrison[115], Ramsey[116], and Mathies[117, 118].

1.4.2 *Motivation*

At first, μTAS was thought to have better performances within chromatographic and electrophoretic separations. To some extent it is true. However, there are some limitations: smaller channels challenge the detection system; they are easy to be blocked and more sensitive to adsorption on the surface. Even though, miniaturization of device has a number of advantages: increased separation efficiency and resolution; decrease cost; decrease time; fewer reagents and analytes; reduced harmful by-products if exist; and more portable[118].

Initially, most of these devices were fabricated in silicon and glass substrates. This was because the technology based on these materials was sophisticated and well developed. However, both of these substrates have certain disadvantages. Silicon cost a lot compared to other substrates and it is not friendly in optical detection due to its opaque in the visible or UV (ultraviolet) region. It is electrically semiconducting which is problematic for use in analytical separations that require high voltage. Although glass is transparent, it is amorphous so that the etched side walls are always not vertical. The silanol groups (Si-OH) supports electroosmotic flow (EOF) which needs to be suppressed

for some applications. Moreover, most of the fabrication needs to be processed in cleanroom and need high-tech instrument which means it is expensive to fabricate[118]. The wet etching method and the dry etching technique of silicon limit the highest aspect ratio of the device. The surface of the substrate materials is charged and many biomolecules, such as DNA or proteins, will stick to the surface via electrostatic interactions and hydrogen bonding[2]. These limitations drive to the development of polymer-based substrate.

Commercial microfluidic products are on the market now[119-121]. For example, DynaflowTM is a microfluidic chip-based system for dose response analysis in drug screening by Cellectricon[119]. Valves and pumps are fabricated into parts of the microfluidic systems by Fluidigm and Biacore[120, 121].

1.4.3 *New materials for Microfluidic Device*

Polymers are getting more and more popular for microsystem technology which is due to several facts. First of all, they are able to be used in mass replication technologies such as injection molding, hot embossing and rapid prototyping. A cleanroom is not necessary once you have a mold. Moreover, polymers are able to provide various channel features, including square channels in different depth and different angle. Second of all, polymeric devices can be manufactured at a lower cost and in a large number, which makes it possible to manufacture disposable microfluidic chips to avoid cross contamination. Third of all, there are many kinds of polymeric materials, providing a

broad range of material properties. Most of them are biocompatible and lack of ionizable groups to suppress EOF (electroosmotic flow)[2].

There are three types of polymers, thermoplastic polymers, elastomeric polymers and thermosetting (Duroplastic) polymers[2]. Thermoplastic polymers are those polymers that will not become soft and remoldable until above the glass transition temperature (Tg) and this shape can be kept even under Tg. The difference between thermoplastic and other two polymers is the interactions between the polymer chains. Van der waals is the main force to hold the chains in thermoplastics while covalent bonds are in thermosets and elastomers. Polyethylenes (PE), polycarbonate (PC), polymethyl methacrylate (PMMA), polyvinylchloride (PVC) are all included in this category. Elastomeric polymers are polymers with the property of elasticity, deforming reversibly under stress. Typical examples are PDMS (polydimethylsiloxane) and epoxy. Thermoplastic polymer and elastomeric polymers are both low crosslinked polymers. The only difference between elastomers and thermosets is the degree of crosslinking. Thermosetting polymers are higher crosslinked molecules that contribute to their hard melting or flowing upon heating. Thermosets is more brittle and more rigid than the other two polymers. Examples are unsaturated polyesters, phenol formaldehyde and vinyl esters[122].

1.4.4 *Polymer properties*

Different parameters of the materials play different roles in kinds of fabrication protocols. In this thesis study, soft lithography was used to make PDMS microfluidic device. Cured PDMS is a soft elastomer at room temperature. Thus elasticity is the key

property of PDMS that is important in our device. At the same time, shelf life is also an important parameter that influences the lifetime of the device. If electric field exists, it is critical for the substrate to have a good dielectric strength so that the electric field will not drop through the substrate material. Furthermore, the substrate needs to be a good heat dissipater. Otherwise, the local temperature of the channels will increase dramatically and influence the performance of the device. Thermal conductivity is always used to evaluate this effect. Except these parameters, auto-fluorescence, biocompatibility and chemical resistance are all related to the success of the device[123].

When choosing a polymer material in microfluidic systems, one of the important issues is surface chemistry. Polymers often do not possess the properties you want it to have. Based on the application requirements, some properties need to be modified, such as the total surface charge density, the types of surface-bound chemical moieties, hydrophobicity, electroosmotic flow mobility, surface charged groups and nonspecific adsorption.

1.5 Microreplication technologies for polymer-based microfluidic applications

1.5.1 *Master Fabrication*

The wide spread of polymer-based microfluidic devices mainly results from the establishment of a low-cost manufacturing process, that is replication technology. Each type of polymer has its own replication methods. However, all of these replication techniques need a replication master, from which copies in the polymer material can be

made. This master includes all the desired structural information of the device in an inverted (negative) form. Thus, the expensive microfabrication happens only once and the master can be replicated multiple times into polymer structures. The replication master can be fabricated by numbers of techniques developed over the 10 years which almost covers the whole area of microfabrication technologies such as wet silicon etching[124], dry silicon etching[125], micromaching[126], electroplating[127], solid object printing[128], LIGA[129], Rapid Prototyping[130, 131] and so on. These different technologies make it possible to freely design of master[122, 132, 133].

The molding techniques that are used to making polymer microfluidic devices are listed in Table 1.1[2].

Table 1.1 Three different replication techniques to make polymer microfluidic devices(adapted from [117]).

Process	Materials	Tool costs	Cycle time	Forces and Temperatures	Geometry	Minimum dimensions Aspect ratios
Hot embossing	Thermoplastics; Thermosetting thin films	Low-medium	Medium-long (3-10min)	High(kN) Around T_g(100-200 ℃)	Planar	nm
Injection molding	Thermoplastics; Thermosets	High	Short-medium (0.3-3min)	High Above melting (150-400 ℃)	Bulk, spherical	Some 10 μm
Casting	Elastomers Epoxies	Low	Long (min-h)	No forces Room temp-80 ℃	Planar	nm about 1

1.5.2 *Hot embossing*

Hot embossing is a popular replication process to fabricate channel structures for thermoplastics-based microfluidic devices[134-136]. The main advantages are that it is simple to optimize the process parameters (temperature, pressure and hold time) for hot

embossing and there is no polymerization needed as casting[137, 138] or injection molding[139, 140]. Hot embossing has straightforward process. The polymer material is always in the form of a planar sheet. Both of the polymer and the master will be put in the vacuum chamber and be heated to a temperature just above the glass transition temperature of the polymer material which makes the polymer available for molding. After holding the embossing force for some hold-time, typically 30-60s, lower the temperature below the glass transition temperature, mold and separate the embossed polymer sheet[141].

1.5.3 *Injection molding*

Injection molding has been the standard method of fabrication in the macroscopic world like well plates or pipettes. It can be used to make any geometry from a wide variety of thermoplastic materials and thermosetting (duroplastic) materials. So it is not surprised to see it has been applied in microsystem world to fabricate microfluidic devices[139, 140]. The molding process starts from the granular polymer material fed into a heated screw. The typical temperature in the heated screw ranges from 200 ℃ to 350 ℃ which melts the polymer material. The melted material is injected under a high pressure into the cavity containing the mold insert as the master structure. A cold-cavity process happens so that the structured parts can be solidified in macroscopic system. For smaller structures, the temperature is higher than the temperature in cold-cavity process so that the structures can be ejected[141].

1.5.4 *Casting*

Casting is a flexible, cheap and widespread process for fabricating planar microchannel structures of elastomeric materials, mostly PDMS. A mixture of PDMS prepolymer and its curing agent are poured over a Si mold, which is made by the master fabrication methods mentioned above. The polymer can be cured at room temperature for one day or at increased temperatures such as 65℃ and 80℃ for 1-2 hours. Curing temperature and the ratio of the curing agent are related to the stiffness of the elastomer. Different applications can be fabricated using different parameters. It is flexible. After curing, peel off the PDMS from the mold. Punch the hole and seal it. Three dimensional structures can be fabricated using such an easy way[131, 137].

There are some direct techniques to build microfluidic device other than microreplication methods such as Laser-based technologies[142, 143], optical lithography in deep resists[144-146], stereolithography[147, 148] and so on. These techniques do not need a master but each single component is fabricated individually which limits the fabrication throughput.

After the finish of the above replication processes, the polymer sheet still need to take several back-end processes to make it usable for microfluidics, such as enclosing, metallization and surface modification[132].

A cover lid is required to make the channels or cavities closed. Several methods are adopted to realize this function. Adhesion, adhesives, solvent bonding, thermal bonding, ultrasonic welding and laser welding are able to enclose the microfluidic device. The

material and geometrical requirements determine which one is chosen. Sometimes a metal layer has to be electroplated on the polymer device to form electrodes that can provide voltage on the device. Surface modification endows the polymer-based device with a large number of changeable properties. Plasma exposure or surface coating can modify the property of hydrophobicity. For PDMS, plasma treatment changes the hydrophobicity to hydrophilicity for temporary. However, it is enough for us to seal the PDMS device irreversibly. So it is an important tool to modify PDMS. Plasma treatment will be introduced as follows[132].

1.5.5 *Plasma Treatment for PDMS device bonding*

Other than hydrophobicity, adhesion, surface charge density, biocompatibility, permeability and other properties can be improved by plasma treatment. This method has been a significant modification technique over these several decades[149]. Both charged and neutral species such as electrons, radicals, atoms, positive and negative ions and molecules can be utilized in this process. Plasma treatment can cause crosslinking, degradation, etching and modification of the exposed surface. Reactor geometry, excitation frequency, power level, gas flow rate, gas composition, gas pressure, sample temperature, and local sample composition will influence the results of the process, and the depth of modification below the surface is typically less than 1μm. Ar,He,Ne,H_2,NH_3,CO,CO_2,O_2,H_2O,N_2,NO_2, F_2 and inert gas are all able to be used in plasma treatment. For example, oxygen-containing plasmas can facilitate etching and surface reactions to engender lots of oxygen functional groups, which probably hydrolyze and induce an increase in the surface charge density. One of the results is the

electroosmotic flow rate increases which is helpful in some microfluidic devices. An H_2O plasma treatment of PMMA will induce hydroxyl and carbonyl groups to the surface which results in more hydrophilic. However, the functionality caused by plasma modification cannot last long which is result from the reactions with the local environment and the high mobility of the polymer chains on the surface. For example, a nitrogen-plasma-treated polyethylene surface lost its effect because of the reactions with the water in air which leads to the loss of nitrogen. An oxygen-plasma-treated PDMS will change back to be hydrophobic. The recovery rate may be correlated to the movement of plasma-induced polar groups from the surface to the bulk material. Therefore, any method to reduce the mobility of polymer chains can be used to decrease the aging rate such as increasing the degree of crosslinking, the crystallinity and the orientation of the polymer surface chains[150, 151].

1.6 Poly(dimethylsiloxane) (PDMS)

Among all of the polymeric materials used in microfluidic devices, PDMS is one of the most attractive materials. Its supreme physical and chemistry properties and its ease to fabrication make it popular in bioanalytical and biochemistry applications[152].

1.6.1 *Composition of PDMS*

PDMS is a silicon-based organic polymer that has another name "silicon rubber". The monomer of PDMS is $[SiO(CH_3)_2]$. The commercial PDMS (Dow Corning) is composed of two parts: base and curing agent, often mixed in a weight ratio of 10:1. [62] The siloxane base oligomers contain a vinyl group(-C=C-) while the curing agent

oligomers contain more than three silicon-hybrid bonds(-Si-H) (Figure 1.3). Upon curing, Si-H bonds of curing agent oligomers are added to the double bonds (the vinyl groups) of the siloxane base oligomers through a hydrosilation reaction, forming Si-CH_2-CH_2-Si linkages. A platinum-based catalyst is included in the curing agent, which catalyzes the hydrosilation reaction[153, 154].

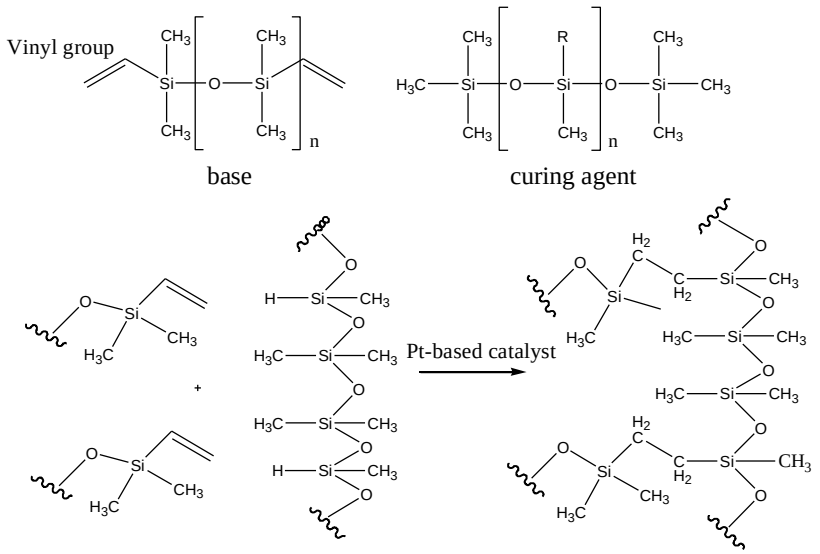

Figure 1.3: The base oligomers are terminated with vinyl groups. The curing agent oligomers contain Si-H bonds. The hydrosilation reaction is catalyzed by the Pt-based catalysts in curing agents, forming Si-CH_2-CH_2-Si linkages. The R group in curing agent is -CH_3 or -H.

The multiple reaction sites on the curing agent oligomers allow for 3-D crosslinking. Different ratios of base to curing agent lead to different properties of the resulting cured elastomer[155]. For Sylgard 184 silicone elastomer, lowering the curing agent percentage by more than 10 percent will lead to a softer and weaker elastomer. Increasing temperature will accelerate the crosslinking reaction. The shrinkage is almost less than 3% after curing as long as there is no solvent on PDMS, which is advantageous when used in casting molding[153, 156].

1.6.2 *Properties of PDMS*

PDMS's unique chemical and physical properties are listed in Table 1.2. The supreme properties endow the microfluidic device with useful functionality and makes PDMS a good structural material for analytical and biology applications[153].

Table 1.2: Physical and Chemical properties of PDMS (adapted from [152])

property	characteristic	consequence
optical	Transparent; UV cutoff,240 nm	Optical detection from 240 to 1100 nm
electrical	Insulating; breakdown voltage, $2*10^7$ V/m	Allows embedded circuits; intentional breakdown to open connections
mechanical	Elastomeric; tunable Young's modulus, typical value of ~750 kPa	Conforms to surfaces; allows actuation by reversible deformation; facilitates release from molds
thermal	Insulating	Insulating Can be used to insulate heated solutions;
Interfacial	Low surface free energy ~20 erg/cm^2	Replicas release easily from molds; can be reversibly sealed to materials
permeability	Impermeable to liquid water; permeable to gases and nonpolar organic solvents	Contains aqueous solutions in channels; incompatible with many organic solvents
reactivity	Inert; can be oxidized by exposure to a plasma	Unreactive toward most reagents; surfaces can be modified to be hydrophilic
toxicity	nontoxic	Can be implanted in vivo; supports mammalian cell growth

As most things in the world, PDMS has advantages and disadvantages. it has some disadvantages. The pros and cons of the PDMS material are summarized in Table 1.3[157].

Table 1.3: pros and cons of PDMS (adapted from[156])

Pros	Cons
Cheap;	Suck up small, hydrophobic molecules[158];
Simple and rapid prototyping fabrication;	Absorb hydrocarbon solvents; swell up like a sponge[159];
Optically transparent from 240 to 1100nm;	
Very low fluorescence; helpful for fluorescence measurements;	Still has some fluorescence; not as good as glass
	Not a solvent-resistant material;
Two methods to bond to itself and other Si-based materials without an adhesive: Reversible and irreversible;	Hydrophobic leads to poor wettability and high non-specific adsorption[158]; easy to trap air bubbles;
Nontoxic and gas-permeable; helpful for cell-based applications;	Evaporation of water through PDMS;
Require less skill than making glass chips	Has some problem with exact replicas of features < 500 nm;

In a summary, PDMS is very cheap which is useful to make disposable devices. It's easy to fabricate which is important for biologists to learn and acquire the skills to make the microfluidic device. What's more, it's superior biocompatibility when compared with silicon and glass materials. The optical detection is favored in PDMS device since it's optically transparent from 240nm to 1100nm[153]. It can be readily sealed reversibly or irreversibly with itself or other materials (glass, silicon, polystyrene, polyethylene, or silicon nitride and PMMA). It is nontoxic, chemically inert and impermeable to water. It is an electrical and thermal insulator which is critical to some specific applications such as PCR and Capillary Electrophoresis devices. However, PDMS has some undesired features such as swelling by organic solvents[159], poor wettability, such up small molecules[158], non-specific adsorption[129] and water evaporation through PDMS device[153]. Even though, PDMS is still chosen as the material to fabricate the device in this thesis.

1.6.3 *PDMS fabrication*

Based on the above discussion about microfabrication techniques for making microfluidic device, PDMS fabrication process is usually separated into three segments: rapid prototyping of the master, replica molding of the master and device bonding.

Rapid prototyping method[131, 137, 153, 160]is used to fabricate almost all of the PDMS devices. A master is fabricated at first and then multiple PDMS replicas were then cast from this master. This process begins with the design of the wanted pattern in a computer-aided design (CAD) program. This design is printed to a chrome mask or a transparency mask. Chrome masks are much more expensive than transparencies and it

needs more time to be made commercially. However, resolution of chrome masks is better than transparency masks which require feature size ≥ 8 μm[160-162]. No matter what masks you choose, they are used as the photomask in contact photolithography. In this process, silicon wafers are cleaned and dried. Photoresist will be coated on the silicon wafer using different spin speed and time[130, 145]. Features with different thickness can be generated[131]. Exposed to UV light, the designed pattern on the mask is transferred to photoresist by photolithography. After developing, the master with a positive relief of photoresist on a silicon wafer is created.

Replica molding of the master is the process to generate PDMS mold using the master. The surface of the master can be treated with fluorinated silanes to prevent irreversibly bonding to PDMS[160]. The PDMS prepolymer which is composed of base and curing agent in a 10:1 ratio is poured over the master and cured until solidified. The liquid PDMS prepolymer conforms to the shape of the master and the resulting cured PDMS bears the designed features with high fidelity (10 nm)[153]. After the PDMS is solidified, it is peeled off the master easily due to the elasticity and low surface free energy. This process can be repeated many times as long as the master remains intact. Small holes are drilled in the PDMS replica to produce inlets and outlets[118].

PDMS are able to seal to itself and has the advantage of sealing to itself as well as to other materials reversibly or irreversibly. For a reversible seal, PDMS and other flat surfaces are brought into conformal contact and the seal is achieved in seconds via van der waals forces. This bonding can withstand pressures greater than ~ 5 psi[118]. There is another way by using adhesive tapes to seal the device[128].

For an irreversible seal, the PDMS and the second surface (such as PDMS, glass, silicon, polystyrene, polyethylene, or silicon nitride) are both exposed to oxygen plasma or corona discharge. Bring the two surfaces into conformal contact quickly and an irreversible sealing is generated. The common explanation is the $–CH_3$ group on the surface is displaced by –OH group formed by the plasma condense, which probably hydrolyze to form Si-O-Si bonds[137, 160]. (see Figure 1.4).

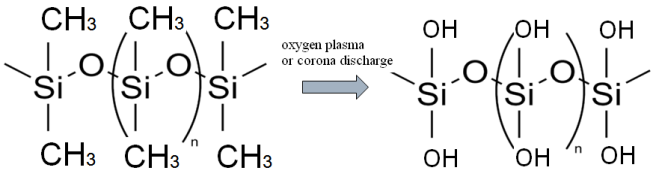

Figure 1.4: Surface groups of PDMS change after oxygen plasma treatment or corona discharge treatment. Before (left): there is CH_3 group on the surface; After(right): there is -OH group on the surface which can be hybridized to form Si-O-Si bonds.

There is another method developed by Quake *et al. which* is able to bond multilayers of PDMS irreversibly[163]. The seal is formed by bring two PDMS slabs into conformal contact when one slab of PDMS has more base agents and another slab of PDMS has more curing agents.

The third method to seal the chip irreversibly was related to "glue" two layers of PDMS together. The two pieces of PDMS are both coated with a thin layer of PDMS prepolymer and brought to contact. The seal is formed by thermocuring the assembly[164].

1.7 Membrane Separation Process

1.7.1 *Types of Membrane Separation Process*

Membranes play an essential role in nature. Biological membranes have an important function by acting as a selective barrier. In the process industry, membrane separation processes are becoming more and more important and have been widely adopted over the last 50 years[165]. The first membrane experiments used membranes of biological origin in the 18th century. However, the rapidly development of industrial membrane-separation process with synthetic membranes happened in the early sixties after the introduction of the asymmetric polymeric membrane[1]. Like biological membrane, the membrane acts as a semipermeable barrier and separation occurs between two liquid phases, two gas phases, or a liquid and a gas phase with membrane controlling the exchange of mass of molecules. Membrane separation processes have two important advantages: energy efficient and capital. People like the membrane devices and systems since they are always compact and modular[165]. Artificial membranes have many biotechnological separation applications such as affinity membrane (e.g. protein purification), biosensors(e.g. glucose sensors), biohybrid organs(e.g. artificial livers) and artificial tissue structures(e.g. artificial skin).

Table 1.4: Some membrane separation processes arranged according to the mechanism of separation (adapted from[1])

Separation mechanism	Membrane separation process
Size exclusion (filtration)	Nano filtration, ultra filtration, micro filtration
Solubility/diffusivity	Reverse osmosis, gas permeation, pervaporation, liquid permeation or dialysis
Charge	Electro dialysis

The main membrane separation processes can be classified into eight major types which function according to three separation mechanisms (see Table 1.4(adapted from[1])).

The membrane phase may be in the following phase: nonporous solid, microporous or macroporous solid with a fluid (liquid or gas) in the pores, a liquid phase with or without a second phase, or a gel[165]. A membrane process is a process of selective and controlled transfer of one species from one bulk phase to another bulk phase separated by the membrane. The intrinsic properties of the membrane are closely related to the success of using membranes. To a great extent, the membrane performance is governed by interfacial interactions between membrane surface, surrounding environment and solutes. These interactions impact significantly on highly-adsorptive-solutes transport in biotechnological and medical applications when fouling of the membrane caused by adsorption of proteins lead to considerable losses in flux, selectivity and performance of the membrane[166].

The following membrane processes are introduced briefly[167].

1. Liquid permeation or dialysis. The membrane phase is between two liquid bulk phases. The small solutes in one liquid phase diffuse through a porous membrane to the second liquid phase due to concentration differences. In another words, solutes move from a region in high concentration to a region in low concentration. It is more difficult for large molecules to move through the membrane. There are several applications that use this membrane separation process such as separation of H_2SO_4 from nickel and copper sulfates in aqueous solutions, food processing, and artificial kidneys.

2. Gas diffusion in porous solid. The membrane is a microporous solid while both phases on two sides of the membrane are gas phase. The pore sizes and the molecular weights determine the rates of molecular diffusion of the gas molecules[168, 169].

3. Gas permeation in a membrane. In this case, the membrane is usually a polymer such as rubber, polyamide, and so on. However, the membrane here is not a porous solid. The gas dissolves in the membrane first and then diffuses in the solid to the other gas phase. It is used to separate a gas mixture due to the fact that each type of molecule diffuses at a different rate through the membrane.

4. Ultrafiltration membrane process. Ultrafiltration membranes are porous membrane with pore sizes range from 5nm to 100nm. It's different from dialysis which is based on diffusion. Ultrafiltration is more convection based. The separation of proteins, polymers, colloidal materials and other relatively high-molecular-weight solutes from the solution is based on molecular size, shape, or chemical structure and it's pressure driven. The osmotic pressure is negligible because of the high molecular weights. Solute is carried in a solution across a semipermeable membrane. This process mimics what actually happen in the kidney.

5. Microfiltration membrane process. This process is similar with ultrafiltration membrane separation process. It is pressure driven as well and the micron-size particles are separated from fluids. The pore size is from 5nm to 5μm. It is used to separate larger particles than those in ultrafiltration, such as bacteria, paint pigment, yeast cells, and so on. Same with ultrafiltration, the membranes are mostly polymeric and can be used in

dead-end and cross-flow mode. All fluid is forced to pass the membrane in the dead-end mode while a tangential flow across the membrane is used in cross-flow mode which helps minimize fouling[1].

6. Reverse osmosis. In the normal osmosis process, the solvent would move from a region with lower solute concentration to a region with higher solute concentration to equalize solvent concentration on each side of a membrane. Reverse osmosis is the process to reverse the natural solvent flow direction by applying an external pressure on one side of the membrane. The membrane is placed between a solute-solvent solution and a pure solvent. This process is always used to produce high quality water such as desalination of seawater. The polymeric reverse osmosis membranes consist of a polymer network in which solutes can be dissolved but without macroscopic pore structure.

7. Gel permeation chromatography. This process is driven by concentration difference beside the porous gel. The diffusion of the low-molecular-weight solutes is retarded by the porous gel. This process is quite useful in analyzing complex chemical solutions and in the purification of very specialized or valuable components.

8. Electrodialysis. In this process, the membrane acts a semi-permeable barrier which allows either positively charged ions (cations) or negatively charged ions (anions) to pass while keeping ions of the opposite charge from passing. The membrane is named under ion-exchange, ion-selective or electrodialysis membranes. Resins composed of cross-linking polymers that possess electrically active functional groups are used in ion

exchangers. A charged molecule (ion) may selectively be exchanged for other charged molecules.

9. Pervaporation. Pervaporation is a membrane process which involves the permeation goes through the membrane and then its evaporation from the other side of the membrane[170]. The membrane acts as a selective barrier between the liquid phase and the vapor phase. Separation of components is achieved based on different transport rate of different components through the membrane. One of the applications is to separate volatile dissolved organics from liquid mixtures[171, 172].

1.7.2 *Membrane Structures*

The structure of the membrane is critical for the membrane performance. The membranes are either symmetrical or asymmetrical. The asymmetrical membrane is composed of a thin selective top layer and a strong support layer which is generally superior to symmetric membrane whose properties do not change throughout the cross section of the membrane[165].

Ceramic membranes have an asymmetrical structure with either a dense or a porous skin layer. The rough porous support layer has a smaller pore size compared with the top layer. The final support layer typically ranges from 1 and 5 μm, which is made of sintered ceramic particles (alumina (Al_2O_3), titania (TiO_2), and zirconia (ZrO_2)). The ceramic membranes are built into a rod instead of a flat disc because flat-discs ceramic membranes are too brittle[1]. Ceramic membranes do not absorb water so that it won't swell as many other membranes. It's not easy for ceramic membrane to change the pore

size causing less retention or change in selectivity. Ceramic membranes are thermally stable, physically hard and chemically resistant which are beneficial for many applications.

A large number of polymeric membranes have been studied and developed in the past decades, as well as a variety of membrane fabrication processes including template leaching, stretching of a polymeric film and phase inversion[173]. Template leaching is the process in the preparation of porous glass membranes by mixing two different components and one of the components is removed by selective leaching after molding. Stretching of a polymeric film is the process to generate voids in dense polymeric films or foils by stretching. Another common technique to prepare asymmetric membranes is phase inversion. It is a thermodynamically driven process[174]. The casting solution can be separated into at least two phases: a solid material-rich phase that forms the porous/non-porous structure of the membrane and a material-poor phase that will be removed from the membrane. By changing the composition of the casting solution, the polymer solidifies and the pores are created. The produced membranes have an inner sponge-like structure which causes an additional fluid resistance[175].

There are also some other membrane structures, such as track etched membranes[176, 177] and anodised alumina membranes[178-180]. The track-etched membrane is produced by two processes. First, dense polymeric films are randomly exposed to collimated, charged particles from a high-energy ion bombardment or particle radiation. As these particles pass through the polycarbonate material, they damage the polymeric chain in the dense film, leaving sensitized tracks. In the second, step the polymer tracks are dissolved with

an etching solution(acid or alkaline solution) to form cylindrical pores. Varying the temperature and strength of the etching solution, and the exposure time to it, produces precisely controlled pore sizes. The pore size is uniform, however, the membrane has a low porosity because of the possibility of an overlap between two pores increases with the porosity (see Figure 1.5) [181].

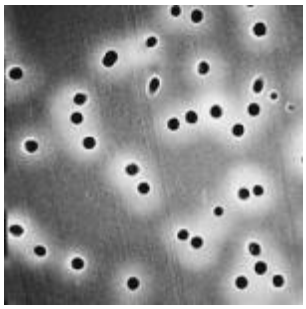

Figure 1.5: SEM micrograph of polycarbonate track etched membrane filter(from sterlitech).

A self-assembling process generate pores of an anodised alumina membrane. A highly ordered structure of pores in the Al_2O_3 matrix can be obtained by anodisation of aluminum in an acidic solution., a self-structuring process is induced and creates the shape and interspacing of the pores due to lattice expansion by the oxidation of the aluminum, An anisotropic potential distribution and heat development during anodisation. The pore size is very uniform, however, the membrane is relatively thin, which may require supported structure depending on the application. And the alumina membrane is brittle, only available in a pore range from 20 to 200mm and has a relatively low flux performance[1, 182].

1.7.3 *Integrating membrane into the device*

Previous processes such as filtration[183] and dialysis[184]have been implemented on microchips. In microfluidic devices, membranes[185-187], gels[188], electrophoresis[189], dielectrophoresis[190, 191] and magnetic filtration[192] are all the methods of filtration now[193]. There is considerable interest in integrating nanoscale structures into microfluidic devices[194, 195]. Macromolecules behave differently as the dimensions of surrounding structures approach the size of the molecule itself[196]. Both preparative and analytical applications that take advantage of these differential properties have been proposed[194-198].

Membranes have been integrated to add functionality and flexibility to microfluidic devices[199, 200]. Fabrication of 3D fluidic networks by integrating membranes containing monodisperse distributions of nanopores into microfluidic devices is relatively straightforward[187, 201, 202]. It becomes more and more popular by using multilayer microfluidic device with membrane filters to separate molecules based on their size, which dramatically reduce the complicated and time-consuming sample pretreatment steps. When the molecules are larger than the pore, none of the molecules will pass and when the molecules are smaller than the pore, the molecules will go through. It is an definite molecular separation compared with the passive analyte-stationary phase interaction. The nanopores of the membrane controls fluidic transport between different planes in the device[203]. The large surface-to-volume ratio maximizes analyte separations based on physical size. Multilayer devices with membranes have great potential for removing impurities and pre-concentrating samples before further analysis in microfluidic devices[185, 204, 205], dramatically reducing offline process time and increasing

sensitivity when coupled with mass spectrometry[186] or capillary isoelectric focusing (CIEF)[206]. Membranes have also been used in cell-related research[207, 208], protein digests[209, 210] bioreactors[210, 211], and bioanalytical chemistry[150]. Membranes are used widely in chemical analysis[212], especially when the sample is mass-limited[205, 213]. Thus, more and more research groups explore molecular transport through membrane nanopores[214].

There are other methods to fabricate porous structures in the microfluidic device, such as chemical etching[116] and photopatterning[215]. Compared with these methods, sandwiching a membrane is cheaper, simpler, more convenient and more universalized to utilize commercial membranes with relatively high throughput.

Nuclear track-etched polycarbonate membranes (PCTE) have precise controlled cylindrical pores whose pore size is from 10 nm to 20 um. The pore density increases as the diameter of the pore decreases. For example, a membrane with 0.2 nm pore size has a pore densities 3×10^{8} cm^{-2}. These membranes are transparent in most pore sizes. They offer the lowest non-specific binding of any filter membrane; there is no sloughing or particle shedding; they are biologically inert; with pressure tolerances in excess of 3000psi. In addition, these filter membranes offer excellent chemical resistance and thermal stability up to 140 ℃. Controlling the applied bias, polarity and density of pores of these membranes, we can obtain a highly selective molecular transport mechanism.

With high surface to volume ratio, it is anticipated the microfluidic device will endow the membranes with maximum performance.

1.8 The Physics of Microfluidics

1.8.1 *Reynolds Number*

Microfluidics is the manipulation and controlling of fluids that are geometrically constrained to micrometer scale. The special dimensions, geometries, and materials in microfluidics devices leads to a specialized set of physical phenomena and flow regimes. Several effects including laminar flow, diffusion, fluidic resistance, surface area to volume ratio, and surface tension play an important role in microfluidics. The most important characteristic feature of fluid flow in microchannels is laminar flow due to the short length scale[216].

The Reynolds number (Re) is a dimensionless group which describes the ratio of inertial forces to viscous forces. The balance between viscous and inertial forces causes the change in velocity. Viscous forces act on the fluid to slow it down, whereas inertial forces act on the fluid to keep it in motion. Viscous forces are closely related to viscosity, while inertial forces depend on the mass or density. The Reynolds number can be expressed in the following equation (equation 1.8.1)[217]:

$$R_e = \frac{inertial\_forces}{viscous\_forces} = \frac{\rho v^2 / L}{\mu v / L^2} = \frac{\rho L v}{\mu} \qquad \text{equation 1.8.1}$$

Where L is a characteristic length (cm); v is a characteristic velocity (cm/s); ρ is the density of the fluid (g/cm^3); and μ is the fluid viscosity ($g / cm \cdot s$).

The Reynolds number also represents the ratio of momentum transport by convection to momentum transport by viscous diffusion[218]. It describes its flow regime: laminar or turbulent. When flow is turbulent, it's unable to predict the position of a particle in the fluid stream as a function of time. The velocity fluctuates randomly. The analysis of turbulent is much more complex than the analysis of laminar flow. When $R_e < 2300$, as calculated from equation 1.8.1, it indicates the flow is laminar flow. When $R_e > 2300$, the flow is considered to be turbulent[219]. Due to the length scale in our device is micro-meter wide and centimeter long, the Reynolds number is much less than 2300 which corresponds to a laminar flow in the device.

1.8.2 *Peclet Number*

Though microscale flow always has low Reynold number, it can have large mass transfer Peclet numbers due to the low diffusivity of macromolecules and particles of interest. The dimensionless Peclet number (Pe) represents the ratio of mass transport by convection to mass transport by diffusion, which is shown in the following equation(equation 1.8.2).

$$P_e = \frac{\text{mass transport by convection}}{\text{mass transport by diffusion}} = (\frac{L^2}{D_{ij}})(\frac{v}{L}) = \frac{vL}{D_{ij}} \qquad \text{equation 1.8.2}$$

Where v is the characteristic velocity; L is a characteristic length, D_{ij} is the diffusion coefficient of the molecule. An alternative way to calculate Pe is to computing the ratio of the diffusion time($t_d=L^2/D_{ij}$) to the convection time ($t_c=L/v$).

When the Peclet number is very large, convection is the dominant force to transport fluid, whereas when the Peclet number is small, diffusion is the dominant force to transport fluid. For the fixed geometry and the fixed velocity, diffusion is most important for transporting small molecules such as gases while convection is most critical for transporting large molecules such as protein and cells[217].

In our device, a syringe pump will drive the solution flow through the device. It is easy to use Peclet number (Pe) to see whether diffusion dominates the movement in the axial direction or convection dominates. For small molecules in aqueous solution, D is about 1×10^{-5} cm^2/s. For 80 base ssDNA molecules, MW is $330\times80=26400$ which corresponds to the diffusion coefficient around 6.9×10^{-7} cm^2/s. v is less than 3.3 cm/s. Therefore Pe>>1, which means convection dominates the flow in the axial direction. The Pe number in the radial direction is calculated in Chapter 3.

1.8.3 *Biot number*

The dimensionless Biot number (Bi) represents the ratio of resistance of mass transfer across a cell layer to the resistance of mass transfer through the tissue by diffusion. This number is used to study the relative importance of transport and reaction processes. Identification of the rate-limiting step can be done by modeling transport and reaction processes. The rate-limiting step is the slowest step in the process. Identifying this rate-limiting step is useful to simplify the reaction model significantly. The rate of reaction can be enhanced by decreasing the characteristic length if the process is limited by diffusion or by increasing the fluid velocity if the process is limited by flow. The Bi number can be calculated by the following equation (equation 1.8.3).

$$B_i = \frac{\text{mass transfer across a cell layer}}{\text{mass transfer by diffusion through tissue}} = \frac{k_m L}{D_{eff}} \qquad \text{equation 1.8.3}$$

Where k_m is the cell layer permeability; L is the distance over which diffusion in the tissue occurs; D_{eff} is the effective diffusion coefficient in the tissue[217].

1.8.4 *Laminar Flow*

Laminar flow is called streamline flow as well. The fluid travels in a steady, time-independent manner at each location and fluid flows in parallel layers are known as steady laminar flow. In steady laminar flow, the velocity does not change with time at each location. Multiple streams can be brought into contact with each other without mixing by turbulence One application is laminar flow patterning. If the channels are wider than they are deep, the Reynolds number is low and the mass transfer Peclet number is high, then the distribution of the solutes in a channel can be controlled by adjusting the input flow rates of each streams which are related to the channel depths, channel widths and input pressures[216].

1.8.5 *Pressure-driven Flow*

Pressure driven flow and electrokinetic driven flow are two major methods to drive the fluids to flow in the microchannels. For pressure-driven flow, $Q=\Delta P/R$[160], where Q is the flow rate (m^3/s), ΔP was the pressure drop across the channel (Pa), and R is the channel resistance (Pa s/m^3). For a circular channel, $R=8\mu L/\pi r^4$. And for a rectangular channel with a high or low aspect ratio ($w << h$ or $h << w$), $R=12\mu L/wh^3$, where μ is the fluid viscosity, L is the channel length, r is the radius of the channel, h is the height and w

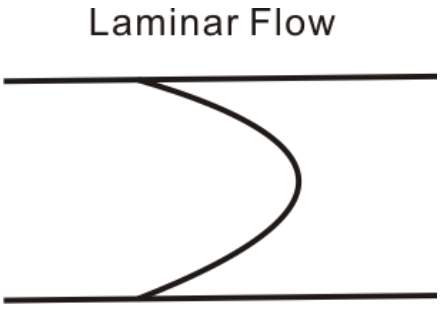

Figure 1.6: Pressure-driven velocity profile which is parabolic.

is the width of the channel. This equation tells us a long narrow channel has more fluid resistance than a short wide channel. If the device has more fluid resistance, it needs more pressure drop across the channel at a definite flow rate. Therefore, a long narrow channel will need more pressure at a certain flow rate. Certainly it is a challenge for the seal of the device. The velocity profile of a cross section is parabolic so that samples undergo axial dispersion and peak broadening see Figure 1.6). It's not good for separation. However, the pressure driven flow is not picky for the buffer composition or the channel material. It's effective for buffers with a wide range of compositions and for channels with a variety of materials.

1.8.6 *Electrokinetic Flow*

The flow can be driven with pressure, but applied electric fields are often more convenient or elegant to actuate these systems. Even if not applied, intrinsic electric fields exist at interfaces in all cases, driven usually by chemical reaction. Therefore, electrodynamics, chemistry, and fluid mechanics are inextricably intertwined, so that electric fields can create fluid flow and fluid flow can create electric fields, with a degree of coupling driven by the surface chemistry.

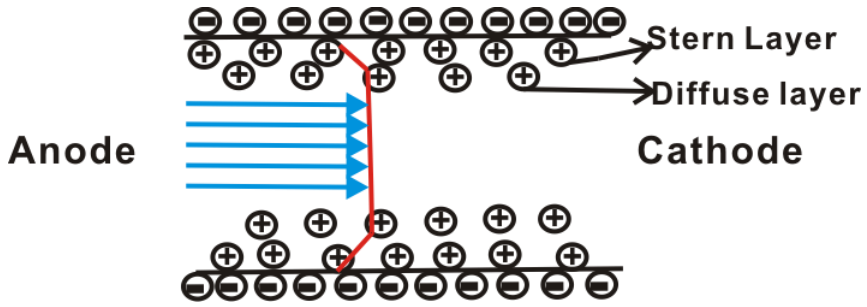

Figure 1.7: Schematic of double layer and the electroosmotic velocity profile. The EOF results from the effect of the applied electric field on the solution double layer at the wall. The direction of the bulk flow is the same with the direction of the counter-ions.

Electrokinetic transport includes electroosmosis and electrophoresis flow. Electroosmosis flow is the motion of ions resulting from the solvent movement, which creates a uniform pluglike flow of fluid down the channel (see Figure 1.7). The EOF is caused by the effect of the applied electric field on the electrical double layer which is formed in a buffer-filled channel. Oppositely charged ions from the ions at the wall of the channel are attracted toward the electrode upon applying the potential through the channel. This will cause the bulk flow in the same direction toward that electrode. EOF is dependent on the surface charge density, electric field, pH, ionic strength of the buffer, material of the channel and so on. The magnitude of EOF can be expressed by $v_{EOF}=(\varepsilon\zeta/\eta)E$, where V_{EOF} is the velocity, ε is the dielectric constant, ζ is the zeta potential and η is the viscosity of the buffer solution. Zeta potential is a potential difference in the double layer. $\zeta=\sigma^*/(\varepsilon\kappa)$, where σ^* is the surface charge density and κ^{-1} is the Debye length. Therefore $v_{EOF}=(\sigma^*/\eta\kappa)E$. And the surface charge is also pH dependent, which means pH influences the EOF. Debye length κ^{-1} is a parameter which characterizes the thickness of the diffuse double layer and it is related to the ionic strength *I*. The Guoy Chapman theory of the electrical double layer is employed to tell the relationship

between κ^{-1} and I (buffer solution concentration) $k^{-1} = [3.29zC^{1/2}]^{-1}$, where z is the charge, C is the electrolyte concentration in mol/L and κ^{-1} is in nm. From this equation, it is obvious that as electrolyte concentration increases, the Debye length decreases[220]. The decrease of Debye length causes the decrease of EOF. All of these shows the EOF can be controlled. When Debye length is large, the EOF will dominate the electrokinetic flow.

Electrophoretic flow is the movement of charged analytes under the influence of an electric field. Analytes with different charge to mass ratio move in different electrophoretic velocities(v_e). $v_e = \mu_e \cdot E$ where μ_e is the electrophoretic mobility and E is the electric field. The electrophoretic mobility can be expressed by $\mu_e = q/(6\pi\eta R)$, where μ_e is the mobility, η is the viscosity of the buffer, q/R is the charge to mass ratio. According to the Nernst-Einstein equation, mobility $\mu_e = zFD/RT$. Therefore $v_e = zFDE/RT$, where v_e is the velocity, z is the charge of the molecule, F is the Faraday constant, R is the gas constant, T is the Kelvin temperature and E is the electric field.

When a transmembrane electric field exists, the flux of a charged molecule is described based on augmented Nernst-Planck equation[221](equation 1.8.4).

$$J = J_{diff} + J_{ep} + J_{EOF} = -D\frac{\partial C}{\partial x} - \frac{zF}{RT}DC - Cv_{EF} \qquad \text{equation 1.8.4}$$

Moreover, electrostatic attraction enhances the transport while repulsion inhibits it[222].So it helps to transport the negative molecules across positively charged nanopores.

For electrokinetic flow, a high surface-to-volume ratio leads to more efficiently dissipation of heat in smaller channels. And the fluid flow can be easily controlled by

turning the electric field off or on. However, electrokinetic flow requires only compatible buffers (those with appropriate pH and ionic strength), the voltage supply, electrolytic bubble formation and evaporation of solvent.

There is also other methods to drive fluid flow in the channel, such as capillary action in plasma-oxidized PDMS[223], centrifugal force in PDMS channels on a plastic disc[224], gradients in surface pressure due to redox-active surfactants in non-PDMS-based devices[225], gradients in temperature[226], patterning of self-assembled monolayers with different surface free energies[227], and capillary action[228].

1.8.7 *Diffusion*

Diffusion and convection are two physical phenomena involved in the transport of molecules. Diffusion is the random motion of molecules that are self-propelled by thermal energy[217]. The diffusion rate depends upon its size and shape, the temperature, and the fluid viscosity[217]. Viewed from macroscopically, the diffusion molecules move from regions of higher concentration to regions of lower concentration which are known as concentration gradients. The common model for diffusion in one dimension is $< d >^2 = 2Dt$, where d is the distance a particle moved in the time t, and D is the diffusion coefficient of the particle[219]. Based on this equation which shows the time required to diffusion increases with the square of the distance over which diffusion occurs, it turns out diffusion is very important in microscale channels. For example, 80nt ssDNA (D=6.9×10^{-7} cm^2/s) in water takes 7.25×10^5 s (about 201 h) to diffuse 1 cm, but only 0.7s to diffuse 10 μm. The polycarbonate membrane in our device has a thickness of

6 μm. Diffusion plays an important role in transport across the membrane in this length scale.

Diffusion coefficient represents the ratio of diffusion flux to the concentration gradient of the particles. The diffusion coefficient is a function of temperature and pressure[217]. Both of the particles and the medium through which diffusion occurs determine the magnitude of the diffusion coefficient. Gases have the largest diffusion coefficient since the intermolecular force is not very important for gases and the molecules physically interact with each other at low frequencies. The diffusion is 10,000 to 100,000 times slower in liquids than in gases because the diffusion molecule cannot travel further distances before colliding with a solvent molecule in liquids. What's more, the diffusion coefficient in membrane is smaller than the diffusion coefficient in the liquid. In complex structures, such as cells and tissues, not only the diffusion distance would increase significantly due to the presence of obstructions, but also these obstructions will exert drag forces on diffusing molecules and retard their movement. Therefore, an effective diffusion coefficient D_{eff} is used to replace the binary diffusion coefficient in Fick's law which is discussed in Chapter 3[217].

ssDNA structures and diffusion coefficient depend on ionic strength of the buffer to some points according to many groups' researches[229-239]. Stellwagen group used capillary electrophoresis to determine the electrophoretic mobility and translational diffusion coefficients of DNA molecules in free solution[230]. They mentioned the diffusion coefficients of small dsDNA oligomers are independent of sequence and the diffusion coefficients of small, dsDNA oligomers are relatively independent of the ionic

composition of the solution. ssDNA diffuse faster than dsDNA which reflect the difference in flexibility between ss and dsDNA molecules. Weill group studied the trend of the persistence length of ssDNA as ionic strength of the buffer changed[229]. They found a total persistence length of about 4nm at 10^{-2} M for ssDNA electrophoresis in sequencing gels. Abstreiter group presented a trend for diffusion coefficient of 24nt ssDNA in a solution of varying ionic strength. As NaCl concentration is increased, the translational diffusion coefficient increased accordingly up to a concentration of ~200mM, from which point the translational diffusion coefficient decreased again. It was believed the initial increase of diffusion coefficient was due to the decrease of electrolyte friction. The later decrease of diffusion coefficient was thought to be caused by the possible conformational changes which was resulted from the effective screening along the chain lowered the electrostatic contribution to the rigidity of oligonucleotides [231].

1.8.8 *Convection*

Another method to transport molecules is by fluid motion. Convection is a mechanism of transport that arises from the bulk motion of fluids (advection). The motion of fluids could result from the application of shear stresses and pressure differences. Shear stresses which are caused by applying forces tangent to a surface lead to relative movement of two contiguous parts of the material. Pressure which is a compressive normal stress could also cause the motion of the fluid[217].

The net motion of solutes differs slightly from the fluid motion because the solute molecules are diffusing at the same time. The Peclet number can be used to determine

whether the diffusion dominates or the convection dominates. If fluid moves slower relative to diffusion, then diffusion dominates. On the contrary, if fluid moves faster relative to diffusion, then convection dominates. Both of diffusion and convection influence transport of energy, momentum and mass in biological systems[217].

1.8.9 *Cocurrent and Counter Current Flow*

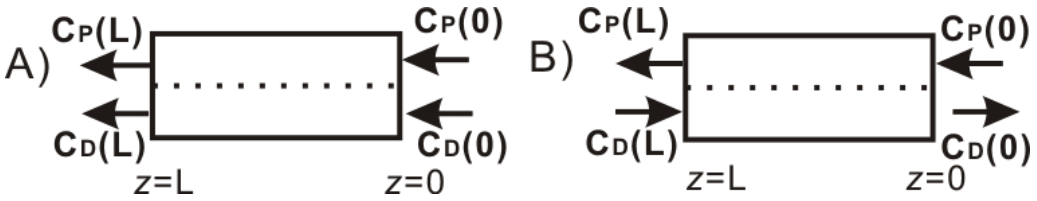

Figure 1.8: Schematic of cocurrent flow(A) and counter current flow(B). (A)Cocurrent flow: permeate flow and dialysate flow are in the same direction. (B): Counter current flow: the permeate flow and the dialysate flow are in the opposite direction.

When the dialysate and permeate fluid flow in the same direction, it is the cocurrent flow(see Figure 1.8). By contrast, when the dialysate and permeate fluid flow in the two opposite directions, it is the counter-current flow (see Figure 1.8). The following two differential equations are used to reflect the material balance on fluid[217]:

$$\begin{cases} permeate: dM = -Q_P dC_p \\ dialysate: dM = Q_D dC_D \\ membrane: dM = k_0 (C_P - C_D) dA_m \end{cases} \qquad \text{equation 1.8.6}$$

Where M is the molar rate; Q_P and Q_D are the flow rates of the permeate and dialysate channels; C_p and C_D is the concentration in the permeate and dialysate channel. A_m is the membrane area. Equation 1.8.6 means the loss of solute from the permeate channel is balanced by the gain from the dialysate. k_0 is the overall mass transfer

coefficient which includes mass transfer on the permeate phase(k_P), mass transfer on the dialysate phase(k_D) and permeability of the membrane(P_m). For a flat-plate dialyser[217],

$$\frac{1}{k_0} = \frac{1}{k_P} + \frac{1}{P_m} + \frac{1}{k_D} \qquad \text{equation 1.8.7}$$

By rearrange equation 1.8.6, $dC_P - dC_D = -dM(\frac{1}{Q_D} + \frac{1}{Q_P})$

$$\ln(\frac{C_P(0) - C_D(0)}{C_P(L) - C_D(L)}) = k_0 A_m(\frac{1}{Q_D} + \frac{1}{Q_P}) \qquad \text{equation 1.8.8}$$

By integrating equation 1.8.6,

$$M = Q_p(C_P(0) - C_P(L)) = -Q_D(C_D(0) - C_D(L)) \qquad \text{equation 1.8.9}$$

Substituting equation 1.8.9 into equation 1.8.8

$$M = k_0 A_m \frac{(C_P(0) - C_D(0)) - (C_P(L) - C_D(L))}{\ln(\frac{C_P(0) - C_D(0)}{C_P(L) - C_D(L)})} \qquad \text{equation 1.8.10}$$

Equation 1.8.10 shows the molar flow rate is related to a log-mean concentration difference.

For counter-current flow, the following equations are used to describe the system:

$$\begin{cases} permeate: dM = -Q_P dC_p \\ dialysate: dM = -Q_D dC_D \\ membrane: dM = k_0(C_P - C_D)dA_m \end{cases} \qquad \text{equation 1.8.11}$$

By using the same method as cocurrent, equation 1.8.8 changes to equation 1.8.12[217]:

$$\ln\left(\frac{C_P(0)-C_D(0)}{C_P(L)-C_D(L)}\right)=k_0A_m\left(\frac{1}{Q_P}-\frac{1}{Q_D}\right) \qquad \text{equation 1.8.12}$$

For the purpose of removing the largest amount of solute from the permeate phase, countercurrent exchange is superior to co-current exchange. It is because the exit concentration on the dialysate side ($C_D(L)$) is slightly less than the outlet concentration on the permeate side ($C_P(L)$) and much less than the inlet concentration on the blood on the permeate side ($C_P(0)$) with cocurrent exchange. However, with countercurrent exchange, dialysate enters from the opposite direction which meant at the outlet concentration on the dialysate side ($C_D(0)$) can then be greater than the outlet concentration on the blood side ($C_P(L)$)[217].

Sherwood number is the dimensionless number in mass-transfer units which represents the ratio of convective mass transfer coefficient to the diffusion mass transfer coefficient. $Sh=\frac{K\cdot L}{D}$. Where K is the mass transfer coefficient, L is the characteristic length, and D is the diffusion coefficient. In the transmembrane process, the transmembrane Sherwood number is expressed as following[217]: $Sh_m=k_mH/D_{eff}=P_mH/D_{eff}$. This number can be used to determine whether the convection mass transfer or the diffusion mass transfer is more important to transport molecules across the membrane[217].

The extraction fraction(E) represents the fraction of solute that is removed from the permeate flow.

For co-current flow, $E = \frac{Q_D}{Q_P} \frac{(C_D(L) - C_D(0))}{(C_P(0) - C_D(0))}$ equation 1.8.13

By using two variables Z which represent the ratio of permeate to dialysate flow rates and FR which represent the ratio of mass transfer resistance to permeate flow rate, the extraction fraction E can be expressed in the following equations[217]:

$E = \frac{1}{1+Z}\{1 - \exp[-FR(1+Z)]\}$, co-current exchange equation 1.8.14

$E = \frac{1 - \exp[FR(1-Z)]}{Z - \exp[FR(1-Z)]}$, counter-current exchange equation 1.8.15

Where $Z = \frac{Q_P}{Q_D}$ and $FR = \frac{k_0 A_m}{Q_P}$

Chapter 2 Fabrication of a PDMS microfluidic device for transporting DNA through a nanopores membrane

2.1 Summary

A microfluidic counter current dialysis device for size based purification of DNA is described. The device consists of two polydimethylsiloxane (PDMS) channels separated by a track etched polycarbonate membrane with a 50 nm pore size. Recovery of fluorescein across the membrane was compared with 10 and 80 nucleotide (nt) ssDNA to characterize the device. Recovery of all three analytes improved with decreasing flow rate. Size selectivity was observed. Greater than 2-fold selectivity between 10 nt and 80 nt ssDNA was observed at linear velocities less than 3mm/s. Increasing the ionic strength of the buffer increased transport across the membrane. Recovery of 80 nt ssDNA increased over 4-fold by adding 30mM NaCl to the buffer. The effect was size dependent as 10 nt showed a smaller increase while the recovery of fluorescein was largely unaffected by increasing the ionic strength of the buffer.

2.2 Introduction

Many groups have studied methods for controlling molecular transport through nanopores[214, 240-247]. Sweedler *et al.* manipulated transport electrokinetically taking advantage of electroosmotic flow and high field strengths in the pores.[202, 214, 245, 248] Kovarik and Jacobson sandwiched a polycarbonate membrane between two PDMS channels to trap particles using electrophoretic and dielectrophoretic forces[243]. Nishizawa *et al.* prepared ion selective membranes which rejected ions of the same polarity as the excess charge on the inner walls of the metal tubules by imposing an electrical bias potential on the membrane[240]. Hou *et al.* modified the surface of gold coated pore walls in polycarbonate membranes to achieve pH-responsive transport of ions due to electrostatic opening and closing of membrane pores[242]. Jirage *et al*. explored the use of gold nanotubules with inner diameters of less than 1 nm to separate small molecules[249]. Schmuhl *et al.* used surfactants to physically open or close nanometer sized channels and pores to gate molecular transport[250]. The Yager group generated laminar fluid interfaces in microfluidic devices for diffusion based sample extraction, separation and detection without using a membrane[251-255].

Short chain nucleic acids are commonly purified using electrophoretic separation on agarose or polyacrylamide gels followed by subsequent recovery of from the gel using electroelution, adsorption, diffusion or gel liquification[80]. It is a slow process not amenable to automation[80, 81]. A nanopore based microfluidic purification device could potentially resolve these issues. The current paper describes our initial work in developing such a device. Fig.1 shows a schematic of the device. A 6 μm thick

polycarbonate membrane was sandwiched between two 250 µm channels. A simple counter current diffusion based design was chosen to make fabrication and operation of the device as simple as possible.

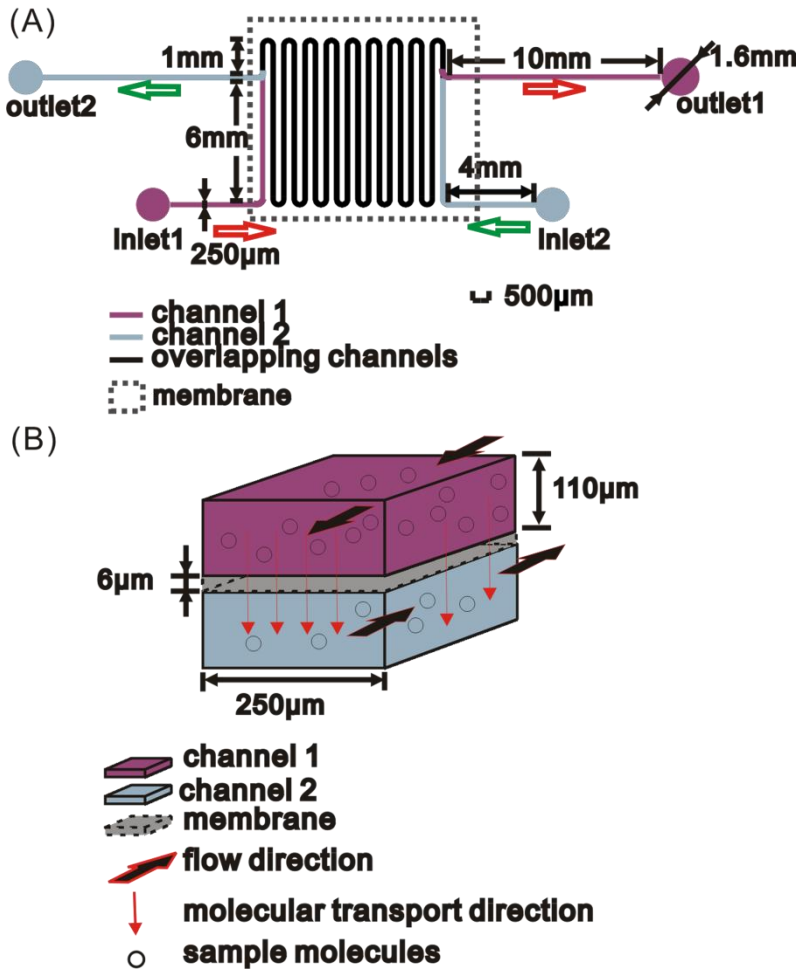

Figure 2.1: (A) Schematic of the counter current dialysis device. Two PDMS channels are separated by a track etched polycarbonate membrane (50 nm pores size). Transport occurs in areas where the channels overlap. A counter current geometry was employed to maximize recovery. (B) Side view illustrating the counter current geometry and transport across the membrane. Not to scale.

2.3 Experimental Section

2.3.1 *Reagents and Chemicals*

PDMS was made using Sylgard 184 silicone elastomer kit (Dow Corning, Midland, MI). Nuclease free water (Integrated DNA technologies, Coralville, IA) was used to prepare all buffer and sample solutions. Fluorescein was purchased from ACROS organics (New Jersey, USA). FAM labeled ssDNA sequences (10 nt: 5'FAM-AGC AGC ACA G and 80 nt: 5'FAM-AGC AGC ACA GAG GTC AGA TGG GAA GCC CGC TGT GAC ATC TGG AGC CGG TTC CCG GAG CCA CCT ATG CGT GCT ACC GTG AA) were synthesized by Integrated DNA technologies (Coralville, IA). Buffers consisted of 2mM NaH_2PO_4,, 300 μM Triton X-100 with various concentrations of NaCl (0, 5mM, 10mM, 30mM, 50mM, 100mM, 200mM), adjusted to pH 7.3 using 100mM NaOH (Mallinckrodt, Paris, KY). Fluorescein and ssDNA solutions were all diluted to 1 μM using in these buffers. All buffer and sample solutions were degassed before use. Piranha solution (3:1 H_2SO_4:H_2O_2, Ashland Chemical, Dublin, OH) was used to clean silicon wafers. Diluted HCl was used to reactivate the PDMS surface. SU8-2050 (Microchem Corp., Newton, MA) was used to fabricate the master. All other reagents and chemicals are from Sigma-Aldrich (St. Louis, MO).

2.3.2 *Fabrication*

The fabrication process is outlined in Figure 2.2. A two-step soft lithography process was used.[256] An SU8 master was fabricated and multiple PDMS replicas were then cast from this master. The chip geometry was designed using CAD software which was then

used to print a transparency film mask. Standard photolithography procedures were used to make the SU8 master. A new silicon wafer was cleaned in piranha solution for 10 min followed by acetone, methanol, isopropanol and deionized water rinses. The negative photoresist SU8 2050 was spin coated on the dried wafer using the manufacture's recommended procedure. The film mask was used to expose the photoresist in a MABA6 aligner (Karl Suss, Munich, Germany). Developing in propylene glycol monomethyl ether acetate (P.M. Acetate) for 6 min yielded a master with the desired geometry. The master was pre-treated with fluorinated silanes (UCT, Bristol, PA). Degassed PDMS prepolymer (10:1 ratio) was then poured onto the master and baked at 70 ℃ for 3 hours. The cured PDMS was removed from the master. A second PDMS layer was made using the same process. The resulting channels were 250 μm wide and 110 μm deep. The total channel length was 14.8cm with an active length where the channels overlapped of 12.8 cm. Inlet and outlet holes were punched into one PDMS layer using a piece of 20 gage stainless steel tubing (McMaster-Carr, Chicago, IL). Both PDMS layers were sonicated in dilute HCl for 10 minutes to reactivate prior to bonding[257]. A 10mm×15mm×6μm polycarbonate membrane with 50nm pore diameter (Sterlitech Corp., Kent, WA) was placed on one layer of PDMS over the transport area of the channel. The PDMS layers were O_2 plasma treated at 600 mTorr and 75 W for 10 s. The two layers were then quickly aligned and bonded irreversibly. The entire assembly was placed on a hotplate at 70 ℃ for 1 hour to complete the bonding process. Two glass substrates were used to support the device and four screws on the corners of the substrates were finger tightened to seal the membrane and the PDMS slabs (see Figure 2.2). 0.5" long pieces of stainless

steel tubing with the same inner and outside diameter as a 21 gage needle (New England Small Tube Corp., Litchfield, NH) were inserted into in the inlet and outlet holes of the device allowing connections to be made with Tygon tubing (0.03 ID, 0.09 OD, Small parts, Inc, Miramar, FL). Buffer was pumped into the device using a syringe pump.

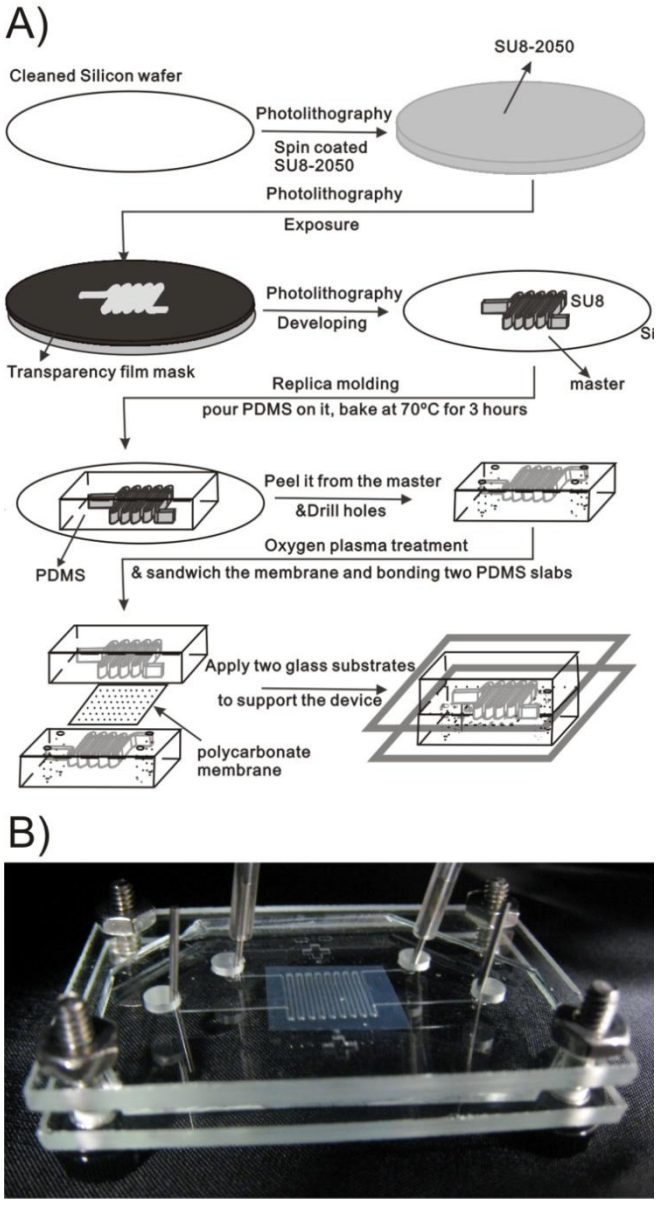

Figure 2.2: A) Schematic of the fabrication procedure of the microfluidic counter current dialysis device. B) Image of the fully assembled device.

2.3.3 *Instrumentation and Data Collection*

An AZ 100 stereomicroscope (Nikon Corp., Tokyo, Japan) mounted with a 120W X-cite metal halide lamp (EXFO Photonic Solutions Inc., Ontario, Canada) and a Cascade 512B CCD camera (Photometrics, Tucson, AZ) was used for fluorescence imaging. Fluorescence was collected through a 1.6× objective with a 3× zoom and filtered using an Endow GFP bandpass filter set (450-490 nm excitation and 500-550nm emmision) and a dichroic mirror (495nm cutoff). Images were recorded and processed using MetaVue software (Downingtown, PA).

2.3.4 *Size Discrimination of the Membrane*

Buffer solution (2mM NaH_2PO_4, 300 µM Triton X-100, 50mM NaCl) and 1 µM fluorescein or fluorescently labelled DNA, dissolved in the same buffer, were simultaneously pumped into inlets #1 and #2 (see Figure 2.1) generating counter current flow in the device. The flow rate was varied from 0.05 ml/hr to 1 ml/hr, corresponding to linear velocities ranging from 0.51 mm/s to 10.1 mm/s. Approximately 10 channel volumes of solution were pumped through the device before data was recorded to ensure stability of the signal. 20 ul solution was collected from outlet #1 to determine the amount of fluorescent analyte that crossed the membrane. This was compared with the intensity of the fluorescent solution pumped into the device (at inlet #2). All fluorescence measurements were made using a Synergy2 plate reader (BioTek Instruments, Winooski, VT) with λ_{ex} = 485nm and λ_{em} = 528nm. Analyte recovery (R) was determined according to:

$$R = \frac{I_{outlet}}{I_{inlet}}$$ equation 2.1

where I_{outlet} is the fluorescence intensity of the solution exiting outlet #1 and I_{inlet} is the fluorescence intensity of the solution entering the device at inlet #2.

2.4 Results and Discussion

2.4.1 *Design Considerations*

The active region of the device consisted of two channels, with dimensions of 12.8 cm long×250 μm wide ×110 μm deep, separated by a polycarbonate track etched membrane. Polycarbonate membranes were chosen due to their mechanical robustness, stability under fabrication conditions and the precisely controlled cylindrical pores typical of these materials. The membrane was 6 μm thick with 50 nm diameter pores. The active region defined by overlapping channels had a total area of 0.32 cm^2 with approximately 1.92×10^8 pores randomly distributed across this area. The membrane was thin enough to allow PDMS to form a good seal during the fabrication procedure.

A counter flow dialysis strategy was adopted to maximize recovery across the membrane. Sample solution and buffer were pumped into each channel in opposite directions. In this device, diffusion is considered to be the major mechanism contributing to transport across the membrane. According to Fick's first law, the rate of diffusion flux is determined by the concentration difference at the boundary[217]. If a cocurrent flow is adopted, transport takes place until equilibrium is reached and the concentration is equal on either side of the membrane. Assuming equal flow rates, recovery in a cocurrent

arrangement is therefore limited to 50% since there is no net transport at equilibrium. However, counter flow dialysis has no such limitation. At every position along the length of the channel, the analyte concentration in the buffer solution is lower than that in the sample solution. The system does not reach equilibrium and net transport occurs along the entire length of the channel with the maximum recovery approaching 100% if the equilibration time is long enough[258-260].

A potential drawback of the counter current approach used here is the generation of pressure differences across the membrane. The nanopores have much higher resistance than the microfluidic channels minimizing flow through the pores at low flow rates. Thus diffusion is the dominant transport mechanism and convection through the nanopores can be considered minimal. However, if bubbles or other obstructions block the channels more significant pressure differences and unpredictable flow patterns can occur. It is therefore important to degas all the solutions. Addition of Triton X-100, a non-ionic surfactant, also decreases bubble size and facilitates their clearance from the device, even at low flow rates[261].

2.4.2 *Characterization of the Device*

Fluorescein and fluorescently labelled ssDNA of two different lengths (10 and 80 bases) were used to characterize the fully fabricated device. The molecular weights for fluorescein, 10 nt DNA and 80 nt DNA were 332 Da, 3583.5 Da and 25278.4 Da, respectively, providing a series of analytes with a wide size range distribution. Figure 2.3 shows fluorescence images of the dialysis channels when the device is perfused with

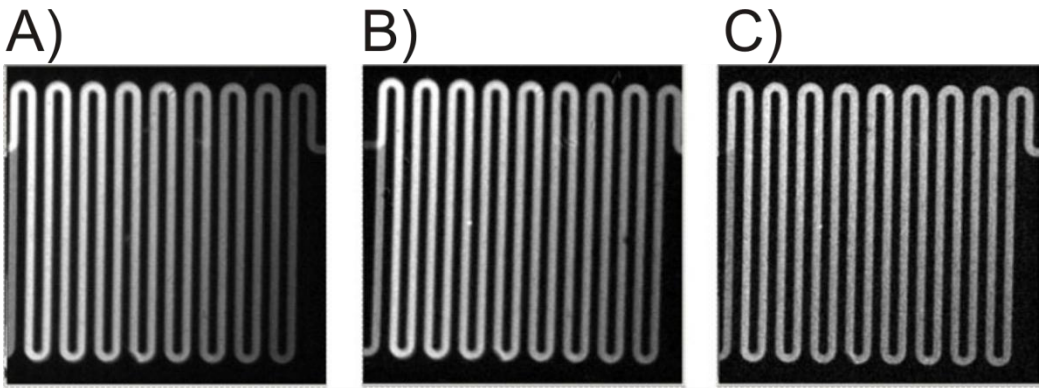

Figure 2.3: Fluorescence image of the membrane region of the counter current dialysis device when perfused with (A) fluorescein, (B) 10 nt DNA and (C) 80 nt DNA. Analyte enters in the lower left channel and exits in the upper right. Buffer enters in the lower right channel and exits in the upper left.

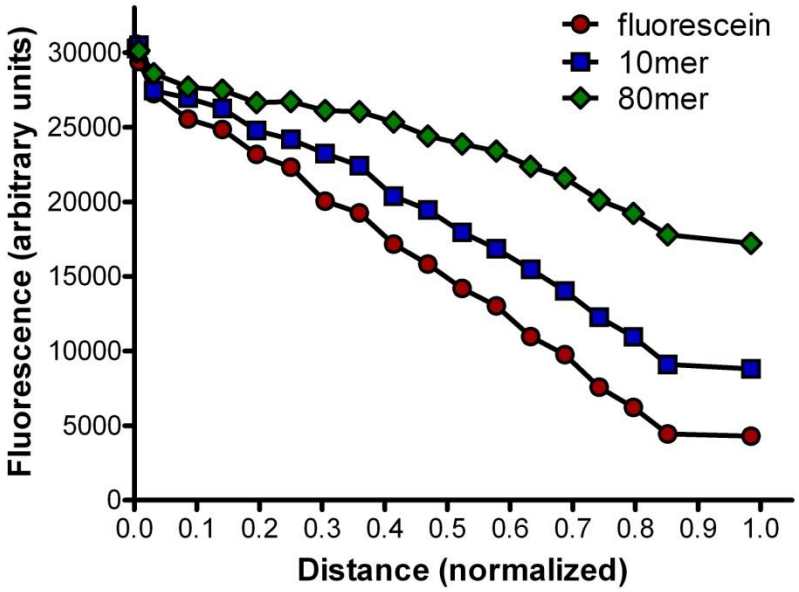

Figure 2.4: Plot of fluorescence intensity vs. distance along the channel for fluorescein (circles), 10 nt ssDNA (squares) and 80 nt ssDNA (diamonds) at 0.5 mm/s in a buffer containing 2 mM NaH_2PO_4, 50 mM NaCl and 300 µM Triton X-100.

fluorescein (A), 10 nt ssDNA (B) and 80 nt ssDNA (C). The sample solution entered the device from the lower left corner and exits through the channel at the top right corner. The buffer solution, on the opposite side of the membrane, enters from the lower right and exits from the upper left channel. Fluorescence intensity decreased along the length of the channel as analyte crossed the membrane and was carried back to the left in the

counter flow. This is especially evident for fluorescein and to a lesser extent 10 nt and 80 nt DNA. Figure 2.4 plots fluorescence intensity along the length of the channel, clearly showing differences in the rate that each analyte crosses the membrane. The trend is consistent with the size dependence expected for diffusion based transport across the nanopores. Images were recorded near the center of the field of view to minimize heterogeneity in the illumination intensity. Sensitivity across this imaging area only varied by less than 1.9% (rsd).

2.4.3 *Recovery and Size Discrimination*

Recovery was assessed by comparing the fluorescence intensity of the analyte solution entering the device to that exiting on the opposite side of the membrane (see eq. 1). Solution was collected and measured offline in a fluorescence plate reader to eliminate the potential for calibration errors in the fluorescence images due to pixel position, differences in channel depth and background generated by the membrane. Recoveries of fluorescein, 10 nt ssDNA and 80 nt ssDNA were measured across a range of flow rates and plotted in Figure 2.5. As would be expected if diffusion dominates, recovery was higher at lower flow rates. The recovery for fluorescein increased from 18.5% to 90% while the recovery for 10 nt ssDNA increased from 9% to 70%. The increase in recovery observed for 80 nt ssDNA was a more modest 7% to 31%. The increase in recovery at lower flow rates is the result of the increased time for equilibration that the analyte is exposed to the membrane. For the 12.8 cm long channel used here, the equilibration time increases from 13 seconds to 4.3 minutes as the linear flow rate is decreased from 10mm/s to 0.5mm/s (1ml/hr to 0.05 ml/hr). Making

measuements at flow rates lower than 0.5mm/s was challenging due to the corresponding increase in time required to collect a reasonable volume of sample.

The size dependence of recovery was maintained across all flow rates. For example,

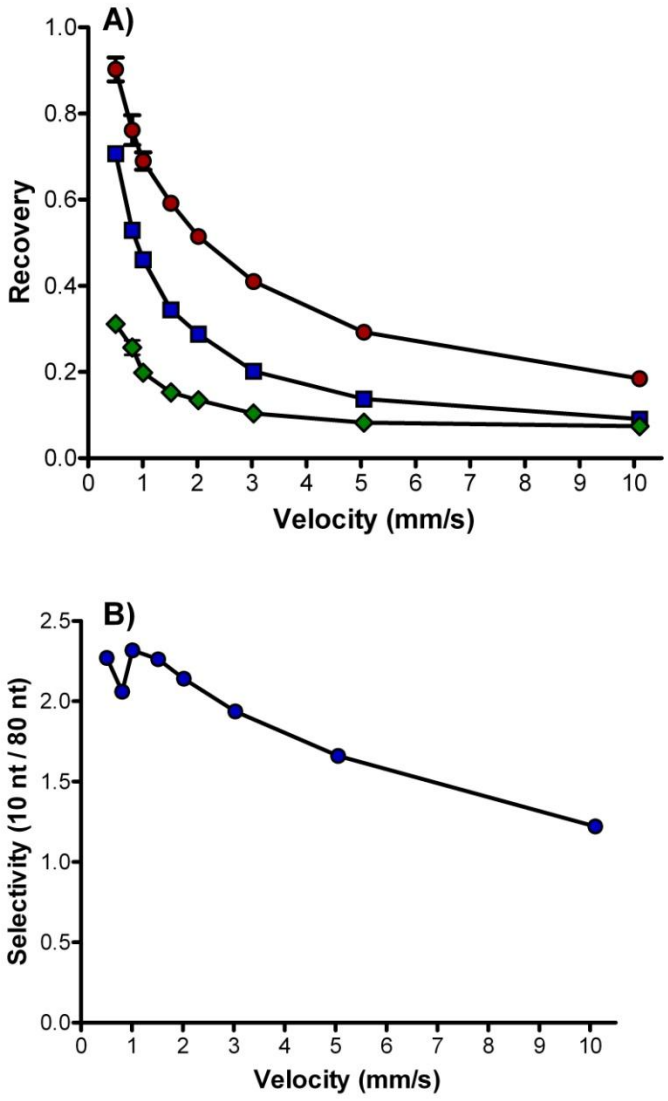

Figure 2.5*:* A) Plot of recovery vs. buffer flow rate for fluorescein (circles), 10nt ssDNA (squares) and 80nt ssDNA (diamonds). Error bars are the standard deviation of three replicate measurements. B) Effect of buffer velocity on the selectivity between 10nt and 80nt ssDNA. The buffer contained 2 mM NaH_2PO_4, 300 μM Triton X-100, and 50 mM NaCl.

at 0.5mm/s, the recovery for fluorescein was 90% while the recovery for 10 nt and 80 nt DNA was 70% and 31%, respectively. The selectivity between 10 nt and 80 nt was 2.3. It should be noted both recovery and selectivity decreased with increasing flow rates (see Figure 2.5). For example, at 10mm/s, the recovery for 10 nt DNA was 9% and the recovery for 80 nt DNA was 7% resulting in a selectivity of only 1.3.

Considering the dimensions of the molecules under study is useful in assessing the mechanism that generates selectivity. The radius of gyration R_g of a chain of contour length L_D=Mb can be estimated using the Kratky-Porod equation[262, 263] :

$$R_g^2 = \frac{pL_D}{3} \times [1 - 3(\frac{p}{L_D}) + 6(\frac{p}{L_D})^2 - 6(\frac{p}{L_D})^3 \times (1 - e^{-\frac{L_D}{p}})] \qquad \text{equation 2.2}$$

where p is the persistence length, M is the number of monomers and b is the contour length of a single monomer. Using b=0.43nm[264] and p=3nm[229], common estimates for ssDNA, the radius of gyration for the 80 nt and 10 nt are approximately 5nm and 1nm, respectively. Both values are significantly smaller than the 50 nm pore size of the membrane suggesting that physical size alone is unlikely to give rise to the selectivity differences observed. Instead selectivity is likely to arise from a combination of steric factors, diffusion constants and interactions with both ions and solution and the surface of the pores[265].

2.4.4 *Ionic Strength of the buffer*

Although the size of the pores is significantly larger than that of the molecules assessed here, the thickness of the double layer also impacts transport of DNA molecules

[214]. Sodium chloride was added to buffers to evaluate DNA and fluorescein transport properties as a function of ionic strength, which in turn impacts the double layer in the pores. As demonstrated in Figure 2.6(A), recovery of each analyte initially increased with increasing ionic strength before reaching a plateau at approximately 30 mM NaCl. Figure 2.6(B) illustrates the effect of ionic strength on the relative recovery of each analyte. The increase in relative recovery showed clear size dependence with 80 nt and 10 nt ssDNA increasing 4.6-fold and 2.1-fold, respectively. Fluorescein was largely unaffected, with relative recovery only increasing 20% with increased ionic strength.

The effect of ionic strength on recovery suggests that the double layer within the pores plays an important role in the transport of the highly negative analytes studied here. The surface of polycarbonate membranes is coated with polyvinylpyrrolidone (PVP) which renders the pore surface hydrophilic. It has been reported that the surface of PVP coated pores typically bears a negative charge at neutral pH [214, 221, 266, 267]. The Guoy-Chapman theory can be used to estimate the Debye length κ^{-1} for dilute aqueous solutions[268]:

$$k^{-1} = (3.29 z C^{\frac{1}{2}})^{-1} \qquad \text{equation 2.3}$$

where κ^{-1} is given in nm and C is the bulk z:z electrolyte concentration in mol/L. The Debye length describes the distance over which ionic effects are observed in solution and can be used to characterize the thickness of the diffuse double layer at a charged surface.

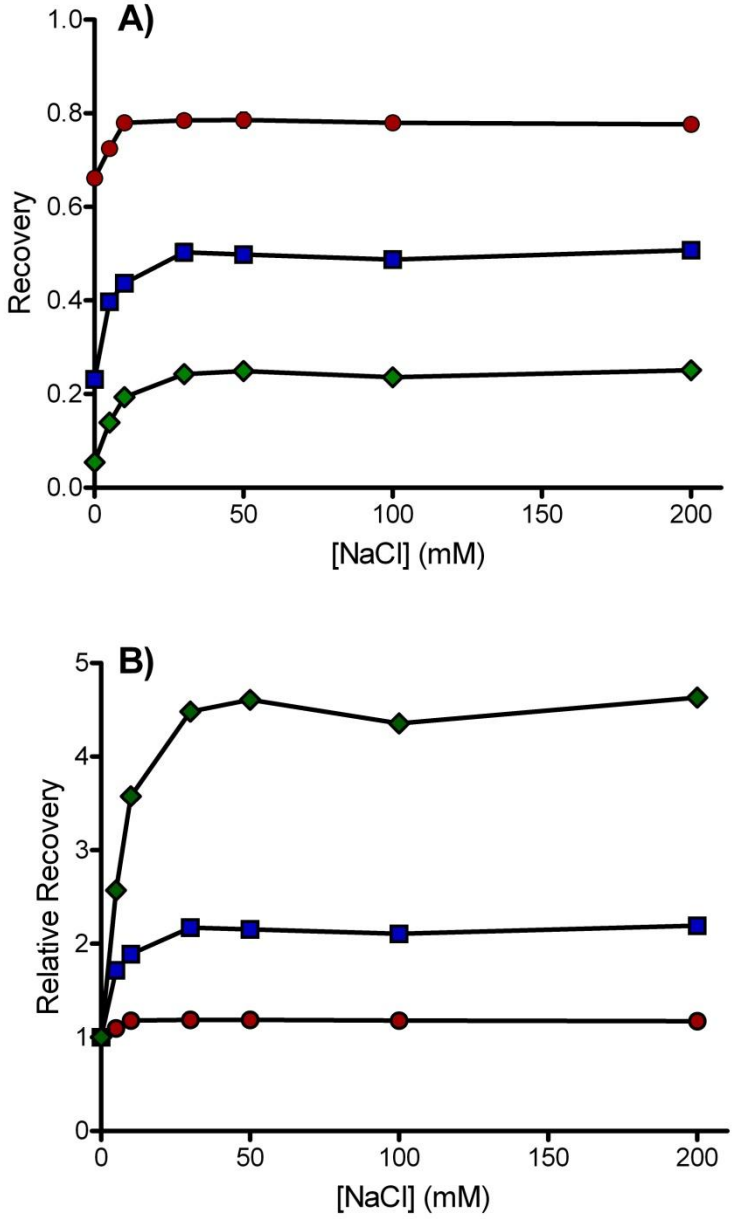

Figure 2.6*:* (A) Plot of recovery vs. NaCl concentration for fluorescein (circles), 10 nt DNA (squares) and 80 nt DNA (diamonds). (B) Plot of recovery normalized to 0 mM NaCl vs. NaCl concentration for fluorescein, 10 nt DNA and 80 nt DNA. Data was recorded in triplicate. Error bars are smaller than the symbols used in the plots. The buffer contained 2mM NaH_2PO_4, 300 µM Triton X-100, and 0–200 mM NaCl.

The Debye length in the buffer was estimated to be 4.67nm in 2mM NaH_2PO_4. Addition of 30 mM NaCl reduces the Debye length to 1.64 nm. Addition of 200 mM NaCl further reduces the Debye length to 0.67 nm.

The formation of a double layer in the pores raises the potential for both coulombic interaction between the charged surface and charged molecules, and increased steric hindrance[220, 240, 269-271]. Increasing the ionic strength of the buffer is expected to reduce the size of the double layer, effectively decreasing the interaction between the charged pore walls and analytes, while increasing the pore size permitting larger molecules to pass through. For example reducing the double layer thickness from 4.67 nm to 0.67 nm increases the cross sectional area of a 50 nm pore by 43%. Beyond affecting the size of the physical barrier of the pore, reducing the Debye length reduces ionic interactions between the analyte and the surface or double layer. Similarly, the radius of gyration of ssDNA decreases as the ionic strength of the buffer increases due to the smaller persistence length of ssDNA[229, 262, 264]. The diffusion coefficient of ssDNA also increases with ionic strength[229, 231]. Through these combined effects increasing the ionic strength improved the recovery of 80 nt DNA 4.6 fold. As expected increasing the effective pore size and decreasing ionic interaction had less of an effect on the smaller and less charged 10 nt DNA, only improving recovery 2.2 fold. The effect on the recovery of fluorescein, already much smaller than the pore size, was negligible.

2.5 Conclusion

We have demonstrated the fabrication and operation of a microfluidic device capable of making size based discrimination of DNA on microliter scale samples. A polycarbonate track etched membrane with 50 nm pores was sandwiched between two PDMS channels and a counter current flow strategy was adopted to maximize recovery. Trends in recovery measured at various flow rates support the premise that diffusion dominated the molecular transport in this device. Recovery increased as the linear velocity decreased. Recovery was also affected by the ionic strength of the buffer suggesting that the thickness and charge of the double layer in the pores play an important role in limiting transport. A theoretical model was built to simulate the transportation process. This model identified diffusion as the major transport mechanism for molecules through the nano pores.

Chapter 3 Modeling to simulate the process for transporting DNA through nanopores

3.1 Summary

Two models were built to simulate the transport process in the microfluidic device. The microfluidic device had two channels with a 50nm polycarbonate membrane sandwiched between them and a counter current flow strategy was adopted to maximize recovery. Both of the models were built based on conservation of mass and constitutive relationships. Diffusion was identified to be the major mechanism to drive molecule through the nanopore. Model 2 assumed there was concentration gradient along the vertical direction (z) in the channel while Model 1 assumed not. COMSOL was used to solve Model 2 to obtain numerical solutions. Trends in recovery measured at various flow rates were consistent with the trends predicted in the two models which support the premise that diffusion dominated the molecular transport in this device. Recovery increased as the linear velocity decreased. Recovery was also affected by the ionic strength of the buffer suggesting that the thickness and charge of the double layer in the pores play an important role in limiting transport which was verified in Model 2. Model 2 also generated surface plots of concentration for three samples (80nt single-stranded DNA(ssDNA), 10nt ssDNA and fluorescein) which visualized concentration distribution in the two channels.

3.2 Introduction

It is important to have a mechanistic and mathematical understanding of transport processes for the design and operation of the devices. Transport-phenomena study always includes the momentum, mass and energy transfer study and the thermodynamics and kinetics of the chemical reactions[217, 272, 273]. The transport process is widely studied in basic research related to molecule, cell and organ function[274-277]; the design and operation of devices, such as filtration units for kidney dialysis[278, 279], high density cell culture and biosensors[280, 281]; and applications including drug and gene delivery[282-284], biological signal transduction[285, 286], and tissue engineering[287, 288].

Many ways have been addressed to describe transport of molecules through membranes including Kedem-Katchalsky approach[289, 290], the hydrodynamic description for neutral components[291] and the Nernst-Planck description for charged solutes[217, 292]. Mass transfer in porous membrane can be analogous to heat transfer in heat exchangers[293-296]. It can be subdivided into diffusive transport and convective transport[297].

Dialysis is a process to transport molecules through the membrane by diffusion which is driven by concentration gradient on both sides of the membrane[167]. The applications of dialysis involve recovery of sulfuric acid from copper leaching solution[165], hemodialysis for removing the metabolic waste from blood[166] and the recovery of acids from various waste solutions by employing ion exchange membranes[298-300], glucose microdialysis for treating diabetes[301] and so on.

Michaels demonstrated an input-output response of a continuous dialysis unit using various flow geometries[294]. Noda& Gryte were among the first to investigate the mass transfer in regular arrays of hollow fibers in countercurrent dialysis[302]. Gill & Bansal developed a predictive mass-transfer model of hollow fiber based on assumption discussed by Happel[303, 304]. Klein focused on the characterization of a hollow fiber bundle using conservation of mass relationships[305]. Shettigar and Jagannathan analyzed the effect of ultrafiltration and dialysate concentration for a tubular haemodialyser thoroughly[306]. Our device had rectangular channels while the above models were all built for hollow fibers which were cylindrical. Walker and Davies studied mass transfer in laminar flow between parallel permeable plates for a Newtonian fluid and found solutions for the concentration profiles and mass transfer rates for various wall Sherwood numbers[307]. However, they assumed both of sides of the channel were permeable while only one boundary was permeable in our device. Cooney, Kim and Davis analyzed the mass transfer in hemodialyzers for laminar blood flow[308]. But their case assumed the concentration in the dialysis stream did not change which was not appropriate for our model. Deen analyzed diffusive and convective transport for mixtures of uncharged solutes by analogy with hydrodynamic transport of a large sphere through a fluid inside a narrow tube[291]. Wesselingh and Noordman recently investigated transport of large molecules through membranes with narrow pores which was not true in our model because we used 50nm pore membrane[297]. Simon group built mathematical model for a countercurrent flow multi-fiber dialyser which related the fractional removal of a solute to mass transfer parameters such as Sherwood number, Peclet number and system

geometry[309]. Yeh investigated the dialysis with external reflux to derive the mass-transfer equations[310] and they also derived mass-transfer equations for dialysis through parallel-flow double-pass rectangular membrane modules[311]. Viehland and Mason focused on statistical-mechanical theory to study membrane transport in a multicomponent systems[312, 313].

Although so many researchers study mass transport through membranes, our problem is unique. It involves mass transfer between two rectangular microfluidic channels through a membrane in a counter-current flow device for 80nt ssDNA, 10nt ssDNA and fluorescein. The model data are compared with the experiment data in this chapter as well.

3.3 Theory

3.3.1 *Definition of Transport Processes*

Diffusion and convection are two physical phenomena involved in the transport of molecules. Diffusion is the random motion of molecules that are self propelled by thermal energy[217]. The diffusion rate depends upon its size and shape, the temperature, and the fluid viscosity[217]. Viewed from macroscopically, the diffusion molecules move from regions of higher concentration to regions of lower concentration which are known as concentration gradients. Convection is a mechanism of transport that arises from the bulk motion of fluids (advection). The motion of fluids could result from the application of shear stresses and pressure differences. Shear stresses which are caused by applying forces tangent to a surface lead to relative movement of two contiguous parts of the

material. Pressure which is a compressive normal stress could also cause the motion of the fluid. Both of diffusion and convection influence transport of energy, momentum and mass in biological systems.

The flux is defined as the amount of the quantity passing through a unit area per unit time in a given direction. Fluxes are vectors which have a magnitude and direction. There is a general relation describing energy, mass and momentum transport which was shown below:

$$\begin{pmatrix}\text{Flux of quantity}\\ \text{being transported}\end{pmatrix} \propto -\begin{pmatrix}\text{gradient of quantity}\\ \text{being transported}\end{pmatrix} \qquad \text{equation 3.3.1}$$

3.3.2 *Conservation Relations*

A control volume is a convenient region of space which is used for examining the flow of mass, momentum, and energy. The analysis and solution of a problem is made easier by using a control volume. The size of the control volume could be fixed or change with time and the location of the control volume could be fixed or move with some arbitrary velocity. In general, the control volume has a volume $V(t)$ and a surface $S(t)$[217].

The equation of conservation of mass(equation 3.3.2) was developed and it involved the concentration of the component under study and the reaction rate and the rate of transport. Equation 3.3.2 can be stated in a differential or integral form as well.

$$\begin{bmatrix}\text{Rate of}\\ \text{accumulation}\\ \text{of i in control volume}\end{bmatrix} = \begin{bmatrix}\text{Moles of i}\\ \text{entering}\\ \text{into control volume}\end{bmatrix} - \begin{bmatrix}\text{Moles of i}\\ \text{leaving}\\ \text{control volume}\end{bmatrix}$$

$$+ \begin{bmatrix}\text{Rate of production of i}\\ \text{by chemical reaction}\\ \text{within control volume}\end{bmatrix} \qquad \text{equation 3.3.2}$$

3.3.3 *Boundary Conditions*

There are several boundary conditions used in mass transport analysis. The concentration may be known at the boundary. The flux may be known at the boundary. The concentrations across a boundary may be not continuous. For example, if the boundary is permeable such as a membrane, the boundary condition may be described in the following equation: $N_i = K(\Phi_i C_i/_2 - C_i/_1)$. K is the permeability, N_i is the flux across the boundary. $C_i/_2$ is the concentration of molecule i at one side of the boundary. $C_i/_1$ is the concentration of molecule i at another side of the boundary. Φ_i is the partition coefficient.

3.3.4 *Fick's Law of Diffusion for Dilute Solutions*

Constitutive relations are required to solve the conservation relation(equation3.3.2). Fick's law of diffusion is one of the most commonly used constitutive relations to solve the problem. It was developed by Adolph Fick from experiments and by analogy with Fourier's law of heat conduction in 1855. Fick's first law of diffusion is valid for dilute solutions and it relates the diffusive flux J_{ix} to the concentration gradient and the

diffusion coefficient under steady state. The net solution diffusion proceeds from a region of higher concentration to a region of lower concentration with a negative sign and a magnitude that is proportional to the concentration gradient(equation 3.3.3).

$$J_{ix} = -D_{ij}\frac{dC_i}{dx} \qquad \text{equation 3.3.3}$$

where D_{ij} is the binary diffusion coefficient of the solute *i* in the solvent *j*(m^2/s). J is the diffusion flux ($\frac{mol}{m^2 \cdot s}$). C_i is concentration in the x direction ($\frac{mol}{m^3}$). *x* is length in the x direction (m). The drive force in one dimention is $\frac{dC_i}{dx}$.

Fick's second law is valid for dilute binary solution under non-steady-state diffusion without chemical reactions occurring. A material balance on component i entering a control volume (from *x* to *x*+Δ*x*) yields:

$$\frac{\partial C_i}{\partial t} = D_{ij}\frac{\partial^2 C_i}{\partial x^2} \qquad \text{equation 3.3.4}$$

3.3.5 *Steady-State Diffusion Across Membranes*

Membrane has different selectivity towards different molecules. Consider a steady-state transport across a membrane of thickness L(as shown in Figure 3.1). Suppose

at *x*=0, $C_m = \Phi C_0$; at *x*=L, $C_m = \Phi C_L$,,

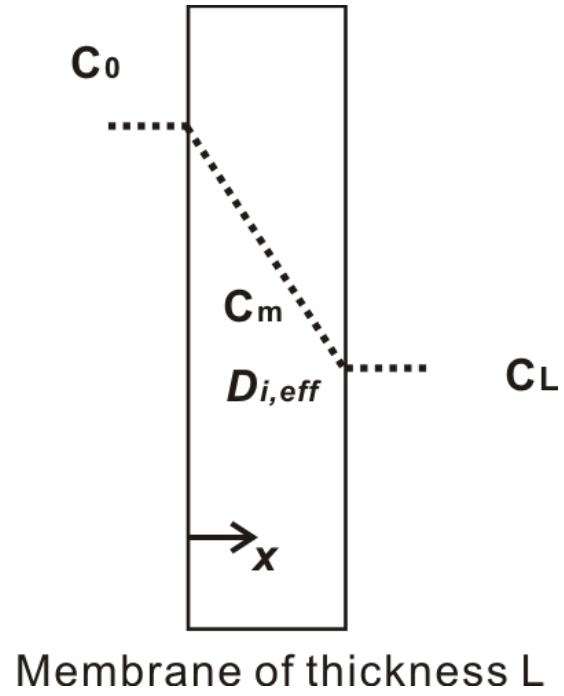

Figure 3.1: Schematic of steady diffusion across a membrane of thickness L that separates two solutions. For this situation, Φ=1.

Based on equation 3.3.4, at steady state, the left side of the equation 3.3.4 is 0. Therefore;

$$0 = D_{i,eff}\frac{d^2C_m}{dx^2} \qquad \text{equation 3.3.5}$$

The solution of equation 3.3.5 is $C_m = Ax + B$

by applying the boundary condition $\begin{cases} x = 0, C_m = \Phi C_0 \\ x = L, C_m = \Phi C_L \end{cases}$,

$$A = -\frac{\Phi(C_0 - C_L)}{L}, C_m = \Phi C_0 - \Phi(C_0 - C_L)\frac{x}{L}$$

So $J_{ix} = -D_{i,eff}\frac{dC_m}{dx} = \frac{D_{i,eff}\Phi}{L}(C_0 - C_L)$ equation 3.3.6

Based on equation 3.3.6, the membrane transport flux is related to the partition coefficient. When Φ<1, it means the surface concentration in the membrane is less than the concentration in the bulk fluid. It was assumed Φ=1 for the convenience of the calculation involved in this chapter. The product $\frac{D_{i,eff}\Phi}{L}$ is referred to as the permeability of the membrane. Obviously, the permeability depends on the thickness of the membrane and diffusion molecules of the molecules and the partition coefficient. It is not an intrinsic property of the membrane. The membrane could have different permeability towards different molecules.

3.4 Experimental Section

3.4.1 *Reagents and Chemicals*

PDMS was made using Sylgard 184 silicone elastomer kit (Dow Corning, Midland, MI). Nuclease free water (Integrated DNA technologies, Coralville, IA) was used to prepare all buffers and sample solutions. Fluorescein was purchased from ACROS organics (New Jersey, USA). FAM labeled ssDNA sequences (10 nt: 5'FAM-AGC AGC ACA G and 80 nt: 5'FAM-AGC AGC ACA GAG GTC AGA TGG GAA GCC CGC TGT GAC ATC TGG AGC CGG TTC CCG GAG CCA CCT ATG CGT GCT ACC GTG AA) were synthesized by Integrated DNA technologies (Coralville, IA). Buffers consisted of 2mM NaH_2PO_4,, 300μM Triton X-100 with various concentrations of NaCl (0, 5mM, 10mM, 30mM, 50mM, 100mM, 200mM), adjusted to pH 7.3 using 100mM NaOH (Mallinckrodt, Paris, KY). Fluorescein and ssDNA solutions were all diluted to 1

μM using in these buffers. All buffer and sample solutions were degassed before use. Piranha solution (3:1 H_2SO_4:H_2O_2, Ashland Chemical, Dublin, OH) was used to clean silicon wafers. Diluted HCl was used to reactivate the PDMS surface. SU8-2050 (Microchem Corp., Newton, MA) was used to fabricate the master. All other reagents and chemicals are from Sigma-Aldrich (St. Louis, MO).

3.4.2 *Fabrication*

The fabrication process is described in previous chapter. A two-step soft lithography process was used.[256] An SU8 master was fabricated and multiple PDMS replicas were then cast from this master. The chip geometry was designed using CAD software which was then used to print a transparency film mask. Standard photolithography procedures were used to make the SU8 master. A new silicon wafer was cleaned in piranha solution for 10 min followed by acetone, methanol, isopropanol and deionized water rinses. The negative photoresist SU8 2050 was spin coated on the dried wafer using the manufacture's recommended procedure. The film mask was used to expose the photoresist in a MABA6 aligner (Karl Suss, Munich, Germany). Developing in propylene glycol monomethyl ether acetate (P.M. Acetate) for 6 min yielded a master with the desired geometry. The master was pre-treated with fluorinated silanes (UCT, Bristol, PA). Degassed PDMS prepolymer (10:1 ratio) was then poured onto the master and baked at 70℃ for 3 hours. The cured PDMS was removed from the master. A second PDMS layer was made using the same process. The resulting channels were 250 μm wide and 110 μm deep. The total channel length was 14.8cm with an active length where the channels overlapped of 12.8 cm. Inlet and outlet holes were punched into one PDMS

layer using a piece of 20 gage stainless steel tubing (McMaster-Carr, Chicago, IL). Both PDMS layers were sonicated in dilute HCl for 10 minutes to reactivate prior to bonding[257]. A 10mm×15mm×6μm polycarbonate membrane with 50nm pore diameter (Sterlitech Corp., Kent, WA) was placed on one layer of PDMS over the transport area of the channel. The PDMS layers were O_2 plasma treated at 600 mTorr and 75 W for 10 s. The two layers were then quickly aligned and bonded irreversibly. The entire assembly was placed on a hotplate at 70 ℃ for 1 hour to complete the bonding process. Two glass substrates were used to support the device and four screws on the corners of the substrates were finger tightened to seal the membrane and the PDMS slabs (see Figure 3.2). 0.5" long pieces of stainless steel tubing with the same inner and outside diameter as a 21 gage needle (New England Small Tube Corp., Litchfield, NH) were inserted into in the inlet and outlet holes of the device allowing connections to be made with Tygon tubing (0.03 ID, 0.09 OD, Small parts, Inc, Miramar, FL). Buffer was pumped into the device using a syringe pump (Harvard Apparatus, Holliston, Massachusetts).

3.4.3 *Size Discrimination of the Membrane*

Buffer solution (2mM NaH_2PO_4, 300μM Triton X-100, 50mM NaCl) and 1μM fluorescein or fluorescently labeled DNA, dissolved in the same buffer, were simultaneously pumped into inlets #1 and #2 (see Figure 3.2) generating counter current flow in the device. The flow rate was varied from 0.05 ml/hr to 1 ml/hr, corresponding to linear velocities ranging from 0.51 mm/s to 10.1 mm/s. Approximately 10 channel volumes of solution were pumped through the device before data was recorded to ensure stability of the signal. 20 ul solution was collected from outlet #1 (see Figure 3.2) to

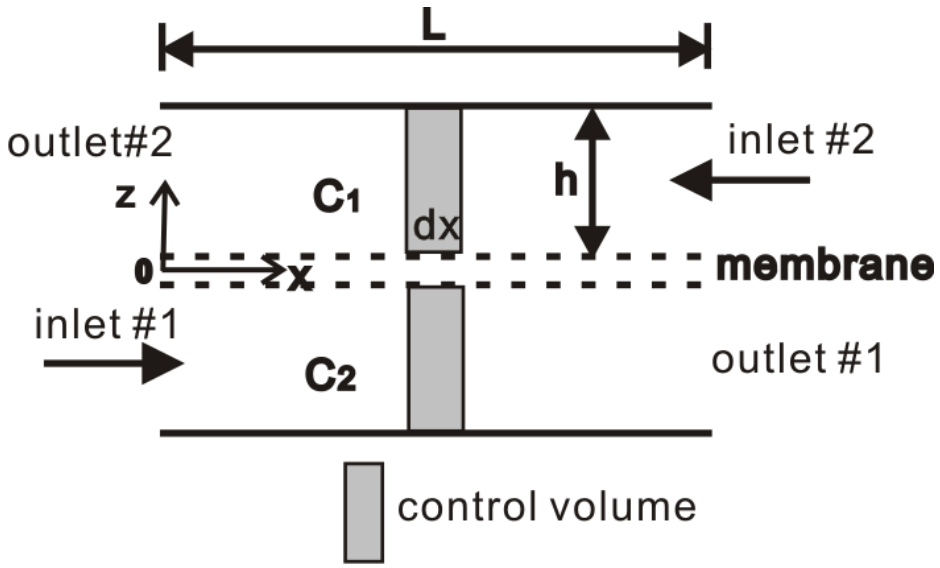

Figure 3.2: Schematic of the model. L is the length of the channel, h is the height of the channel.C_1 is the sample concentration in the dialysis channel. C_2 is the sample concentration in the perfusion channel. At x=0, C_2=0. At x=L, C_1=1 μM.

determine the amount of fluorescent analyte that crossed the membrane. This was compared with the intensity of the fluorescent solution pumped into the device (at inlet #2). All fluorescence measurements were made using a Synergy2 plate reader (BioTek Instruments, Winooski, VT) with λ_{ex}=485nm and λ_{em}=528nm. Analyte recovery (R) was determined according to:

$$R = \frac{I_{outlet}}{I_{inlet}} \qquad \text{equation 3.4.1}$$

where I_{outlet} is the fluorescence intensity of the solution exiting outlet #1 and I_{inlet} is the fluorescence intensity of the solution entering the device at inlet #2.

3.5 Model and Discussion

3.5.1 *Model 1*

The following equations were used to calculate the resistance of nanopore and the resistance of the channel[219].

$$R_n = \frac{8\mu h_m}{\pi r^4} \cdot \frac{1}{N_n} \qquad \text{equation 3.5.1}$$

$$R_c = \frac{12\mu L}{wh^3}[1 - \frac{h}{w}(\frac{192}{\pi^5}\sum_{n=1,3,5}^{\infty}\frac{1}{n^5}\tanh(\frac{n\pi w}{2h}))]^{-1} \qquad \text{equation 3.5.2}$$

Where h_m is the thickness of the membrane; r is the radius of the nanopore, μ is the viscosity of the solution, N_n is the number of nanopores in the overlap region of the membrane. w is the width of the channel, h is the depth of the channel, L is the length of the channel. h_m=6μm, r=25nm, h=110μm, w=250μm, L=12.8cm, N_n=192×10^6, so the magnitude of R_n is about 2 orders of magnitude of R_c. It would prefer to flow through the channel instead of the nanopores. Convection through the nanopores can be ignored and diffusion was assumed to be the major mechanism to drive the molecules through the nanopores.

In this model, several assumptions were made including diffusion was the major mechanism to drive the molecules through the membrane, a constant mass transfer coefficient and no concentration gradient in z direction (see Figure 3.2). The model domain is shown in Figure 3.2. The sample molecules were transported by convection in

the channel, whereas diffusion was considered the only transport mechanism to drive the molecules across the membrane.

Based on equation 3.3.2 (the conservation of mass equation), equation 3.5.3 was derived for top channel:

$$\frac{d}{dt}[hdxC_1] = (vC_1/_{x+dx} - vC_1/_x)h - dxK(C_1 - C_2) \qquad \text{equation 3.5.3}$$

Divide equation 3.5.3 by dx and let $dx \to 0$

$$h\frac{d}{dt}(C_1) = vh\frac{dC_1}{dx} - K(C_1 - C_2) \qquad \text{equation 3.5.4}$$

Because it's under stable state, the left side of equation 3.5.4 is equal to zero,

$$\frac{dC_1}{dx} = \frac{K}{vh}(C_1 - C_2)$$

Similarly, the following equation was derived for the bottom channel,

$$-h\frac{d}{dt}(C_2) = vh\frac{dC_2}{dx} - K(C_1 - C_2) \qquad \text{equation 3.5.5}$$

Under stable condition, the left side of equation 3.5.5 is equal to zero,

$$\frac{dC_2}{dx} = \frac{K}{vh}(C_1 - C_2)$$

In a summary, the following mass transport equations (equation 3.5.6) were formulated to describe the device.

$$\begin{cases} \dfrac{dC_1}{dt} = v\dfrac{dC_1}{dx} - \dfrac{K}{h}(C_1 - C_2) \\ \dfrac{dC_2}{dt} = -v\dfrac{dC_2}{dx} + \dfrac{K}{h}(C_1 - C_2) \end{cases}$$ equation 3.5.6

where C_1 is the sample concentration in the dialysis channel; C_2 is the sample concentration in the perfusion channel; K was the mass transfer coefficient; v was the average linear velocity in the channel; h was the height of the channel; L was the length of the channel; W was the width of the channel. The partition coefficient was assumed to be 1. R was recovery. When recovery was zero, no analyte was transported through the membrane. When recovery was one, all of the molecules were transported through the membrane.

The boundary condition is:

$$\begin{cases} C_1(x = L) = C_0, \ when \ x = L \\ C_2(x = 0) = 0, \ when \ x = 0 \end{cases}$$ equation 3.5.7

where C_0 is the initial concentration in the inlet of the dialysate channel.

Recovery was obtained by solving equation 3.5.6 and 3.5.7 at steady state.

Under steady state, the left side of the equation 3.5.6 is equal to zero, therefore

$$\begin{cases} v\dfrac{dC_1}{dx} = \dfrac{K}{h}(C_1 - C_2) \\ v\dfrac{dC_2}{dx} = \dfrac{K}{h}(C_1 - C_2) \end{cases} \Rightarrow \frac{dC_1}{dx} = \frac{dC_2}{dx} \Rightarrow \frac{dC_1 - dC_2}{x} = 0 \Rightarrow C_1 - C_2 = H$$

where H is constant.

So that

$$\begin{cases} \dfrac{dC_1}{dx} = \dfrac{K \cdot H}{h \cdot v} \Rightarrow C_1 = C_1(x=0) + \dfrac{K \cdot H}{h \cdot v} x \\ \dfrac{dC_2}{dx} = \dfrac{K \cdot H}{h \cdot v} \Rightarrow C_2 = C_2(x=0) + \dfrac{K \cdot H}{h \cdot v} x = 0 + \dfrac{K \cdot H}{h \cdot v} x = \dfrac{K \cdot H}{h \cdot v} x \end{cases}$$

Since $C_1 - C_2 = H$, $C_1(x=0) = C_2(x=0) + H = H \Rightarrow C_1 = H + \dfrac{K \cdot H}{h \cdot v} x = H(1 + \dfrac{K}{h \cdot v} x)$

$$C_1(x=L) = C_0 \Rightarrow C_1(x=L) = H(1 + \frac{K}{h \cdot v} L) = C_0 \Rightarrow H = \frac{C_0}{1 + \dfrac{K}{h \cdot v}}$$

Therefore: $R = \dfrac{C_2(x=L)}{C_1(x=L)} = \dfrac{\dfrac{KHL}{h \cdot v}}{H(1 + \dfrac{KL}{h \cdot v})} = \dfrac{KL}{vh + KL} = \dfrac{1}{\dfrac{Q}{KLW} + 1}$ equation 3.5.8

Thus the recovery is a function of value of how fast the molecules diffuse through the membrane (determined by *KLW)* versus how long the solution stays in the channel (determined by flow rate Q).

The mass transfer rate of a molecule through the membrane can be expressed in equations of the surface area, the concentration difference and the overall mass transfer coefficient. The overall mass transfer coefficient is usually determined experimentally[294]. The mass transfer coefficient *K* was obtained by linearly fitting the experiment data to the following equation in Model 1.

$$\frac{1}{R}-1=\frac{1}{K}\cdot\frac{Q}{LW} \qquad \text{equation 3.5.9}$$

The data ($\frac{1}{R}-1$) can be plotted as a function of $\frac{Q}{LW}$ with the slope of the line being $\frac{1}{K}$.

3.5.2 *Compare between Model 1 and Experiment Data*

By obtaining the data of recovery from the experiment and plotting ($\frac{1}{R}-1$) as a function of $\frac{Q}{LW}$, the mass transfer coefficient (*K*) was determined. For example, the overall mass transfer coefficient (*K*) for 10 nt DNA was determined to be 6.9×10^{-4}mm/s using Figure 3.3 (2A). This value for *K* was used to calculate the theoretical recovery across a range of flow rates as shown in Figure 3.3(2B). Overall this strategy was successful in describing the trends observed in recovery, validating the assumptions made in developing this model.

Similarly, the mass transfer coefficients (*K)* were estimated to be 1.92×10^{-3} mm/s and 2.73×10^{-4} mm/s for fluorescein and 80nt ssDNA, respectively. The back fitting theoretical results are shown in Figures 3.3(1B) and 3. 3(3B). For fluorescein, the model data fits the experiment data well for most flow rates. Although the model predicted the recovery trend for 80nt DNA, more deviation from the experimental data was observed. In general our model was more successful in predicting recovery for smaller molecules such as fluorescein and 10 nt ssDNA than larger molecules such as 80nt ssDNA. There are two possible contributors to this phenomenon. The first relates to the boundary layer. As analytes cross the membrane a concentration gradient can be generated across the

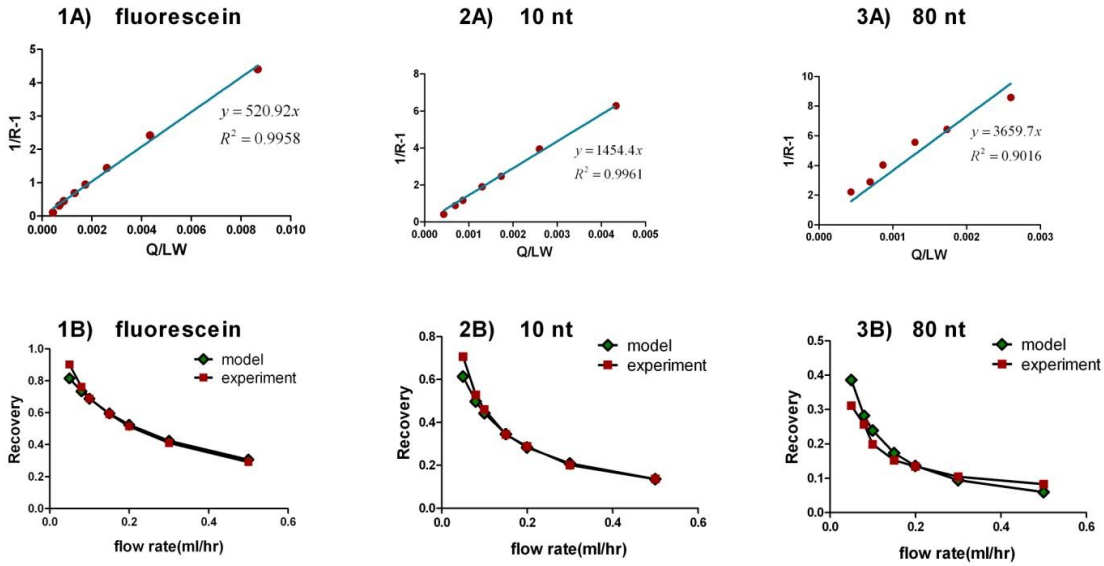

Figure 3.3: Top: Plot of (1/R-1) as a function of *Q/LW* for fluorescein(1A), 10nt DNA (2A) and 80nt DNA(3A). The slope of each curve is 1/*K*. Bottom: Plot of recovery vs. flow rate for fluorescein(1B), 10 nt DNA(2B) and 80nt DNA(3B) comparing experimental data (squares) vs. values predicted by the model(diamonds).

depth of the channel. Model 1 assumes constant concentration across the depth of the channels and does not account for this gradient. Molecules with higher diffusion constants equilibrate more quickly across the channel depth, decreasing the magnitude of this effect. Convection within the pores is a second potential contributor to the observed deviations. This model assumes that diffusion is the only mechanism that contributes to transport across the membrane. However, a consequence of the counter current flow used in our device is a pressure difference across the membrane, which would be expected to generate a small convective flow. For small molecules this convective flow is small in comparison to diffusion and little deviation from the model is observed. For larger molecules, convection plays a more significant role in transport through the nanopores, leading to larger deviations from the model. The Sherwood number can be used to represent the ratio of convective mass transport to diffusive mass transport. For 80nt

ssDNA, $Sh = \frac{K \cdot h_m}{D} = 0.0237 = \frac{convective\ mass\ transport}{diffusive\ mass\ transport}$, which demonstrated the relative importance of diffusive transport to convective transport through the nanopores for 80nt ssDNA. Similarly, *Sh*=0.0192 for fluorescein and *Sh*=0.0197 for 10nt ssDNA, which proved diffusion was more important to transport fluorescein, 10nt ssDNA and 80nt ssDNA through the nanopores. By comparing the Sherwood number for three samples, convective played a more significant role to transport 80nt ssDNA across the membrane. In Model 2, the boundary layer will be considered to extend the model to predict recovery for larger molecules or faster flow rates. This model demonstrated that diffusion was the major mechanism of transport for the molecules and flow rates studied here, confirming the utility of our simplified model under these conditions.

3.5.3 *Model 2*

Let's compare the diffusion time across the cross section of the channel (τ_c) and the diffusion time across the membrane (τ_m) to see whether it is necessary to consider the boundary layer into the model. Graphical notation was demonstrated in Figure 3.4. τ_c and τ_m were calculated using the following equation (equation 3.5.10).

$$\frac{\tau_m}{\tau_c} = \frac{\frac{h_m^2}{D_m}}{\frac{h^2}{D_c}} = \frac{h_m^2 D_c}{h^2 D_m} = \frac{h_m}{h} \cdot \frac{D_c}{Kh} \qquad \text{equation 3.5.10}$$

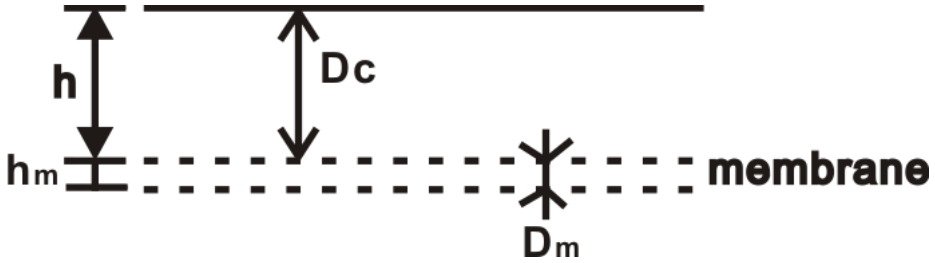

Figure 3.4: Schematic of diffusion time across the channel and diffusion time across the membrane. h_m is the thickness of the membrane; h is the height of the channel; D_C is the diffusion coefficient in the dialysis channel; D_m is the diffusion coefficient across the membrane.

Where h_m is the thickness of the membrane, h_m is the height of the channel, D_c is the diffusion coefficient in the channel, D_m is the diffusion coefficient across the membrane, K is the mass transfer coefficient which is equal to $\frac{\Phi D_m}{h_m}$. Assuming the partition coefficient Φ=1, $K = \frac{D_m}{h_m}$.

Table 3.1: Parameters of 80 nt ssDNA, 10 nt ssDNA and fluorescein to calculate τ_m / τ_c. h_m is the thickness of the membrane, h is the height of the channel. D_C is the diffusion coefficient in the dialysis channel. K is the mass transfer coefficient obtained from model 1.

Analyte	h_m (μm)	h (μm)	D_c (cm^2/s)	K (mm/s)	$\frac{\tau_m}{\tau_c}$
80 nt ssDNA	6	110	6.9×10^{-7} [233]	2.73×10^{-4}	0.125
10 nt ssDNA	6	110	2.1×10^{-6} [233]	6.9×10^{-4}	0.151
fluorescein	6	110	6×10^{-6} [314]	1.92×10^{-3}	0.155

The above parameters for 80 nt ssDNA, 10 nt ssDNA and fluorescein are listed in Table 3.1, $\frac{\tau_m}{\tau_c}$ value was 0.125 for 80 nt ssDNA, 0.151 for 10nt ssDNA and 0.155 for fluorescein. It demonstrated the diffusion across the channel was much slower than diffusion across the membrane which meant diffusion across the channel would influence

the transport process across the membrane. Boundary layer is needed to be considered. Therefore, we built another model which considered the concentration gradient in the z direction (see Figure 3.5). Though, in this model (Model 2), it still assumed diffusion was the major mechanism to drive the molecules through the membrane and ignored the convection transport through the membrane. The model domain is shown in Figure 3.5.

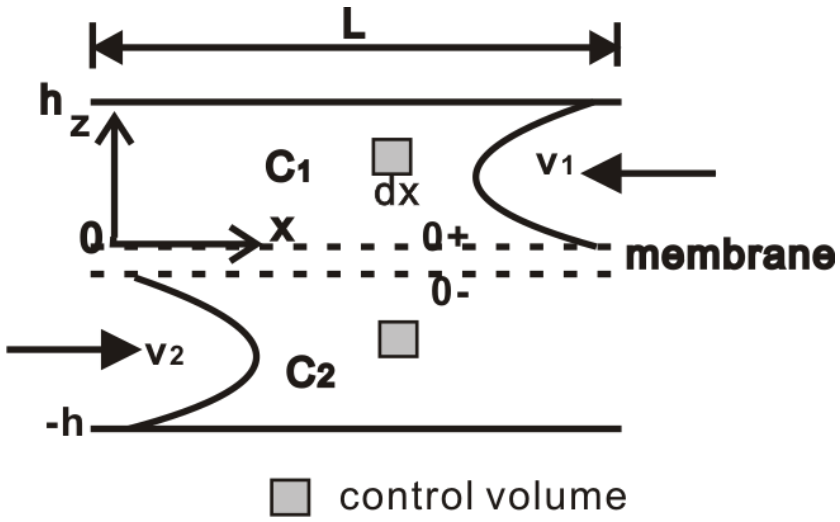

Figure 3.5: Schematic of the model 2. *h* is the height of the channel.C_1 is the sample concentration in the dialysis channel. C_2 is the sample concentration in the perfusion channel. At x=0. C_2=0. At x=L. C_1=1 uM.

The following equations (equation 3.5.11) were derived to describe the condition of the device.

$$\begin{cases} \dfrac{\partial C_1}{\partial t} = v_1 \dfrac{\partial C_1}{\partial x} + D_c \dfrac{\partial^2 C_1}{\partial z^2}, 0 < z < h \\ \dfrac{\partial C_2}{\partial t} = -v_2 \dfrac{\partial C_2}{\partial x} + D_c \dfrac{\partial^2 C_2}{\partial z^2}, -h < z < 0 \end{cases} \qquad \text{equation 3.5.11}$$

The initial condition was:

t=0, $C_1(x=L)$=1.0uM, $C_2(x=0)$=0

The boundary condition was:

$$\begin{cases} \dfrac{\partial C_1}{\partial z} = 0, \ \ when \ z = h \\ \dfrac{\partial C_2}{\partial z} = 0, \ \ when \ z = -h \\ -D_c \dfrac{\partial C_1}{\partial z} /_{z=0^+} = -K[C_1(0^+) - C_2(0^-)] \\ -D_c \dfrac{\partial C_2}{\partial z} /_{z=0^-} = K[C_1(0^+) - C_2(0^-)] \end{cases}$$

equation 3.5.12

The flow profile inside of the channel was parabolic[197, 315]. The following expression was used to describe the velocity in the channel.

$$\begin{cases} v_1 = \dfrac{3Q}{2Wh}(1 - \dfrac{4(z - \frac{h}{2})^2}{h^2}) \\ v_2 = \dfrac{3Q}{2Wh}(1 - \dfrac{4(z + \frac{h}{2})^2}{h^2}) \end{cases}$$

where C_1 was the concentration in the top channel(0<z<h); C_2 was the concentration in the top channel(-h<z<0); D_c was the diffusion coefficient in the channel, K was the mass transfer coefficient; the partition coefficient was assumed to be one. W was the width of the channel.

By assuming $C_1 = X \cdot Z$, where X is a function of x, Z is a function of z,

$$\frac{\partial C_1}{\partial x} = Z\frac{dX}{dx}, \frac{\partial C_1}{\partial z} = X\frac{dZ}{dz}, \frac{\partial^2 C_1}{\partial z} = X\frac{d^2 Z}{dz^2}$$

Under steady state, the left side of equation 3.5.11 was zero,

$$v_1(z)\cdot Z\frac{dX}{dx} + D_c \cdot X\frac{d^2 Z}{dz^2} = 0 \Rightarrow \frac{\frac{dX}{dx}}{X} = -\frac{D_c\frac{d^2 Z}{dz^2}}{v_1(z)\cdot z} = \lambda$$

$$\begin{cases} \dfrac{\frac{dX}{dx}}{X} = \lambda \Rightarrow X = Ae^{\lambda x} \\ -\dfrac{D_c\frac{d^2 Z}{dz^2}}{v_1(z)\cdot z} = \lambda \Rightarrow \dfrac{d^2 Z}{dz^2} = -\dfrac{-\lambda v_1(z)Z}{D_c} = -\dfrac{3\lambda Q}{2D_c Wh}\left(1-\dfrac{4(z-\frac{h}{2})^2}{h^2}\right)Z \\ \qquad = -\dfrac{3\lambda Q}{2D_c Wh}\left(-\dfrac{4}{h^2}z^2 + \dfrac{4}{h}z\right)Z = \dfrac{6\lambda Q}{D_c Wh^3}z^2 Z - \dfrac{6\lambda Q}{D_c Wh^2}zZ) \end{cases}$$ equation 3.5.13

However, we cannot solve equation 3.5.13. The analytical solution from equation 3.5.13 was not obtained. A finite element method modeling software COMSOL was used to obtain the numerical solution for equation 3.5.11.

3.5.4 *Model 2- COMSOL Modeling*

Two separate domains are formulated in this model: the dialysate and the permeate. The model domain appears in Figure 3.6. The molecule is transported by diffusion between two domains.(dialysate and permeate domain) The following mass transport equations can be formulated to describe the system.

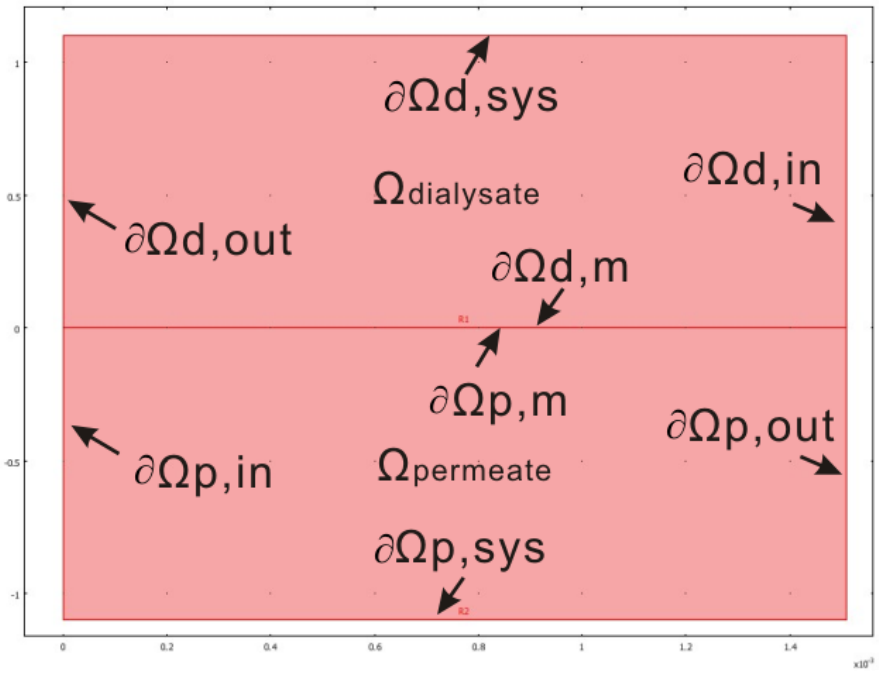

Figure 3.6: Diagram of the device and boundaries for the modeled system. Two domains are formulated in the model (dialysate domain and permeate domain). There is a membrane between two domains. $\partial\Omega$ denotes the boundary.

$$\nabla \cdot (-D_c \nabla C_1 + C_1 v_1) = 0 \qquad in \quad \Omega_{dialysate}$$

$$\nabla \cdot (-D_c \nabla C_2 + C_2 v_2) = 0 \qquad in \quad \Omega_{permeate}$$

Where C_1 denotes the concentration in the dialysate domain (top channel); C_2 denotes the concentration in the permeate domain (bottom channel); D_c is the diffusion coefficient in the channel; v_1 is the velocity in the dialysate channel; v_2 is the velocity in the dialysate channel.

The boundary condition are defined below according to 3.5.12 (Figure 3.6).

At the inlet to the modeled domain, the concentration conditions are defined as:

$$C_1 = C_0, at\ \partial\Omega_{d,in}$$
$$C_2 = 0, at\ \partial\Omega_{p,in}$$

No flux is across the boundary $\partial\Omega_{d,sys}$, $\partial\Omega_{p,sys}$.

At the outlet, convective is assumed to contribute to the mass transport.

$$J = C_1 v_1, at\ \partial\Omega_{d,out}$$
$$J = C_2 v_2, at\ \partial\Omega_{p,out}$$

Between two domains, assuming the partition coefficient is equal to one, the boundary condition is:

$$J = K(C_2 - C_1), at\ \partial\Omega_{d,m}$$
$$J = K(C_1 - C_2), at\ \partial\Omega_{p,m}$$

Take 80nt ssDNA for example, the parameters used in COMSOL are listed in the following table (Table 3.2). D_c and K for 10nt ssDNA and fluorescein are listed in Table 3.1. The other parameters are the same for all of the three samples.

Table 3.2: Parameters used in the COMSOL model for 80nt ssDNA.

Property	Value	Description
D_c	6.95×10^{-11} [m^2/s]	Diffusion Coefficient, channel
Q	0.05×10^{-6}/3600[m^3/s]	Volumetric Flow Rate
W	250×10^{-6} [m]	Channel Width
H	110×10^{-6} [m]	Channel Depth
h_m	6×10^{-6} [m]	Membrane Depth
C_0	1×10^{-6} [mol/liter]	Inlet Concentration, dialysate
K	2.73×10^{-7} [m/s]	Mass Transfer Coefficient

The total amount of C_2 is calculated by integrating C_2 along the boundary $\partial\Omega_{p,out}$. The total amount of C_1 is calculated by integrating C_1 along the boundary $\partial\Omega_{d,in}$.

Recovery is calculated by the following equation (equation 3.5.14).

$$R = \frac{\int_{\partial\Omega_{p,out}} C_2}{C_0 \cdot h_m}$$ equation 3.5.14

The surface plot (Figure 3.7(A)) from COMSOL visualized the concentration distribution throughout the two domains: the dialysate domain is on the top and the permeate is on the bottom. The contour plot (Figure 3.7(B)) visualized the same concentration distribution in the two domains. As the plots demonstrates (Figure 3.7), the concentration in the dialysate domain decreased along the direction of x and the concentration was not constant along the z direction. The figures shows the concentrations on the two sides of the membrane are different. There is diffusion layers resulting from the concentration gradients on both sides of the membrane. And the concentration jumps at the boundary of the membrane.

Similarly, the surface plots for 10nt ssDNA(Figure 3.8 (A)) and for fluorescein (Figure 3.8 (B)) are obtained using the same modeling method as 80nt ssDNA (Figure 3.7(A)). Compared with Figure 3.7(A), it was significant to see the concentration along the *x* direction drops more quickly for 10nt ssDNA and fluorescein. More 10nt ssDNA and fluorescein are transported through the membrane into the permeate domain. 80nt ssDNA is the biggest molecule among the three samples. It has the smallest diffusion coefficient (Table 3.1). 10nt ssDNA and fluorescein diffuse faster than 80nt ssDNA so that the effect of Taylor dispersion was compromised by diffusion to some extent. The contour in Figure 3.7(B) was more parabolic compared with the contour of 10nt ssDNA(Figure 3.9(A)) and fluorescein(Figure 3.9(B)).

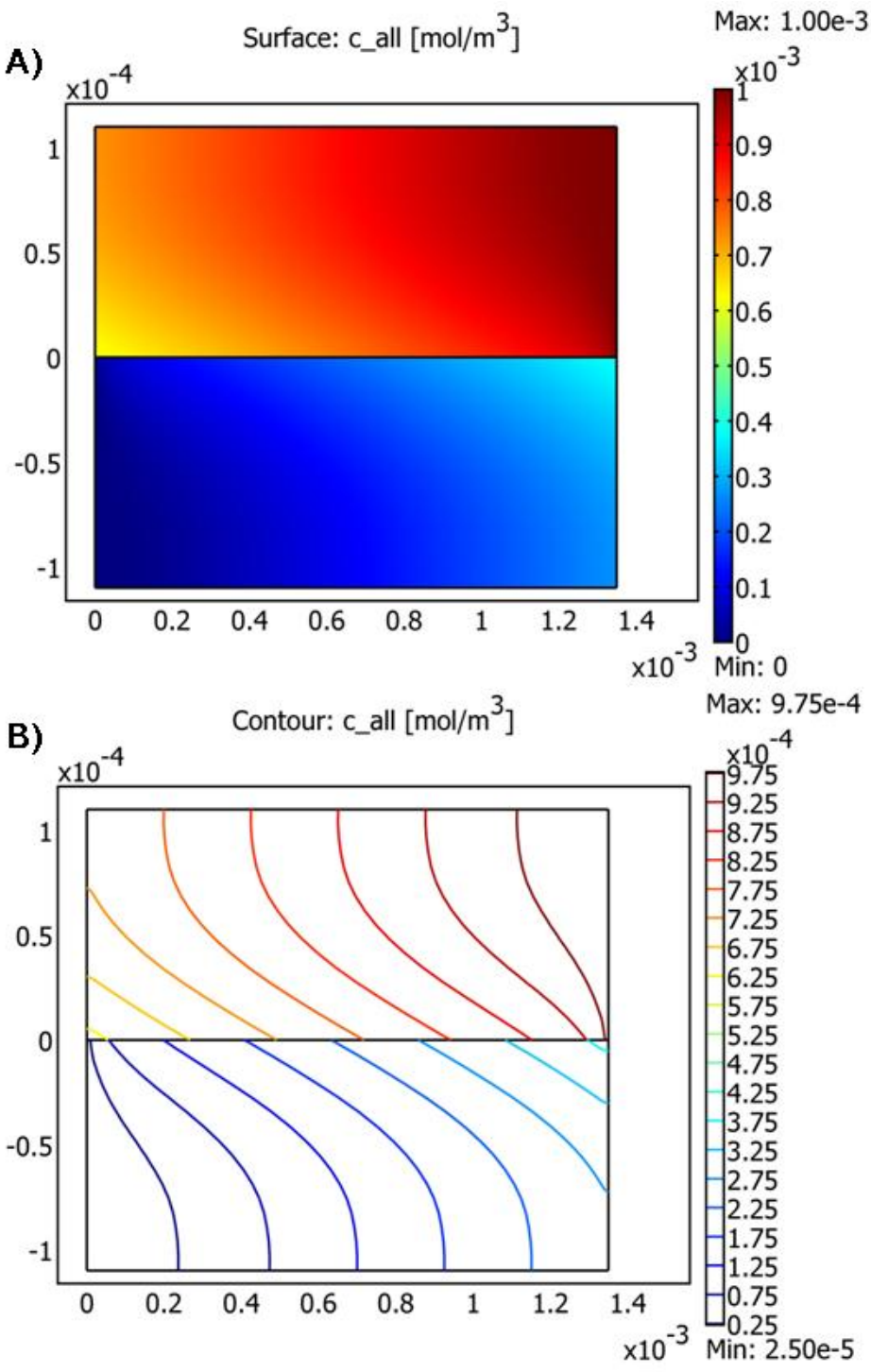

Figure 3.7:A) Surface plot of concentration B) Contour plot of concentration for 80nt ssDNA at 0.05ml/hr flow rate. It visualizes the surface concentration distribution(A) and the contour concentration distribution (B) in the two domains. Top: dialysate domain. Bottom: permeate domain. The flow direction in the dialysate domain is from right to left while the flow direction in the permeate domain is from right to left. Buffer consists of 2mM NaH_2PO_4, 300 µM Triton X-100, 50mM NaCl.

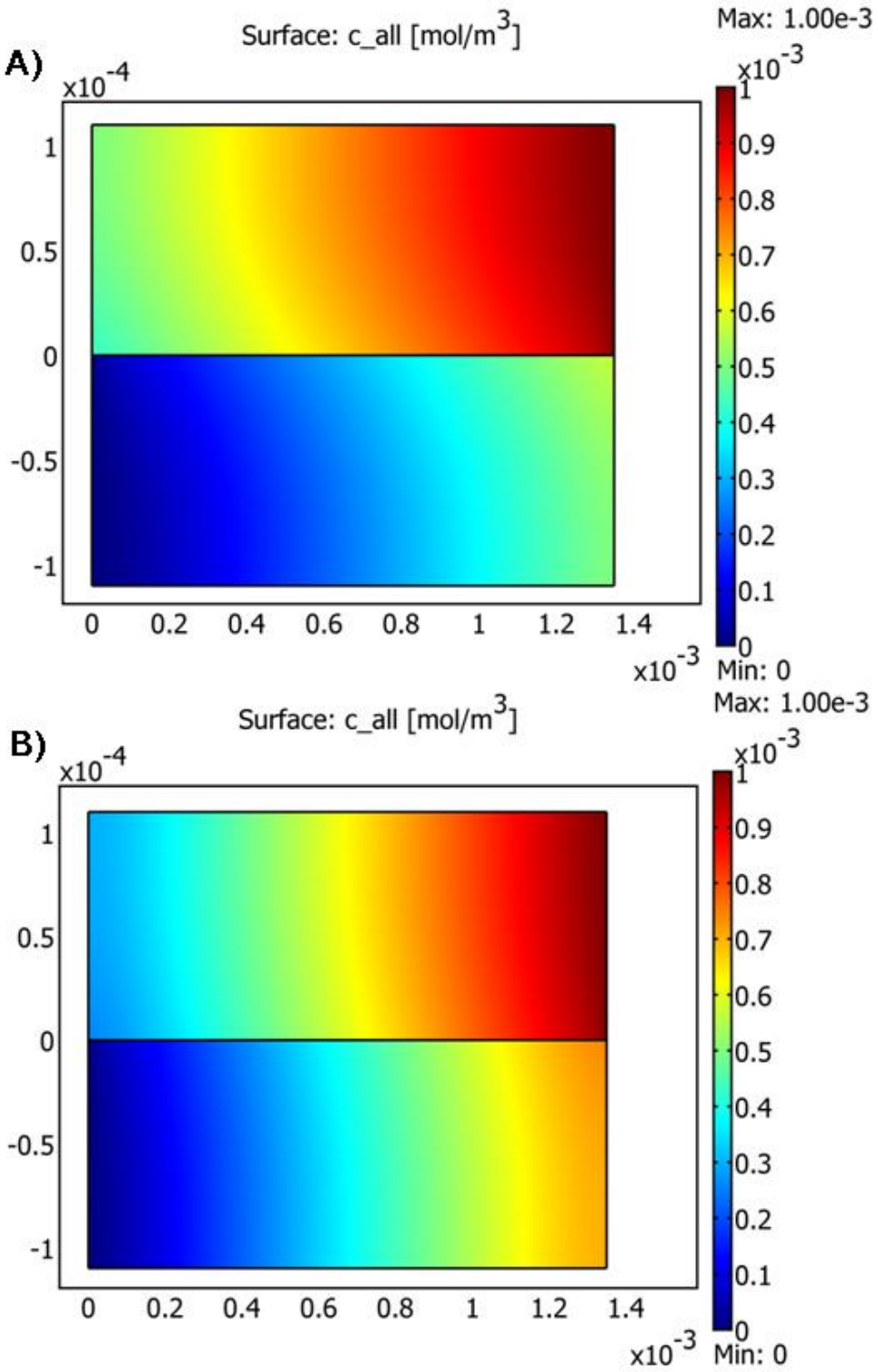

Figure 3.8: Surface plot of concentration for 10nt ssDNA(A) and fluorescein(B) at 0.05ml/hr flow rate. It visualizes the concentration distribution in the two domains. Top: dialysate domain. Bottom: permeate domain. The flow direction in the dialysate domain is from right to left while the flow direction in the permeate domain is from right to left. Buffer consists of 2 mM NaH_2PO_4, 300 μM Triton X-100, 50 mM NaCl.

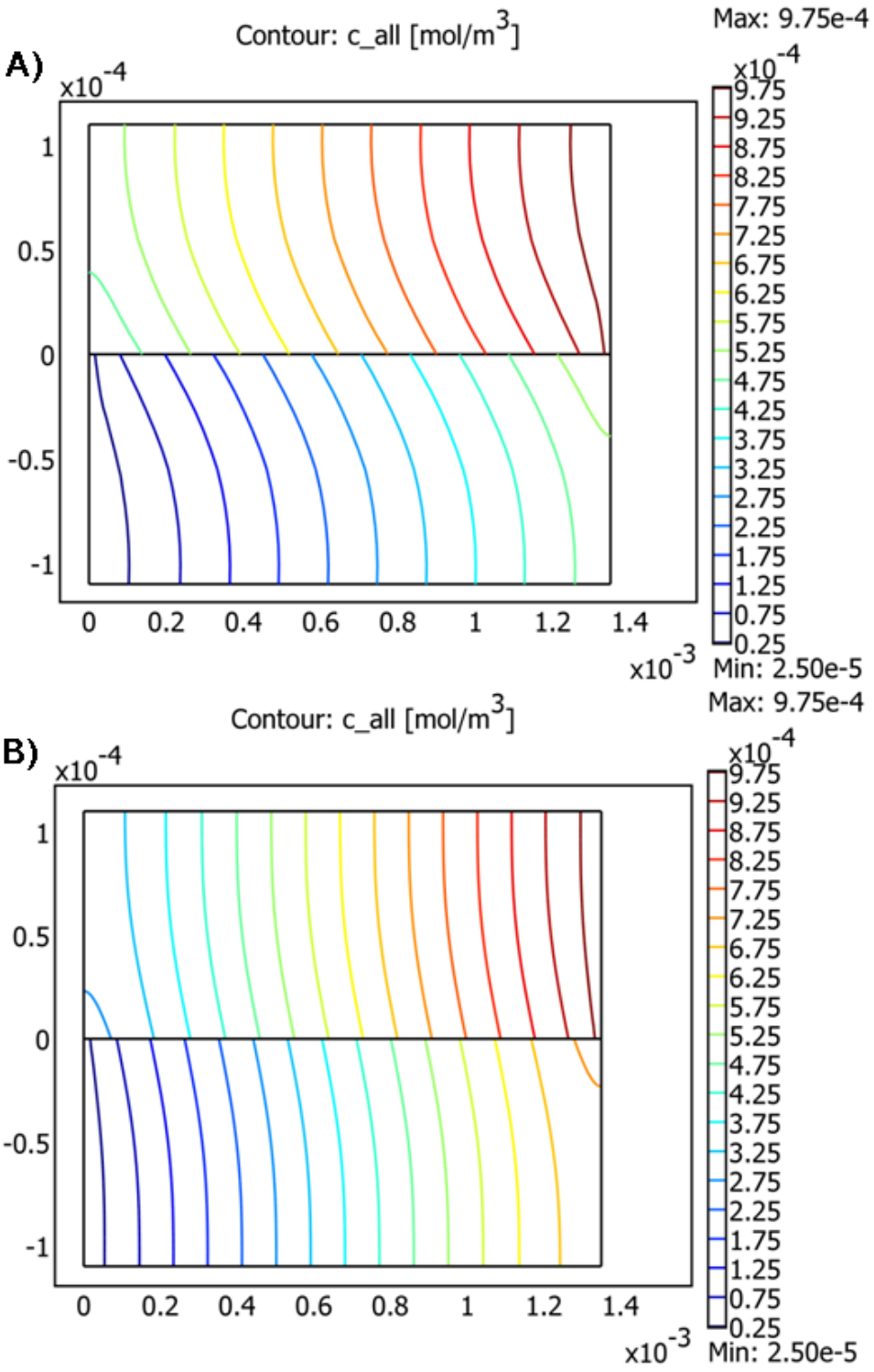

Figure 3.9: Concentration Contour plot for 10nt ssDNA(A) and fluorescein(B) at 0.05ml/hr flow rate. It visualizes the concentration contour distribution in the two domains. Top: dialysate domain. Bottom: permeate domain. The flow direction in the dialysate domain is from right to left while the flow direction in the permeate domain is from right to left. Buffer consists of 2 mM NaH_2PO_4, 300 μM Triton X-100, 50 mM NaCl.

3.5.5 *Compare between Model 2 and Experiment Data*

By setting different flow rates (1.0ml/hr, 0.5ml/hr, 0.3ml/hr, 0.1ml/hr, 0.08ml/hr and 0.05ml/hr) in COMSOL, the corresponding recovery can be calculated according to equation 3.5.14. The results are shown in Figure 3.10. Each plot has two data sets. The green-triangle data is calculated from Model 2 while the red-square data is from the experiment. The model fits the experiment well for most of the flow rates. Several reasons may contribute to the deviation from the experiment. due to counter flow in the device. The pressure difference resulting from the counter flow in the two channels can cause convection transport through the nanopores. Convection transport through the nanopores may not be ignored. The mass transfer coefficient used in Model 2 was obtained from Model 1 which may be not so right for this model. However diffusion still can be seen as the dominant force to drive the molecules through the membrane.

The formation of a double layer in the pores raises the potential for both coulombic interaction between the charged surface and charged molecules, and increased steric hindrance[220, 240, 269-271]. Increasing the ionic strength of the buffer is expected to reduce

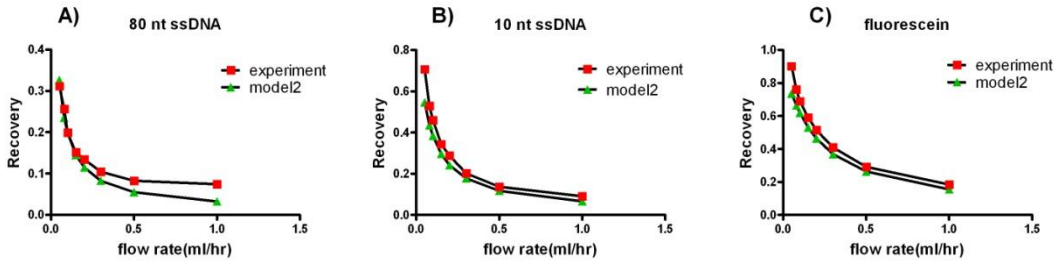

Figure 3.10: Comparisons between recovery calculated from the model and recovery measured from the experiments. A) 80nt ssDNA; B) 10nt ssDNA; C) fluorescein. Buffer consists of 2mM NaH_2PO_4, 300μM Triton X-100, 50mM NaCl. Flow rate was 0.08ml/hr.

the size of the double layer, effectively decreasing the interaction between the charged pore walls and analytes, while increasing the pore size permitting larger molecules to pass through. For example reducing the double layer thickness from 4.67 nm to 0.67 nm increases the cross sectional area of a 50 nm pore by 43%. Beyond affecting the size of the physical barrier of the pore, reducing the Debye length reduces ionic interactions between the analyte and the surface or double layer. Similarly, the radius of gyration of ssDNA decreases as the ionic strength of the buffer increases due to the smaller persistence length of ssDNA[229, 262, 264]. The diffusion coefficient of ssDNA also increases with ionic strength[229, 231].

To some extent, Model 2 can be used to predict how recovery changes as ionic strength of the buffer changes. The diffusion coefficient of the ssDNA increases as ionic strength increases[229, 231]. The recovery obtained from Model 2 changes as ionic strength of the buffer changes. The results are demonstrated in Figure 3.11. The trend of recovery from Model 2 when the ionic strength of the buffer increases is consistent with the trend coming from experiments. The recovery would increase as the ionic strength of the buffer increases. However, the recovery measured from the experiment would increase more

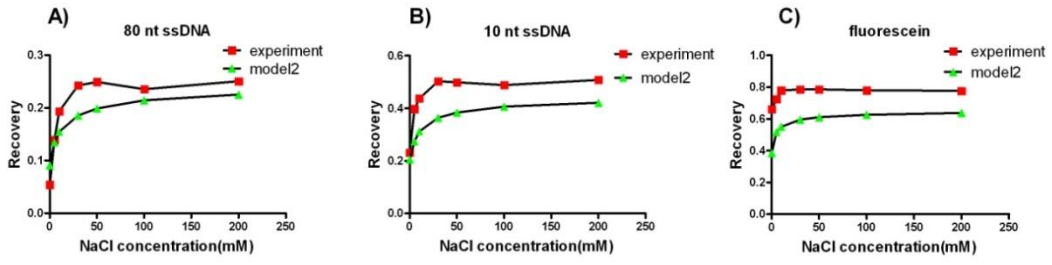

Figure 3.11: Comparisons between recovery calculated from the model and recovery measured from the experiments. A) 80nt ssDNA; B) 10nt ssDNA; C) fluorescein. Buffer consists of 2mM NaH_2PO_4, 300 μM Triton X-100. 0, 5mM, 10mM, 30mM, 50mM, 100mM and 300mM NaCl were added into the buffer to change the ionic strength of the buffer. Flow rate was 0.08ml/hr.

significantly. It may be resulted from other factors that could not be reflected in the model including steric factors, interaction between ions in the solution and surface of the nanopores, the size of the molecules and so on. All of these factors contribute to the increase of the mass transfer coefficient as ionic strength of the buffer changes. A more appropriate model would be built by trying different mass transfer coefficient in the Model 2 and then obtain a best fit between experiment data and Model 2 data. The mass transfer coefficient used in Comsol under that condition would be most accurate in Model2. What's more, another model that integrate convection transport and diffusion transport through the nanopores needs to be developed to describe more realistic condition in the devices.

3.6 Conclusion

We have demonstrated two models which were built based on conservation of mass and constitutive relationships. Diffusion was identified to be the major mechanism to drive molecule through the nanopores. Model 1 assumed there is no concentration gradient along the vertical direction (z) in the channel while Model 2 assumed there existed concentration gradient in the z direction. COMSOL was used to solve Model 2 to obtain numerical solutions. Recovery calculated from the model was compared with recovery measured from the experiments by changing flow rates or by changing the ionic strength of the buffer. Experiments were conducted in a microfluidic device which had two channels with a 50nm polycarbonate membrane sandwiched between them and a counter current flow strategy was adopted to maximize recovery. Trends in recovery measured at various flow rates were consistent with the trends predicted in the two

models which support the premise that diffusion dominated the molecular transport in this device. Recovery increased as the linear velocity decreased. Recovery was also affected by the ionic strength of the buffer suggesting that the thickness and charge of the double layer in the pores play an important role in limiting transport which was demonstrated in Model 2. Increasing the ionic strength of the buffer increased transport across the membrane. Surface plots of concentration for three molecules(fluorescein, 10nt ssDNA and 80nt ssDNA) were demonstrated in this chapter and it visualized the concentration distribution in the two channels. 80nt ssDNA diffused more slowly than 10nt ssDNA or fluorescein. Concentration dropped more slowly along the dialysate channel compared with 10nt ssDNA or fluorescein. The predictive capabilities of models are quite good. However, another model combining convection and diffusion transport through the nanopores is needed to make the model more accurate to predict results.

Chapter 4 Developing a microfluidic device for Single-stranded DNA generation and separation

4.1 Summary

Single-stranded DNA(ssDNA) generation was an important step for SELEX and other biotechnology applications that require ssDNA only. A microfluidic dialysis device for single-stranded DNA generation from double-stranded DNA(dsDNA) is described. The device consists of two polydimethylsiloxane (PDMS) channels separated by a track etched polycarbonate membrane with an 800 nm pore size. Two steps were adopted to generate single-stranded DNA. Streptavidin-coated polystyrene beads were immobilized with dual-biotin labeled dsDNA and alkaline treatment was adopted to denature dsDNA and release the non-biotinylated ssDNA. The whole process happened automatically in the device. The purity and the yield from six different NaOH concentrations and five different flow rates were compared in this paper. 25mM NaOH was found to be the optimum concentration in this device with over 95% purity regardless of what flow rates are used. However, lower flow rates would help to get higher ssDNA yield up to 50% of the initial dsDNA amount. The ssDNA generation process was also time-based. Purity from the chip experiments was even better than the result from an off-chip method when NaOH concentration was higher than 25mM. Capillary Electrophoresis results confirmed ssDNA was the major component in the collected solution.

4.2 Introduction

Single stranded DNA (ssDNA) has broad applications in therapeutics[23, 29, 316-318], diagnositcs[8, 319-322], biosensing[46, 323-328] and sequencing technologies[41, 63, 329, 330]. Unlike double-stranded DNA(dsDNA), ssDNA contains unpaired regions and it undergoes three dimensional folding and possessed a unique conformation under some conditions. Diverse structural conformations are formed including hairpin structures[8, 9], pseudoknots[10, 11] and quadruplex structures formed by planes of two neighbouring G-quartets[12, 13]. These conformations are very useful for some technologies like Systematic Evolution of Ligands by Exponential enrichment (SELEX)[3-5] and single-stranded conformation polymorphism (SSCP)[36, 37]. With unique base-paring mechanism, single stranded DNA templates can also be used in technologies which used hybridization-based detection schemes such as single-nucleotide polymorphism (SNP) which detects point mutations in DNA[38-40], pyrosequencing technology[41-43], solid phase DNA sequencing[44, 45], and sensing in DNA chips and microarrays[46-49].

Several groups have already made microfluidic devices to isolate aptamers. Park and Ahn developed a microfluidic device for binding nucleic acids to multiple immobilized proteins and eluting and recovering nucleic acids using sol-gel arrays system[331]. Soh group demonstrated an M-SELEX system which manipulated small numbers of beads to isolate high-affinity aptamers rapidly[332, 333]. Bowser group isolated the aptamer in a μFFE(micro free flow electrophoresis) device[88]. Lee group presented a magnetic bead-based microfluidic system which integrated a ssDNA incubation module with an on-chip nucleic acid amplification module[334]. However, these microfluidic SELEX systems only

realized some steps such as aptamer extraction process and PCR, not the entire SELEX process. Integrating the ssDNA generation step into these microfluidic SELEX is important because it could make the whole process cycled and the microfluidic SELEX was automatic and continuous from start to end.

As far as we know, Soh group developed a microfluidic electrochemical DNA sensor which integrated symmetric PCR, ssDNA generation and sequence-specific electrochemical detection on a single chip [335]. Lambda exonuclease digestion was used to generate ssDNA. The same group also used this method to generate ssDNA molecules to analyze genetic information of H1N1 influenza virus in a microfluidic system[336]. Mathies group used a streptavidin-coated gel in a microfluidic device to capture PCR products and released single stranded DNA by thermally heating the device to 67℃[337]. Nuzzo group discriminated SNP by immobilizing DNA on agarose beads followed with alkaline dehybridization[338]. Seidel group developed a chemiluminescence flow-through DNA microarray system applying a streptavidin-coated magnetic beads with alkaline denaturation in a μColumn commercially available[48]. As we know, this is the first polymer based microfluidic device with a polycarbonate membrane sandwiched between two channels to generate ssDNA by streptavidin-coated beads immobilization and alkaline denaturation. This is a fast, efficient and automatic method with high purity and yield. Little labor was involved. It can be integrated into other microfluidic systems to realize automatic ssDNA generation. It was a free-flow device. No streptavidin-coated gel or magnetic field is needed. Recently, several reports mentioned this ssDNA generation method may be unsuitable because the complementary ssDNA may re-anneal

with the non-biotinylated ssDNA and the release of streptavidin may cause cell aggregation in the selection process[98, 339, 340]. In this chapter, by labeling the dsDNA with dual biotin, the ratio between two single stranded DNA was quantitatively and qualitatively compared under different conditions and the purity was measured to reach over 95% and the yield could be as high as 42 ±5% of the original dsDNA amount under a reasonable flow rate in the device, which is 84 ±5% from the maximum possible ssDNA amount for this device. It's higher than 39.19 ±2.48% of the starting dsDNA amount reported in the literature[60] and 21.1 ±9.1% from the maximum possible ssDNA amount[340]. The yield in this device could be improved by decreasing the flow rate with a maximum yield was 50% of the original dsDNA amount. The over 95% purity was also higher than 90% reported in other literatures[335, 341]. Capillary electrophoresis was applied to qualitatively analyze the sample which confirmed ssDNA was the major component in the collected solution.

4.3 Experimental Section

4.3.1 *Reagents and Chemicals*

PDMS was made using Sylgard 184 silicone elastomer kit (Dow Corning, Midland, MI). Piranha solution (3:1 H2SO4:H2O2, Ashland Chemical, Dublin, OH) was used to clean silicon wafers. Diluted HCl was used to reactivate the PDMS surface. SU8-2050 (Microchem Corp., Newton, MA) was used to fabricate the master. All DNA samples were purchased from Integrated DNA technologies (Coralville, IA). Tris EDTA(TE) buffers consisted of 10mM Tris(hydroxymethyl)aminomethane(Tris), 1mM

Ethylenediamenetetraacetic acid disodium salt(EDTA), 150mM NaCl(Spectrum Chemical, New Brunswick, NJ) and 0.002% Triton X-100, adjusted to pH 7.5 using 1M HCl. TE buffer were degassed before use. 12.5mM, 18.75mM, 25mM, 50mM, 100mM and 300mM NaOH were prepared to denature dsDNA. 1.26μm streptavidin-coated polystyrene beads(Spherotech, Lake Forest, IL) were used to capture biotinylated dsDNA. Wash buffer was comprised of 5mM Tris, 0.5mM EDTA, 1mM NaCl and 0.05% Tween 20, adjusted to pH 7.5 using 1M HCl. Binding buffer consisted of 10mM Tris, 1mM EDTA and 2M NaCl, adjusted to Ph7.5 using 1M HCl. TBE buffer(Tris 89mM, Boric acid 89mM, EDTA 2mM) with 10% glycerol(Invitrogen, Grand Island, NY, purity>=99.5%) was used as CE running buffer. 8% Linear polyacrylamide(LPA)(MW600,000-1,000,000, polysciences, Inc, Warrington, PA) in TBE buffer with 10% glycerol was prepared and filtered through a 0.45μm membrane filter. Poly(ethylene oxide) (PEO) was dissolved in deionized water to 0.2% by mass with 0.1M HCl at a water bath around 95℃ with stirring. All buffer solutions were prepared using nuclease free water (Integrated DNA technologies, Coralville, IA) and filtered through a 0.2μm membrane before use. All other reagents and chemicals are from Sigma-Aldrich (St. Louis, MO).

4.3.2 *Fabrication*

The fabrication process is described previously[138]. A two-step soft lithography process was used.[256] An SU8 master was fabricated and multiple PDMS replicas were then cast from this master. The chip geometry was designed using CAD software which was then used to print a transparency film mask. Standard photolithography procedures

were used to make the SU8 master. The master was pre-treated with fluorinated silanes (UCT, Bristol, PA). Degassed PDMS prepolymer (10:1 ratio) was then poured onto the master and baked at 65 ℃ for 3 hours. The cured PDMS was removed from the master. A second PDMS layer was made using the same process. The resulting channels were 250 μm wide and 110 μm deep. The total channel length was 17cm with an active length where the channels overlapped of 15.3 cm. Inlet and outlet holes were punched into one PDMS layer using a piece of 21 gage stainless steel tubing (McMaster-Carr, Chicago, IL). Both PDMS layers were sonicated in dilute HCl for 10 minutes to reactivate prior to bonding[257]. A 12mm×20mm×6 μm polycarbonate membrane with 800nm pore diameter (Sterlitech Corp., Kent, WA) was placed on one layer of PDMS over the transport area of the channel. The PDMS layers were O2 plasma treated at 600mTorr and 75W for 10 s. The two layers were then quickly aligned and bonded irreversibly. The entire assembly was placed in the oven at 65 ℃ for 2 hours to complete the bonding process. Two glass substrates were used to support the device and eight screws on the edges of the substrates were finger tightened to seal the membrane and the PDMS slabs. 0.5" long pieces of stainless steel tubing with the same inner and outside diameter as a 23 gage needle (New England Small Tube Corp., Litchfield, NH) were inserted into in the inlet and outlet holes of the device allowing connections to be made with Tygon tubing (0.02 ID, 0.06 OD, Small parts, Inc, Miramar, FL). Buffer was pumped into the device using a syringe pump (Harvard Apparatus, Holliston, Massachusetts).

4.3.3 *Instrumentation and Data Collection*

A Synergy2 multi-mode microplate reader (BioTek, Winooski, VT) mounted with a Tungsten Halogen lamp and the filter set (λ_{ex}=485nm, λ_{em}=528nm) was used for fluorescence intensity measurement. Fluorescence data were recorded and processed using Gen5Reader Control and Data Analysis software (BioTek, Winooski, VT). Capillary electrophoresis was performed on a P/ACE MDQ capillary electrophoresis system (Beckman Coulter Inc., Fullerton, CA) equipped with laser induced fluorescence detection (λ_{ex}=488nm, λ_{em}=520nm) module. 32 Karat Software(Beckman coulter Inc., Fullerton, CA) was used for collecting and recording data.

4.3.4 *Sample Preparation*

Two 80nt ssDNA sequences (5'biotin-biotin- TT CAC GGT AGC ACG CAT AGG CGA TCA TAA AGC CTC CAT AGC ATT GTA CGT CGA AAC CTG CCA TCT GAC CTC TGT GCT GCT-FAM-3' and the complementary sequence 5'- AGC AGC ACA GAG GTC AGA TGG CAG GTT TCG ACG TAC AAT GCT ATG GAG GCT TTA TGA TCG CCT ATG CGT GCT ACC GTG AA -3') were synthesized by Integrated DNA technologies (Coralville, IA) and annealed to dsDNA1 in the following steps. Both of ssDNA sequences were dissolved in Nuclease Free Duplex Buffer (Integrated DNA technologies, Coralville, IA) to 100μM. Equal volume of each ssDNA solution were mixed together and the mixture was heated to 94℃ for 2min followed by cooling down to room temperature gradually. The resulting dsDNA1 product were diluted in TE buffer to 10μM and was stored in -20℃ for future use. Another two 80nt

ssDNA sequences (5'biotin-biotin- TT CAC GGT AGC ACG CAT AGG CGA TCA TAA AGC CTC CAT AGC ATT GTA CGT CGA AAC CTG CCA TCT GAC CTC TGT GCT GCT-3' and the complementary sequence 5'FAM- AGC AGC ACA GAG GTC AGA TGG CAG GTT TCG ACG TAC AAT GCT ATG GAG GCT TTA TGA TCG CCT ATG CGT GCT ACC GTG AA -3') were synthesized by Integrated DNA technologies (Coralville, IA) and annealed to dsDNA2 in the same procedure as above for dsDNA1. The only difference between dsDNA1 and dsDNA2 was the location of the dye FAM (Figure 4.1). Due to some synthesis technique limitations, two dsDNA (dsDNA1 and dsDNA2, Figure 4.1) were synthesized as two samples to characterize the ssDNA-generation results instead of single dsDNA sample with two dyes labeled on the two strands.

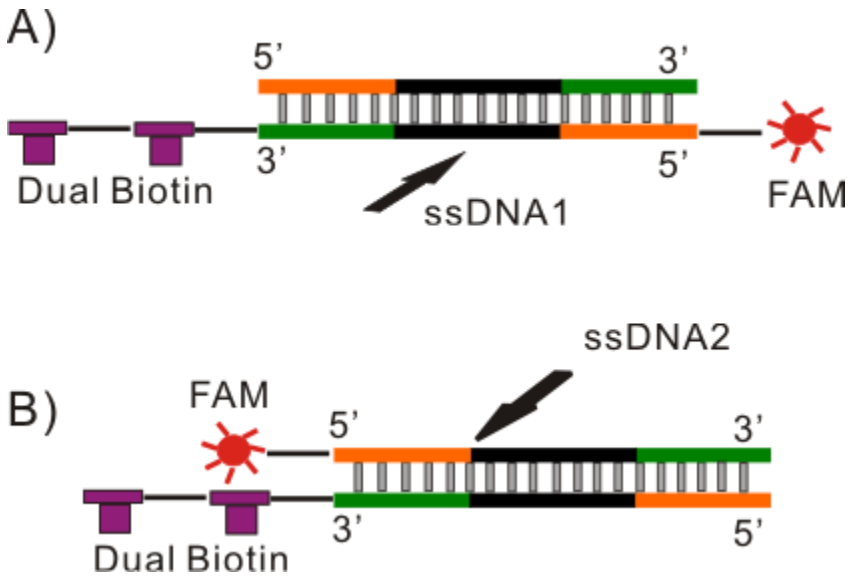

***Figure 4.1*:** (A) dsDNA1; Dual biotin and FAM were labeled on the same strand.The fluorescence signal was from the complementary strand(ssDNA1); (B) dsDNA2; Dual biotin was labeled on the complementary strand and FAM was labeled on the goal single strand(aptamer). The fluorescence signal was from aptamer(ssDNA2).

4.3.5 *Binding of dsDNA to beads*

150µl streptavidin-coated polystyrene beads suspension was centrifuged at 15000rpm for 5min in order to remove the storage buffer. Washing buffer was used to prewash the beads for three times at 15000rpm for 5 min and the result beads were resuspended in 300µl binding buffer after removing the supernatant. 200pmol dsDNA in 300µl nuclease-free water was mixed with beads suspension and incubated at room temperature for 15min. The supernatant was collected after centrifuge and the fluorescence intensity was measured to determine how much free dsDNA existed in the supernatant. By knowing how much dsDNA were added and how much dsDNA were left, the amount of dsDNA binding to the beads can be determined. Washing buffer was used to clean the beads with dsDNA (dsDNA-beads) for twice and TE buffer was added to resuspend dsDNA-beads in which dsDNA concentration was 100nM.

4.3.6 *ssDNA generation by alkaline denaturation*

dsDNA-beads solution was spiked with the same volume of freshly prepared NaOH solution. This mixture was injected to the chip as the sample. The mixture of TE buffer and NaOH solution in one to one volume ratio were injected to the chip as the buffer(Figure 4.2). It was supposed to use downstream buffer in the buffer channel for convenience. The reason to use the same buffer as the sample channel was for the easy conversion from fluorescence intensity to DNA concentration. The ratio between two single strands at six different NaOH concentrations were compared in this paper(12.5mM, 18.75mM, 25mM, 50mM, 100mM and 300mM).

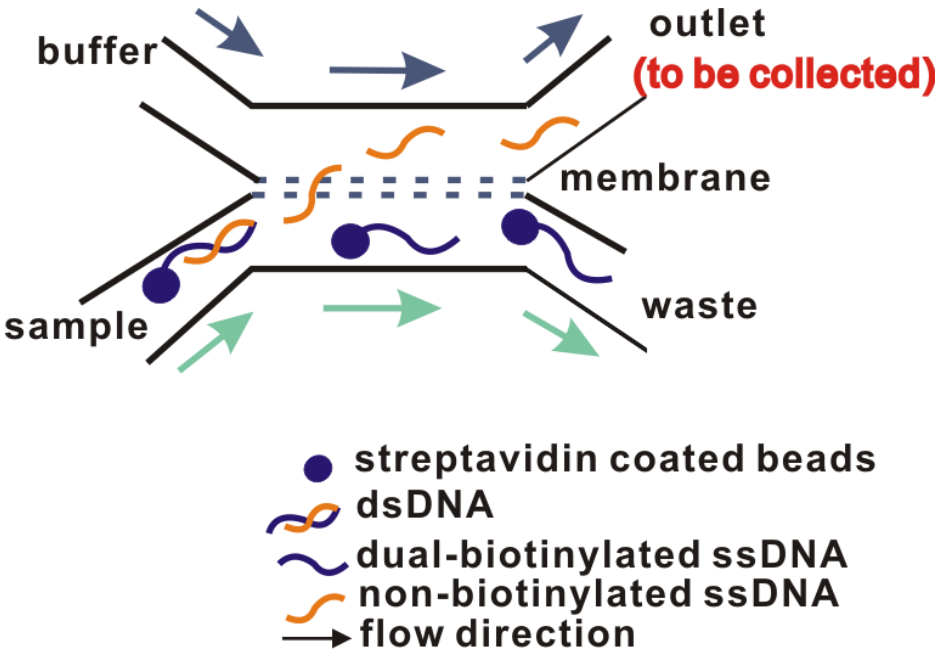

Figure 4.2: Cocurrent flow schematic: buffer and sample solution were injected into the device in the same direction. One of the single strands was dual biotinylated which lead to dsDNA was attached to the streptavidin-coated beads. As dsDNA denatured, non-biotinylated single-stranded DNA(ssDNA) were able to go across the membrane and be collected at the outlet for downstream use. However, beads attached dual-biotinylated ssDNA was bigger than the nanopores of the membrane and they were transported into waste vials.

A co-current flow strategy (Figure 4.2) was adopted in the device which meant the flow direction in the buffer channel and in the sample channel was the same. The flow rate was set to be 0.2ml/hr which corresponded to 2.2mm/s. NaOH could denature dsDNA and the separated non-biotinylated ssDNA(5nm)[138] would be smaller than the membrane pores(0.8μm) and it was going to be transported through the membrane and be collected at the outlet of the buffer channel. The two single-stranded DNA had no size difference. However, the single strand with beads(1.26μm) attached was bigger than the pores and it cannot go across the membrane. The solution from the buffer channel would be collected and measured by the plate reader. However, NaOH not only denatured dsDNA but also disrupted interaction between streptavidin and biotin which could cause

both of single strands enter the solution and go across the pores into the buffer channel. After neutralization, the biotinylated ssDNA would re-anneal with the non-biotinylated single strand which was bad for the applications that only require the non-biotinylated ssDNA. The perfect result would be all non-biotinylated single strands go to the buffer channel while the beads-attached single strands stay in the sample channel. For dsDNA2, the fluorescence intensity came from the non-biotinylated single strand(which was denoted as ssDNA2) or from the whole detached dsDNA2; and for dsDNA1, the fluorescence intensity came from the biotinylated single strand(which was denoted as ssDNA1) or from the whole detached dsDNA1. Capillary electrophoresis results demonstrated the fluorescence intensity was mainly from ssDNA not from dsDNA which would be mentioned as follows. Therefore, the fluorescence intensity from the collected solution would be assumed to come from ssDNA2 or ssDNA1. The concentration of DNA can be calculated by converting the measured fluorescence intensity to concentration according to the calibration curve. C_{ssDNA2}/C_{ssDNA1} (the ratio of concentration of ssDNA2(C_{ssDNA2}) to concentration of ssDNA1(C_{ssDNA1})) would be calculated under different NaOH concentrations, where C_{ssDNA2} was the concentration of ssDNA2 at the outlet of the buffer channel and C_{ssDNA1} was the concentration of ssDNA1 at the outlet of the buffer channel. The experiments were conducted for three times for error bars. A control experiment was done by mixing dsDNA-beads with equal volume of TE buffer followed by collecting the outlet solution from the buffer channel.

A reference method was used to compare the two results. dsDNA-beads suspension was transferred into seven centrifuge tubes and six tubes were spiked with the same

volume of NaOH (12.5mM, 18.75mM, 25mM, 50mM, 100mM and 300mM). The last one was spiked with the same volume of TE buffer as the control. After incubating for 15 min at room temperature, the solution was centrifuged under 15000rpm for 5min and followed by collecting the supernatant. C_{ssDNA2}/C_{ssDNA1} was determined. The experiments were conducted for three times for error bars.

4.3.7 *Determine the relationship between ssDNA generation and the flow rate in the device*

Equal volume of beads-dsDNA suspension and 25mM NaOH solution was mixed and the mixture was injected to the device as the sample. Equal volume of TE buffer and 25mM NaOH was mixed and the mixture was injected to the device as the buffer. C_{ssDNA2}/C_{ssDNA1} would be calculated under five different flow rates (0.5ml/hr, 0.3ml/hr, 0.2ml/hr, 0.1ml/hr and 0.05ml/hr). The solutions from the outlet of the buffer channel were collected between 15min to 20min counting from the moment of adding NaOH into dsDNA-beads in order to minimize errors.

4.3.8 *Determine the influence of incubation time to ssDNA generation*

Equal volume of beads-dsDNA suspension and 25mM NaOH solution was mixed and the mixture was injected into the device as the sample. Equal volume of TE buffer and 25mM NaOH was mixed and the mixture was injected into the device as the buffer. The outlet solution of the buffer channel was collected every 6min at a rate of 0.2ml/hr (2.2m/s). Therefore, the incubation time increased(8min, 14min, 20min……). The

experiments were conducted for dsDNA1 and dsDNA2. The impact caused by incubation time to dsDNA1 and dsDNA2 were compared.

4.3.9 *Coating capillary and loading gels for Capillary electrophoresis characterization*

A 40cm-long, 75μm-ID, 360μm-OD uncoated fused-silica separation capillary (Polymicro Technologies, Phoenix, AZ) was used. Electroosmotic flow(EOF) was suppressed by applying Iki and Yeung's method for coating a capillary using PEO[342]. The capillary was rinsed with 0.1M NaOH, H2O, 1M HCl, 0.2% PEO/0.1M HCl and TBE buffer containing 10% glycerol . Each step lasted for 10 min with 20 psi rinse pressure. Barron Group's method for separating ssDNA and dsDNA was adopted in the capillary electrophoresis experiment[343, 344]. 8% w/v LPA (MW600000-1,000,000) in TBE buffer containing 10% glycerol was used to be the sieving matrix for separating 80nt ssDNA and 80bp dsDNA. Glycerol was reported to improve resolution by some research groups[345, 346]. Linear polyacrylamide (LPA) was filtered through a 0.45μm membrane filter and degassed through centrifuge with 12000 rpm for 1min. All the other solutions were filtered through a 0.2μm membrane filter. LPA was loaded into the 40cm capillary in the MDQ capillary electrophoresis system by using 20psi for 20min. Samples were injected using 2kV voltage for 15s. The separation was performed under the following conditions: 10kV voltage (reverse polarity), laser detection at 488/520nm and 15℃. TBE buffer containing 10% glycerol was used as the running buffer. Before performing separation, the LPA-loaded capillary were conditioned under 10kV voltage (reverse polarity) overnight to ensure an equalibrated gel structure which helps to obtain consistent mobility time for each sample from run to run.

4.4 Results and Discussion

4.4.1 *Design considerations*

In suspension, beads would tend to settle down in the bottom of the syringe which makes it hard to inject them into the device. The settling velocity is related to the balance of viscous drag and gravity force. According to Stoke's law:

$$V_m = \frac{g(\rho_s - \rho_m) \cdot d^2}{18\eta_0}$$

which is derived by solving the Stokes flow limit for small Reynolds numbers of the general Navier-Stokes equation[347-350].

where: V_m is the maximum settling velocity (cm/sec); g is the acceleration of gravity (980.7 cm/sec^2); η_0 is the viscosity of the external phase in poises(g/cm sec); ρ_s is the density of solid sphere (g/cm^3); ρ_m is the density of the medium(g/cm^3); d is the mean diameter of the suspended particles(*cm*).

The rate of sedimentation is related to the density and the diameter of the particles. Therefore, the size and the material of beads are crucial to the continuously running of the device. According to the manufactures' data about density and diameter of the beads, streptavidin-coated polystyrene beads had the lowest density compared with silica and magnetic beads. Polystyrene(PS) beads also have a series of diameters from low nm to high μm. Based on the requirements of the device, beads should have a diameter bigger than the membrane pores as well as have a smaller density which keeps beads suspended

in the solution for a longer time. The lower rate of sedimentation was beneficial for the continuously running of the device which is vital for the automatic system. In order to keep recovery high, a bigger pore membrane (800nm) was used in the device so that 1.26μm polystyrene beads were used for this paper.

Alkaline denaturation was the method adopted in this paper to generate ssDNA. However, alkaline solution not only denatured dsDNA but also interrupted streptavidin-biotin interaction which caused the collected solution was contaminated with the complementary strand. A dual-biotin label was used to increase the stability of streptavidin and biotin interaction upon adding NaOH. Similar design was proved successful in PCR cycles as reported in the literature[351]. Our data (not shown here) demonstrated dual-biotin design was able to achieve a higher purity than the single-biotin design. The ideal sample would be a single dsDNA sample with dual biotin labeled on the complementary strand and two different dyes labeled on each single strand without any cross talk between two dyes. However, due to some synthesis technique and lab facilities limitations, the ideal sample cannot be obtained. Two dsDNA (dsDNA1 and dsDNA2, Figure 4.1) were synthesized as two samples to characterize the ssDNA-generation results. Both of two dsDNA have the same concentration in the initial solution (100nM). Removing the complementary strand is very important in ssDNA generation. The fluorescence signal from dsDNA1 was from ssDNA1 and the fluorescence signal from dsDNA2 was from ssDNA2. The ratio between the amount of ssDNA2 and the amount of ssDNA1(purity) will be compared as follows.

4.4.2 *Study ssDNA generation by alkaline denaturation and strand separation in the device*

The biotinylated dsDNA was immobilized onto the streptavidin-coated polystyrene beads. Subsequently the beads with dsDNA (dsDNA-beads) were mixed with sodium hydroxide (NaOH) solution to denature dsDNA. dsDNA was incubated with NaOH in situ and the two single strands were separated by a membrane filter in the microfluidic device with a 0.2ml/hr flow rate. No labor was involved and the only thing was to collect the outlet solution of the buffer channel. The dsDNA would be denatured and the non-biotinylated single strand would go across the membrane and be collected at the outlet of the buffer channel. The whole process happened automatically and continuously.

Alkaline treatment is known to be a reliable and convenient way to denature double-stranded DNA in a mechanism related to the deprotonation of guanine and cytosine segments[352-355]. However, the three-dimensional structure of streptavidin, as well as the hydrophobic, van der Waals forces and hydrogen bonds between biotin and streptavidin are fractured which leads to the biotinylated strand enters the solution and being transported through the nanopores to be collected with the non-biotinylated strand[95, 98, 103].

In order to characterize the experiment, the fluorescence intensity was measured in a plate reader and converted to the concentration of ssDNA according to a calibration curve. The concentration of NaOH was significantly related to dsDNA denaturation and

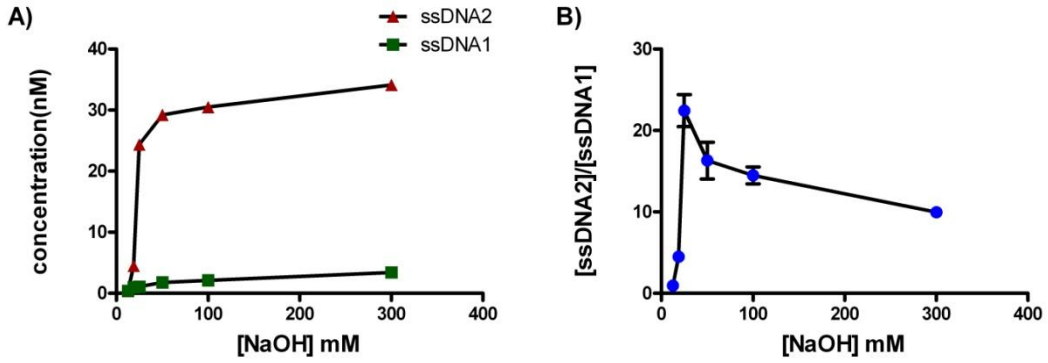

***Figure 4.3*:** Six different concentrations of NaOH were used to generate ssDNA. Denature and separation of the two single strands was automatically and continuously carried out in a microfluidic device. The denatured ssDNA would go across the filter membrane and be collected at the outlet of the buffer channel. A) Plot of [ssDNA2] and [ssDNA1] vs. [NaOH]. Both [ssDNA2](triangles) and [ssDNA1](squares) increased with [NaOH] increased. B) The ratio ([ssDNA2]/[ssDNA1]) (circles) increased with [NaOH] increased until reach an optimum concentration(25mM). The purity could reach 95.7%. After that, the ratio decreased as [NaOH] increased. Data was recorded in triplicate. Error bars were smaller than the symbols used in the plots. The flow rate was 0.2ml/hr and buffer contained 10mM Tris, 1mM EDTA, 150mM NaCl and 0.002% Triton X-100.

streptavidin-biotin dissociation. Six different NaOH concentrations were used in this experiment. It was found there was a window that dsDNA was strongly denatured while most of streptavidin-biotin interaction was still active for some NaOH concentration. Figure 4.3A demonstrated that both of the concentration of ssDNA2(C_{ssDNA2}) and the concentration of ssDNA1(C_{ssDNA1}) at the outlet of buffer channel increased as NaOH concentration increased. C_{ssDNA2} increased from 0.3nM to 34nM as NaOH increased from 12.5mM to 300mM. Especially from 18.75mM to 25mM NaOH concentration, ssDNA2 concentration increased from 4.5nM to 24nM at a steep rate. However, C_{ssDNA1} increased with a more moderate rate even when NaOH concentration changed from 12.5mM to 25mM. The ratio between C_{ssDNA2} and C_{ssDNA1}(C_{ssDNA2}/C_{ssDNA1}) was determined as NaOH concentration changed. Figure 4.3B demonstrated the optimum ratio was achieved at 25mM NaOH when most of dsDNA2 had been denatured but streptavidin-biotin

interaction was still maintained. The maximum ratio could be as high as 22 which meant the purity reached 95.7%. The yield of the non-biotinylated ssDNA(amount of ssDNA2 recovered from the device) was related to the flow rate chosen in the device. At 0.2ml/hr, the yield was 48±0.3% from the maximum possible ssDNA amount for this device. For SELEX, the presence of complementary strand can cause the rehybridization of two single strands and loss of selected high affinity aptamers. Therefore, the purity is very important for this ssDNA generation process. In this microfluidic device, only 4.3% sequence would have the chance to be contaminated by the complementary (biotinylated) strands. With NaOH concentration less than 25mM, the process of DNA denaturation was less strongly driven. With NaOH concentration higher than 25mM, too much streptavidin-biotin interaction was interrupted which caused more biotinylated ssDNA were collected. The ratio between two single strands decreased as well. However, compared with lower NaOH concentration, it was still better to use higher NaOH concentration to obtain higher purity and higher yield in the ssDNA generation process.

4.4.3 *Study ssDNA generation using different flow rates in the device*

When the solution flowed through the device in different flow rates, the time for equilibration that the analyte was exposed to the membrane would be different. For the 15.3cm long channel used here, the equilibration time increased from 30.6s to 4.2min as the flow rate decreased from 0.5ml/hr to 0.06ml/hr (5mm/s to 0.61mm/s). Therefore, the recovery for analytes would increase as flow rates decreased which was demonstrated in Figure 4.4(A) and 4(B). The recovery of ssDNA2 was defined as the yield. The yield changed as flow rate changed. Lower flow rates helped to achieve a higher yield.

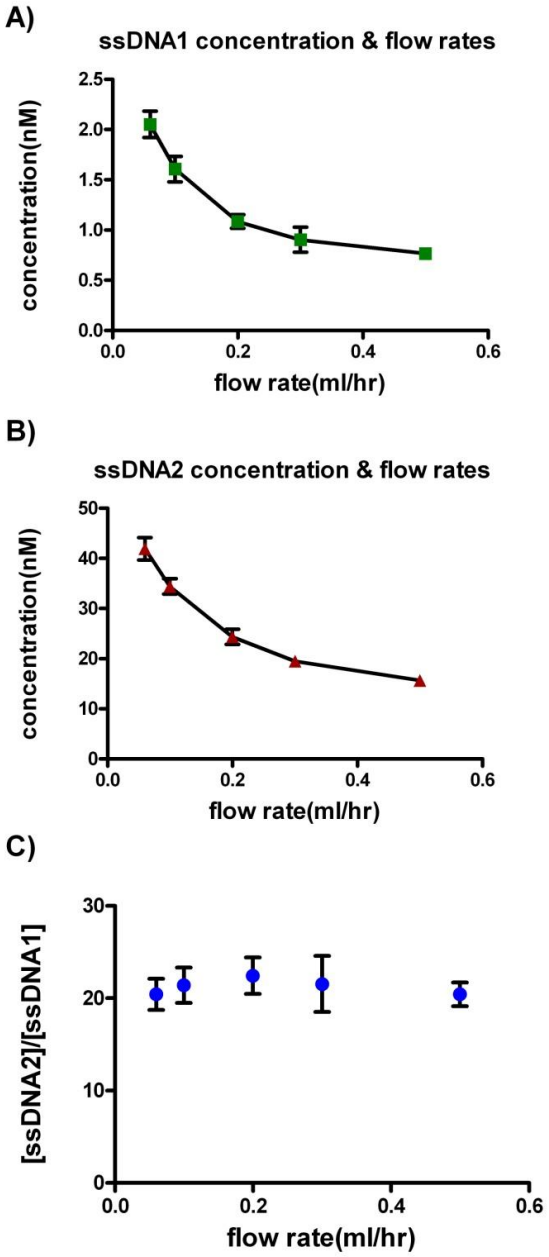

***Figure 4.4*:** Five different flow rates were used to change equilibrium time in the device which could influence the recovery of the ssDNA molecules. At lower flow rates, the time for equilibration that the analyte was exposed to the membrane increased. The recovery for ssDNA molecules increased. (A) beads with dsDNA1(dsDNA1-beads) was the sample molecule; plot of [ssDNA1](squares) vs. flow rates; B) beads with dsDNA2(dsDNA2-beads) was the sample molecule; plot of [ssDNA2](triangles) vs. flow rates; Both recovery of ssDNA1 and ssDNA2 increased as flow rates decreased with a similar rate. (c) plot of [ssDNA2]/[ssDNA1](circles) vs. flow rates. Changing flow rates in the device changed the recovery of ssDNA1 and ssDNA2 at a similar rate. The ratio of [ssDNA2]/[ssDNA1] was similar for the five different flow rates. The purity was above 95% for the selected five flow rates. Data was recorded in triplicate. The NaOH concentration was 25mM and buffer contained 10mM Tris, 1mM EDTA, 150mM NaCl and 0.002% Triton X-100.

At 0.06ml/hr (which corresponds to 0.61mm/s linear velocity), the yield can reach 84±5% from the maximum possible ssDNA amount for this device. The recovery for ssDNA1 and ssDNA2 changed in a similar rate as flow rate changes. The ratio C_{ssDNA2}/C_{ssDNA1} would remain relatively stable no matter what flow rate was used. The purity was changing from 95.3% to 95.7%. In another word, the purity remained unchanged as the flow rate changed. NaOH concentration was 25mM in this experiment.

4.4.4 *Study the influence of incubation time to the ssDNA generation*

The incubation time also impacts the denaturation of dsDNA and the dissociation of streptavidin and biotin. Denaturation of dsDNA leads to ssDNA2 generation and denaturation of streptavidin leads to ssDNA1 generation. 25mM NaOH was used to denature dsDNA and 0.2ml/hr was used to flow the solution through the device. As demonstrated in Figure 4.5, the generation of ssDNA1 was linearly related to the incubation time. However, ssDNA2 was generated quickly and the amount of ssDNA2 remained relatively stable from 8min to 40min which is the time range for all of the experiments in this paper. The sudden decrease and increase of ssDNA2 was thought to be related to the unpredictable flow pattern in the channel due to blocking of the channel or pores by air bubbles, beads and other obstructions. Although all of the solutions were degassed and filtered through a 0.2μm membrane filter, it was still unavoidable to inject air bubbles and other obstructions into the device. Figure 4.5 also illustrated that it was beneficial to finish the experiments in a reasonable short time because the amount of non-biotinylated ssDNA1 would continuously increase as time increased while ssDNA2 would not change after 8 min (the shortest time from start of incubation to the end of

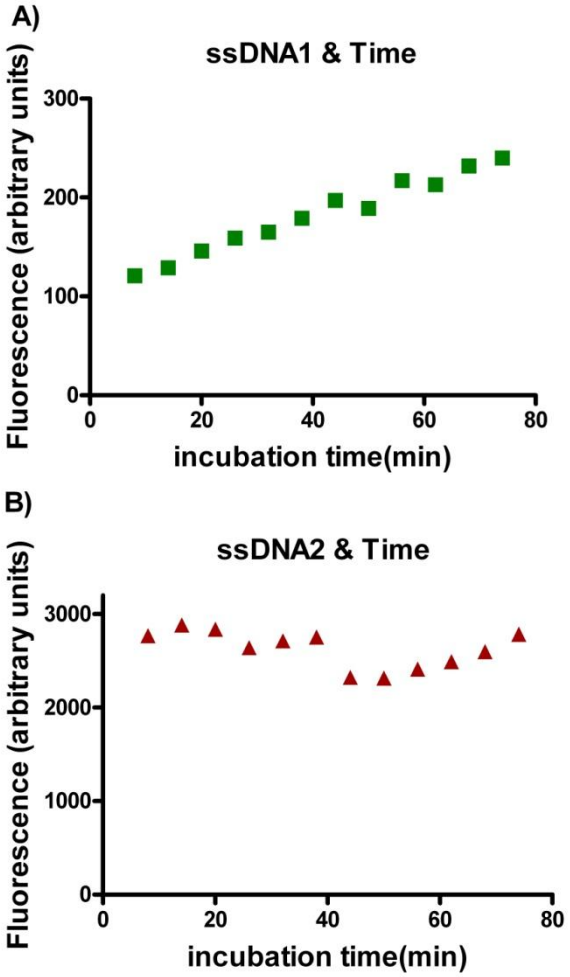

Figure 4.5: A) Plot of fluorescence intensity signal from ssDNA1 (squares) vs. incubation time; B) Plot of fluorescence intensity signal from ssDNA2 (triangles) vs. incubation time; ssDNA1 increased with a steeper rate as incubation time increased while ssDNA2 stayed more stable as incubation time increased. Incubation time played a more important role to the denaturation of streptavidin.

collection at 0.2ml/hr). For 14min, 20min and 26min, the relative standard deviation from ssDNA1 was 10% while the relative standard deviation from ssDNA2 was only 4.6%. This error was thought to be included in the error bars because the operation time was not the same from run to run. And it may explain why the error from ssDNA2 was usually smaller than the error from ssDNA1.

4.4.5 *Comparison purity between two methods*

The ssDNA generation and two strands separation were conducted in the experiments using the microfluidic device. The whole process was automatic and no labor was involved which was good for avoiding errors relating to the operation of the experiments. The second method was named under reference method which generated ssDNA off the chip. After incubating with NaOH at room temperature for 10min, the dsDNA-beads suspension were settled at the bottom of the tube via centrifuge at 15000rpm for 5min. The supernatant containing denatured ssDNA was transferred to another clean centrifuge tube by pipetting. The fluorescence intensity was measured in the plate reader. And the ratio C_{ssDNA2}/C_{ssDNA1} was determined at different NaOH concentration. This reference method involved many manual-operation procedures which led to loss of the target ssDNA and contamination of the complementary strand particularly through transferring supernatant to the clean tubes by pipetting. As illustrated in Figure 4.6, the ratio C_{ssDNA2}/C_{ssDNA1} from these two methods was close. However, the microfluidic-device method yielded a better purity when NaOH concentration was higher than 25mM. This phenomenon was thought mainly caused by supernatant contamination by dsDNA-beads in the transferring process. From this perspective, the microfluidic-device method should be counted as “reference” method because it involved less human errors during the experiments.

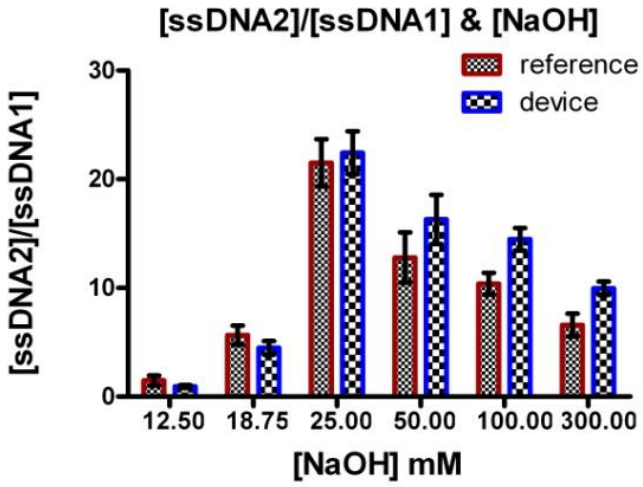

Figure 4.6: Reference method was done by manually denaturizing dsDNA and separating the two single strands in the centrifuge followed by removing the supernatant; Device method was done by automatically denaturing dsDNA and separating two single strands in a microfluidic device.

4.4.6 *Determine ssDNA or dsDNA existence in the collected solution using capillary electrophoresis*

The solution from the outlet of the buffer channel would be collected and neutralized by diluting10 times in the neutralizing buffer which contained Tris 100mM and EDTA 1mM (pH7.5). After neutralization, 15µl solution would be used as the sample in the capillary electrophoresis system. 10µl 100nM dsDNA2 solution was mixed with 10µl 100nM ssDNA2 and this mixture was used as the sample in the capillary electrophoresis system to identify peaks. So did 20nM dsDNA2 and 100nM ssDNA2. ssDNA and dsDNA peaks were identified in the electropherogram which was displayed in Figure 4.7 (A). The front peak belongs to dsDNA2 and the later peak (around 10min) belongs to ssDNA2. As demonstrated by Figure 4.7(B), ssDNA2 peak increased as NaOH concentration increased. Especially when NaOH concentration changed from

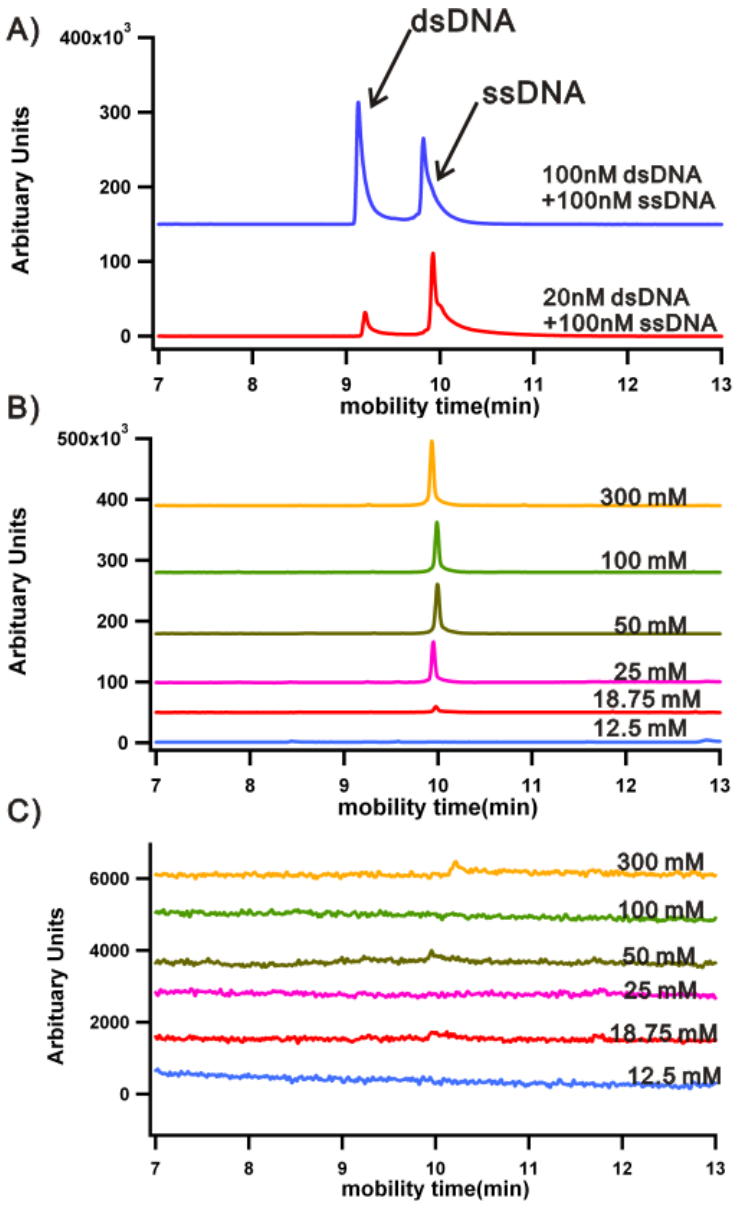

Figure 4.7: A) peak identification; 100nM dsDNA2 was mixed with equal volume of 100nM ssDNA2 and the mixture was injected into the Capillary Electrophoresis (CE) system(Top); 20nM dsDNA2 was mixed with equal volume of 100nM ssDNA2 and the mixture was injected into the CE system(Bottom);The earlier peak was identified as dsDNA and the later peak was identified as ssDNA. B) dsDNA2-beads suspension was incubated with six different NaOH concentrations (12.5mM, 18.75mM, 25mM, 50mM, 100mM and 300mM) and the mixture was injected into the device at 0.2ml/hr. The outlet solution from buffer channel was collected, neutralized and finally injected into the CE system. The electropherogram was recorded. C) dsDNA1-beads suspension was incubated with six different NaOH concentrations (12.5mM, 18.75mM, 25mM, 50mM, 100mM and 300mM) and the mixture was injected into the device. The outlet solution from buffer channel was collected, neutralized and finally injected into the CE system. The electropherogram was recorded.

18.75mM to 25mM NaOH, the peak increased to a level which was as high as peaks when NaOH concentration was 50mM and 100mM. The peak from 300mM NaOH was highest. Therefore, it was clear that higher NaOH concentration was useful to increase ssDNA generation but it was not very significant when NaOH concentration was higher than 25mM. There was no significant dsDNA2 peak in Figure 4.7(B).It might be caused by the concentration of dsDNA was below the detection limit, which revealed that the dsDNA2 concentration was very low and ssDNA2 can be treated as the major component in the solution. No significant ssDNA peak or dsDNA peak can be detected in Figure 4.7(C) when dsDNA1-beads suspension was used as the sample in the device. FAM was labeled at the complementary strand which proved few ssDNA1 went across the membrane and single strand was the major DNA form in the collected solution which was crucial for SELEX and other molecular and biotechnology applications which require ssDNA.

4.5 Conclusion

We have demonstrated a microfluidic device which can automatically and continuously generate ssDNA and separate two single strands at the same time. A polycarbonate track etched membrane with 800nm pores was sandwiched between two PDMS channels as a filter and 1.26μm streptavidin-coated polystyrene beads were used to generate size difference between two single strands. dsDNA was immobilized with streptavidin-coated beads first. NaOH was used to denature dsDNA and the non-biotinylated ssDNA was collected at the outlet of the buffer channel to be used in the downstream application. However, NaOH would not only denature dsDNA but also

disrupt streptavidin-biotin interaction which causes the biotinylated ssDNA enters the solution and be transported through the membrane. Two double stranded DNAs (dsDNA1 and dsDNA2) were used to detect how much ssDNA1 and ssDNA2 were collected at the outlet of the buffer channel. Both of two double stranded DNAs were dual biotinylated and the biotinylated ssDNA would be removed because beads were bigger than the pores. If the collected solution was contaminated by the complementary strand, this strand would re-anneal with the non-biotinylated ssDNA to form dsDNA. For SELEX, the formation of dsDNA would cause loss of high affinity aptamers that show binding to the target before.

Six different NaOH concentrations were used to denature dsDNA and 25mM was demonstrated to be the optimum concentration which can strongly drive the dsDNA denaturation process while still keeping most streptavidin biotin-interaction active. 95.7% of collected DNA at the outlet of the buffer channel were non-biotinylated single strands. Although different flow rates could impact the equilibration time the analytes are exposed to the membrane area, the purity remained relatively stable even the flow rates changed. However, it is helpful to lower the flow rates in order to obtain a higher yield of the non-biotinylated ssDNA which is important in the SELEX process. At 0.06ml/hr, the yield could reach 84±5% from the maximum possible ssDNA amount for this device. The interaction between streptavidin and biotin was fractured more significantly as incubation time increased. However, NaOH will denature dsDNA quickly and the amount of ssDNA remained stable as time goes by. Therefore, it's beneficial to finish the whole experiments in a shorter time to prevent more and more biotin streptavidin dissociated

which would generate a larger amount of biotinylated ssDNA at the outlet of the buffer channel. Purity from the chip experiments was even better than the result from an off-chip method when NaOH concentration was higher than 25mM. No labor was involved during the operation of the microfluidic device which avoided some errors result from manual operations like pipetting and transferring solution. The capillary electrophoresis results revealed that ssDNA was the major molecule in the collected solution which is very important for SELEX and other techniques which only requires ssDNA.

Chapter 5 Summary and Future Directions

5.1 Summary of Research

Microfluidic devices are becoming more and more popular in biology and chemistry labs. Systematic Evolution of ligands by Exponential Enrichment (SELEX) is still adopted by most of people to isolate aptamers with high affinity and specificity. Aptamers rival antibodies both in therapeutic and diagnostic areas. However, a conventional SELEX process takes weeks to months from the first selection to the finish of cloning and sequencing. SELEX could move into a higher-speed and simpler system if it moved to a chip-based microfluidic environment. Single stranded DNA generation is an important step in not only SELEX but also in other sample processing methods such as single-stranded conformation polymorphism (SSCP), single-nucleotide polymorphism (SNP), pyrosequencing technology, solid phase DNA sequencing, and sensing in DNA chips and microarrays. The single strands will reanneal with the complementary single strands to prevent them from forming many different structure confirmations which are important in target-aptamer binding. An innovative nanopore based microfluidic device has been developed for single stranded nucleic acids sizing and generation for SELEX. The objective of my research is to design, fabricate, test and model this device.

Chapter 2 focused on the design, fabrication and characterization of the device. The design is based on the theory that different-molecular-weights molecules have different physical sizes. The membrane with nanopores could be used to separate different-sizes molecules. This nanopore based microfluidic device consists of two polydimethylsiloxane (PDMS) channels separated by a polycarbonate membrane with a 50 nm pore size. The master was fabricated first by using rapid prototyping and multiple

PDMS replicas were then cast from this master. Oxygen plasma treatment was applied to bond two PDMS layers and glass substrates were used to support the whole device. A counter current flow strategy was adopted to maximize recovery. Recovery of fluorescein across the membrane was highest compared with 10 and 80 nucleotide (nt) single stranded DNA(ssDNA). And the recovery of all of the three analytes improved with decreasing flow rate. The device was found to have different transport rate towards different-lengths ssDNA. Greater than 2-fold selectivity between 10 nt and 80 nt ssDNA was observed at linear velocities less than 3mm/s. Increasing the ionic strength of the buffer increased transport across the membrane. The effect was size dependent as 10 nt showed a smaller increase compared with 10 nt ssDNA while the recovery of fluorescein was largely unaffected by increasing the ionic strength of the buffer.

Chapter 3 demonstrated two mathematical models which were built to simulate the process of DNA transportation in the microfluidic device. Both of the models were built based on conservation of mass and constitutive relationships. Diffusion was identified to be the major mechanism to drive molecule through the nanopores. The first model assumes no concentration gradient along the channel depth and an analytical solution was obtained to express the relationship between recovery and mass transfer coefficient of the membrane. The second model was closer to real situation. However, it was solved by the finite element software COMSOL and only numerical solutions were obtained. Trends in recovery measured at various flow rates were consistent with the trends predicted in the two models which support the premise that diffusion dominated the molecular transport in this device. These models showed recovery increased as the linear velocity decreased

and Models 2 demonstrated recovery was also affected by the ionic strength of the buffer. In addition, Model 2 generated surface plots of concentration for three samples (80nt single-stranded DNA(ssDNA), 10nt ssDNA and fluorescein) which visualized concentration distribution in the two channels. Overall, these two models are critical to identify the mechanism to drive DNA molecules through the nanopores and explain phenomena relating to size selectivity of three samples and trends of recovery as the flow rate changes and as the ionic strength of the buffer changes.

In Chapter 4, the microfluidic device was applied to generate ssDNA and separate two single strands simultaneously for SELEX. Streptavidin-coated polystyrene beads were immobilized with dual-biotin labeled dsDNA and alkaline treatment was adopted to denature dsDNA and release the non-biotinylated ssDNA. Six different NaOH concentrations were used to denature dsDNA and 25mM was demonstrated to be the optimum concentration which can strongly drive the dsDNA denaturation process while still keeping most streptavidin biotin-interaction active. 95.7% of collected DNA at the outlet of the buffer channel were non-biotinylated single strands. Although different flow rates could impact the equilibration time the analytes are exposed to the membrane area, the purity remained relatively stable even the flow rates changed. However, it is helpful to lower flow rated in order to have a higher yield of the non-biotinylated ssDNA which is important in the SELEX process. At 0.06ml/hr, the yield could reach 84±5% from the maximum possible ssDNA amount for this device. The ssDNA generation process was also time-based. Purity from the chip experiments was even better than the result from an off-chip method when NaOH concentration was higher than 25mM. Capillary

Electrophoresis results confirmed ssDNA was the major component in the collected solution. It usually took four to five hours to denature dsDNA and remove one single strand by regular laboratory procedures. This microfluidic chip could make this process much simpler and more convenient. Turn it on, let it go! It saved time and labor. Single stranded DNA was generated and strands were separated successfully in this nanopore based microfluidic device.

5.2 Future Directions

5.2.1 *Integrated the microfluidic device into CE-SELEX*

It was planned to integrate the microfluidic single stranded DNA generation device into the micro-SELEX system, which consists of micro-Free Flow Electrophoresis(μFFE) separation device[356, 357], microPCR amplification device and microfluidic ssDNA generation and purification device. However, the microfluidic PCR device has not been developed successfully yet in our group. Therefore, the ssDNA generation device is going to be integrated into the CE-SELEX system[33, 34] to replace the steps of single stranded DNA generation and purification in the CE-SELEX protocol. The procedure of ssDNA generation and purification in CE-SELEX involves streptavidin beads immobilization, alkaline denaturation, ethanol precipitation and drying. The device that has been developed in Chapter 4 can be used for ssDNA generation. However there are other ingredients such as salts, primers and *Taq* polymerase in the PCR matrix that have to be removed for the CE-SELEX process[35]. Two membranes will be integrated into the

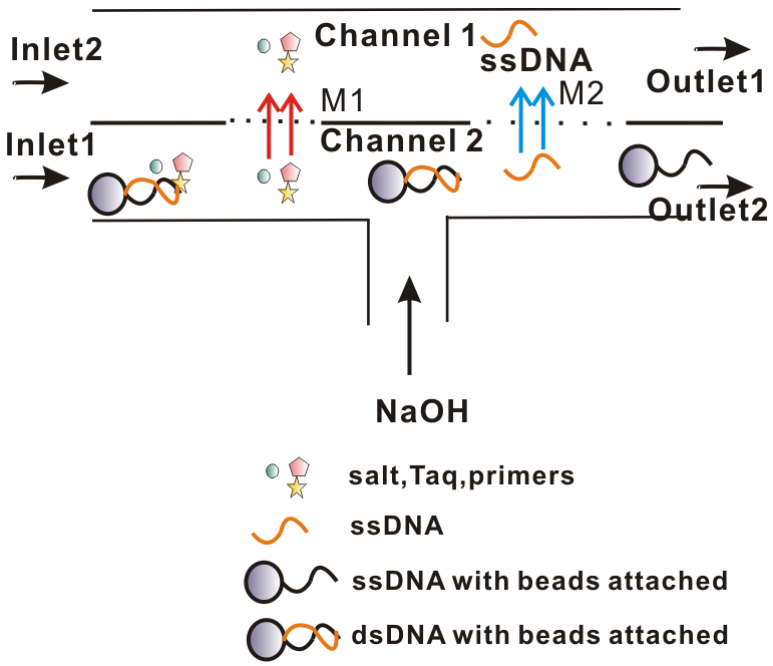

Figure 5.1: Schematic of the device for ssDNA generation and purification. The PCR product and water are injected into the device through Inlet1 and Inlet2. Salt, *Taq* and primers are removed first and flushed in a faster speed in the channel 2. In the channel 1, the beads-dsDNA suspension is incubated with NaOH which is injected into the device through the third inlet. As dsDNA denatured, the non-biotinylated ssDNA can go across the membrane and be collected at Outlet1, which is free of salt, *Taq*, Primers and the complementary ssDNA.

same chip(see Figure 5.1). The membrane M1 is used to remove salts, *Taq* and primers, while the membrane M2 is adopted to remove the beads attached ssDNA.

It is not necessary to have the same membrane for M1 and M2. After immobilized with streptavidin beads, the PCR product is injected into the channel 1 from Inlet1 and water enters another channel 2 from Inlet2. Different flow rates can be used in the two channels in order to remove salt, *Taq* and primers as more as possible, which is also helpful to cause time delay between salt, *Taq*, primers collected at outlet 1 and the non biotinylated ssDNA collected at outlet1. 25mM NaOH is injected from the third inlet at the same flow rate as channel 2 and incubated with beads-dsDNA suspension in the chip

and the denatured ssDNA will go across the membrane and be collected at the outlet1, which is free of salts, *Taq*, and primers. This ssDNA solution can be used for the further rounds of SELEX selection.

There are some problems which can be anticipated for this device. As we known, the microfluidic chip has the advantage of consuming fewer reagents compared with regular lab operations. However, when this device is integrated with the regular lab procedures such as CE-SELEX, this advantage turns into a disadvantage since CE-SELEX requires larger volume of reagents which may take longer to run in the microfluidic device. For example, PCR yielded around 800 μl solution which need to be purified in the device. According to Chapter 4, it takes about 4 hr to finish the experiment if 0.2ml/hr is used as the flow rate in the channel 2 by using the microfluidic device. In another words, it may lose the advantage of "take less time" when integrate the microfluidic device with the regular CE-SELEX system. The second problem is related to the concentration of the final single stranded DNA. A faster flow rate may be used in order to obtain a higher yield of the ssDNA which may be diluted by the massive buffer in Channel 1. And the final ssDNA solution may need to be neutralized before concentrated in the concentrator. However, I think it's practical to integrate the microfluidic ssDNA generation and purification device into the CE-SELEX system to test the ssDNA generation results. This procedure paves the way for the successful completion of micro-SELEX system in the future.

5.2.2 *Improve the recovery of the device*

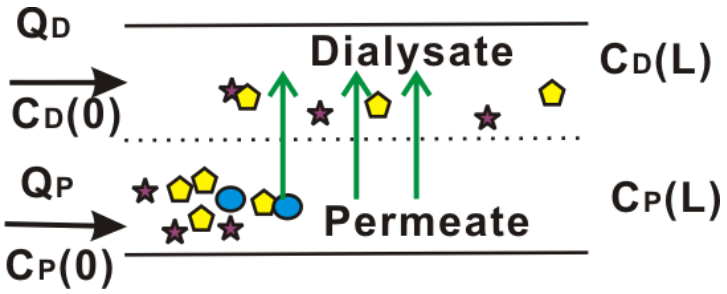

Figure 5.2: Schematic of cocurrent flow. Two channels (Dialysate and permeate channel) are separated with a membrane. The flow rate in the dialysate channel is Q_D and the flow rate in the permeate channel is Q_P. The fraction of solute that is removed from the permeate flow is related to the ratio of permeate to dialysate flow rates Q_D/ Q_P.

Cocurrent flow strategy was adopted in the ssDNA generation device due to beads adsorption problem, which sacrifices the recovery of ssDNA(see Figure 5.2). In Chapter 4, the cocurrent flow is adopted as the flow strategy and the highest recovery is only up to 50% of the initial DNA in the permeate solution when the flow rates in the dialysate and in the permeate channel are the same. In SELEX process, the yield of single stranded DNA is very important since we don't want to lose high affinity aptamers in the purification step. The ideal recovery would be 100% of the initial DNA in the permeate channel. It is critical to increase the recovery of the microfluidic device if we want to integrate it into the SELEX system.

There are two possible ways to increase the recovery. The first method is to increase the recovery by adopting different flow rates in the device. Based on the extraction ratio which represents the fraction of solute that is removed from the permeate flow, $E = \frac{Q_D}{Q_P}\frac{(C_D(L) - C_D(0))}{(C_P(0) - C_D(0))}$ for cocurrent flow[217]. This equation demonstrates the fraction

of solute that is removed from the permeate flow is increased as the ratio $\frac{Q_D}{Q_P}$ is increased. Recovery has the same definition as the fraction of solute that is removed from the permeate flow(E). In another words, recovery increases as the ratio $\frac{Q_D}{Q_P}$ increases as well. This is understandable because transport is driven by diffusion, which is also driven by concentration difference between two sides of the membrane. When the flow rate in the dialysate channel is much higher than the permeate channel, the solute concentration in the dialysate channel is much lower than the permeate channel which can be seen 0 if the flow is fast enough. Therefore, the recovery can be improved as the ratio of permeate to dialysate flow rates increases.

Another way to increase the recovery of the device is to adopt another membrane which has high porosity, small pore diameter and the counter current flow strategy is adopted in the device. The beads adsorption problem may be caused by the convection transport through the nanopores due to pressure differences in the two channels. Based on the experiment results which are not shown in this thesis, when the membrane has a smaller pore diameter (<30nm), the beads adsorption problem is much less significant even though the flow is adopted in the counter current strategy. However, when the pore diameter decreases, the recovery decreases a lot. It is even not as good as that obtained with a bigger-pore membrane in a cocurrent flow strategy. This phenomenon was thought to be related to the membrane used in this device. The polycarbonate track etched membrane which is used in this device is made by a two-process method. First, the production of "tracks" is created by means of nuclear bombardment, and then the tracks

are etched by means of a chemical bath, which creates the "pores". The pore size is uniform; however, the membrane has a low porosity because of the possibility of an overlap between two pores increases with the porosity. The ideal membrane would have higher porosity than polycarbonate track etched membrane does, such as alumina membrane. However, the alumina membrane has a relatively thick thickness which is around 60 μm[358-360]. It is really a challenge to bond two layers of PDMS with a thick membrane between them. It is critical to find a thin membrane with high porosity in a small pore diameter which can be operated in the continuously flowing system without beads adsorption problem and a counter current flow is adopted in the microfluidic device such as a block polymer membrane in Siegel's group[361].

References

(1) Rijn, C. J. M. v. *Nano and micro engineered membrane technology*; Amsterdam ; Boston : Elsevier 2004.
(2) Becker, H.; Gärtner, C. *Electrophoresis* **2000**, *21*, 12-26.
(3) Ellington, A. D.; Szostak, J. W. *Nature* **1990**, *346*, 818-822.
(4) Tuerk, C.; Gold, L. *Science* **1990**, *249*, 505-510.
(5) Ellington, A. D.; Szostak, J. W. *Nature* **1992**, *355*, 850-852.
(6) Syed, M.; Pervaiz, S. *Oligonucleotides* **2010**, *20*, 215-224.
(7) Hermann, T.; Patel, D. J. *Science* **2000**, *287*, 820-825.
(8) Dominik, K.; Yin-Shan, E. N.; TShima, D. T. *Biochemical Society Transactions* **2009**, *37*, 1201-1206.
(9) Chou, S.-H.; Chin, K.-H.; Wang, A. H.-J. *Nucleic Acids Research* **2003**, *31*, 2461-2474.
(10) Tuerk, C.; MacDougal, S.; Gold, L. *Proceedings of the National Academy of Sciences* **1992**, *89*, 6988-6992.
(11) Schneider, D. J.; Feigon, J.; Hostomsky, Z.; Gold, L. *Biochemistry* **1995**, *34*, 9599-9610.
(12) Macaya, R. F.; Schultze, P.; Smith, F. W.; Roe, J. A.; Feigon, J. *Proceedings of the National Academy of Sciences* **1993**, *90*, 3745-3749.
(13) Jing, N.; Rando, R. F.; Pommier, Y.; Hogan, M. E. *Biochemistry* **1997**, *36*, 12498-12505.
(14) Famulok, M. *Current Opinion in Structural Biology* **1999**, *9*, 324-329.
(15) Shangguan, D.; Li, Y.; Tang, Z.; Cao, Z. C.; Chen, H. W.; Mallikaratchy, P.; Sefah, K.; Yang, C. J.; Tan, W. *Proceedings of the National Academy of Sciences* **2006**, *103*, 11838-11843.
(16) Berens, C.; Thain, A.; Schroeder, R. *Bioorganic & Medicinal Chemistry* **2001**, *9*, 2549-2556.
(17) Famulok, M. *Journal of the American Chemical Society* **1994**, *116*, 1698-1706.
(18) Sassanfar, M.; Szostak, J. W. *Nature* **1993**, *364*, 550-553.
(19) Burgstaller, P.; Famulok, M. *Angewandte Chemie International Edition in English* **1994**, *33*, 1084-1087.
(20) Mayer, G.; Ahmed, M.-S. L.; Dolf, A.; Endl, E.; Knolle, P. A.; Famulok, M. *Nat. Protocols* **2010**, *5*, 1993-2004.
(21) Tombelli, S.; Minunni, M.; Mascini, M. *Biosensors and Bioelectronics* **2005**, *20*, 2424-2434.
(22) Jayasena, S. D. *Clinical Chemistry* **1999**, *45*, 1628-1650.
(23) Lee, J. F.; Stovall, G. M.; Ellington, A. D. *Current Opinion in Chemical Biology* **2006**, *10*, 282-289.
(24) Deng, Q.; German, I.; Buchanan, D.; Kennedy, R. T. *Analytical Chemistry* **2001**, *73*, 5415-5421.
(25) Pavlov, V.; Xiao, Y.; Shlyahovsky, B.; Willner, I. *Journal of the American Chemical Society* **2004**, *126*, 11768-11769.
(26) Tombelli, S.; Minunni, M.; Mascini, M. *Biomolecular Engineering* **2007**, *24*, 191-200.
(27) Fichou, Y.; Ferec, C. *Trends in Biotechnology* **2006**, *24*, 563-570.
(28) Schachat, A. P. *Ophthalmology* **2005**, *112*, 531-532.
(29) Ng, E. W. M.; Shima, D. T.; Calias, P.; Cunningham, E. T.; Guyer, D. R.; Adamis, A. P. *Nat Rev Drug Discov* **2006**, *5*, 123-132.
(30) Cox, J. C.; Rudolph, P.; Ellington, A. D. *Biotechnology Progress* **1998**, *14*, 845-850.
(31) Hybarger, G.; Bynum, J.; Williams, R.; Valdes, J.; Chambers, J. *Analytical and Bioanalytical Chemistry* **2006**, *384*, 191-198.
(32) Misono, T. S.; Kumar, P. K. R. *Analytical Biochemistry* **2005**, *342*, 312-317.
(33) Mendonsa, S.; Bowser, M. *J. Am. Chem. Soc* **2004**, *126*, 20-21.
(34) Mendonsa, S. D.; Bowser, M. T. *Journal of the American Chemical Society* **2005**, *127*, 9382-9383.
(35) Mosing, R. K.; Mendonsa, S. D.; Bowser, M. T. *Analytical Chemistry* **2005**, *77*, 6107-6112.
(36) Aguade, M.; Meyers, W.; Long, A. D.; Langley, C. H. *Proceedings of the National Academy of Sciences* **1994**, *91*, 4658-4662.
(37) Orita, M.; Iwahana, H.; Kanazawa, H.; Hayashi, K.; Sekiya, T. *Proceedings of the National Academy of Sciences* **1989**, *86*, 2766-2770.

(38) Okamoto, A.; Tanaka, K.; Fukuta, T.; Saito, I. *Journal of the American Chemical Society* **2003**, *125*, 9296-9297.
(39) Liu, M.; Yuan, M.; Lou, X.; Mao, H.; Zheng, D.; Zou, R.; Zou, N.; Tang, X.; Zhao, J. *Biosensors and Bioelectronics* **2011**, *26*, 4294-4300.
(40) Ji, M.; Hou, P.; Li, S.; He, N.; Lu, Z. *Mutation Research/Fundamental and Molecular Mechanisms of Mutagenesis* **2004**, *548*, 97-105.
(41) Groth, M.; Huse, K.; Reichwald, K.; Taudien, S.; Hampe, J.; Rosenstiel, P.; Birkenmeier, G.; Schreiber, S.; Platzer, M. *Analytical Biochemistry* **2006**, *356*, 194-201.
(42) Pourmand, N.; Elahi, E.; Davis, R. W.; Ronaghi, M. *Nucleic Acids Research* **2002**, *30*, e31.
(43) Sen, R.; Ishak, H. D.; Estrada, D.; Dowd, S. E.; Hong, E.; Mueller, U. G. *Proceedings of the National Academy of Sciences* **2009**, *106*, 17805-17810.
(44) Hultman, T.; Stahl, S.; Hogan, E.; Uhlen, M. *Nucleic Acids Res.* **1989**, *17*, 4937-4946.
(45) Murphy, M.; Hammond, H.; Caskey, C. *Methods in Molecular Biology* **1996**, *65*, 163-176.
(46) Zhou, W.-J.; Halpern, A. R.; Seefeld, T. H.; Corn, R. M. *Analytical Chemistry* **2012**, *84*, 440-445.
(47) Wang, J.; Onoshima, D.; Aki, M.; Okamoto, Y.; Kaji, N.; Tokeshi, M.; Baba, Y. *Analytical Chemistry* **2011**, *83*, 3528-3532.
(48) Donhauser, S. C.; Niessner, R.; Seidel, M. *Analytical Chemistry* **2011**, *83*, 3153-3160.
(49) Famulok, M.; Mayer, G. *Accounts of Chemical Research* **2011**, *44*, 1349-1358.
(50) Walder, R.; Hayes, J.; Walder, J. *Nucleic Acids Res.* **1993**, *21*, 4339-4343.
(51) Williams, K.; Bartel, D. *Nucleic Acids Res.* **1995**, *23*, 4220-4221.
(52) Nordstrom, L. J.; Clark, C. A.; Andersen, B.; Champlin, S. M.; Schwinefus, J. J. *Biochemistry* **2006**, *45*, 9604-9614.
(53) Stoltenburg, R.; Reinemann, C.; Strehlitz, B. *Analytical and Bioanalytical Chemistry* **2005**, *383*, 83-91.
(54) Gyllensten, U.; Elrlich, H. *Proc natl Acad Sci USA* **1988**, *85*, 7652-7656.
(55) Boiziau, C.; Dausse, E.; Yurchenko, L.; Toulme, J.-J. *Journal of Biological Chemistry* **1999**, *274*, 12730-12737.
(56) Fukusaki, E.-i.; Kato, T.; Maeda, H.; Kawazoe, N.; Ito, Y.; Okazawa, A.; Kajiyama, S.-i.; Kobayashi, A. *Bioorganic & Medicinal Chemistry Letters* **2000**, *10*, 423-425.
(57) Low, S. Y.; Hill, J. E.; Peccia, J. *Biochemical and Biophysical Research Communications* **2009**, *378*, 701-705.
(58) Javaherian, S.; Musheev, M. U.; Kanoatov, M.; Berezovski, M. V.; Krylov, S. N. *Nucleic Acids Research* **2009**, *37*, e62.
(59) Reske, T.; Mix, M.; Bahl, H.; Flechsig, G.-U. *Talanta* **2007**, *74*, 393-397.
(60) Citartan, M.; Tang, T.-H.; Tan, S.-C.; Gopinath, S. *World Journal of Microbiology and Biotechnology* **2011**, *27*, 1167-1173.
(61) Higuchi, R. G.; Ochman, H. *Nucleic Acids Res.* **1989**, *17*, 5865.
(62) Dastjerdi, K.; Tabar, G. H.; Dehghani, H.; Haghparast, A. *Biotechnology and Applied Biochemistry* **2011**, *58*, 226-230.
(63) Hultman, T.; Stahl, S.; Hornes, E.; Uhlen, M. *Nucleic Acids Res.* **1989**, *17*, 4937-4946.
(64) Wilson, R. *Nucleic Acids Therapeutics* **2011**, *21*, 437-440.
(65) Espelund, M.; Stacy, R.; Jakobsen, K. *Nucleic Acids Res.* **1990**, *18*, 6157-6158.
(66) Dwivedi, H.; Smiley, R.; Jaykus, L.-A. *Applied Microbiology and Biotechnology* **2010**, *87*, 2323-2334.
(67) Daniels, D. A.; Chen, H.; Hicke, B. J.; Swiderek, K. M.; Gold, L. *Proceedings of the National Academy of Sciences* **2003**, *100*, 15416-15421.
(68) Keefe, A. D.; Pai, S.; Ellington, A. *Nat Rev Drug Discov* **2010**, *9*, 537-550.
(69) Walder, R. Y.; Hayes, J. R.; Walder, J. A. *Nucleic Acids Research* **1993**, *21*, 4339-4343.
(70) Kim, Y. S.; Hyun, C. J.; Kim, I. A.; Gu, M. B. *Bioorganic & Medicinal Chemistry* **2010**, *18*, 3467-3473.
(71) Wilson, C.; Szostak, J. W. *Chemistry & Biology* **1998**, *5*, 609-617.
(72) Ding, J. L.; Gan, S. T.; Ho, B. *Journal of Innate Immunity* **2009**, *1*, 46-58.

(73) Surina, E. R.; Morozkina, E. V.; marchenko, A. N.; A.A., A.; Mitkevich, O. V.; Kushinirov, V. V.; Teravanesyan, M. D.; Benevolensky, S. V. *Molecular Biology* **2009**, *43*, 623-631.
(74) Ferreira, C.; Papamichael, K.; Guilbault, G.; Schwarzacher, T.; Gariepy, J.; Missailidis, S. *Analytical and Bioanalytical Chemistry* **2008**, *390*, 1039-1050.
(75) Yang, Q.; Goldstein, I. J.; Mei, H.-Y.; Engelke, D. R. *Proceedings of the National Academy of Sciences* **1998**, *95*, 5462-5467.
(76) Yunusov, D.; So, M.; Shayan, S.; Okhonin, V.; Musheev, M. U.; Berezovski, M. V.; Krylov, S. N. *Analytica Chimica Acta* **2009**, *631*, 102-107.
(77) Low, S. Y.; Hill, J. E.; Peccia, J. *Biochemical and Biophysical Research Communications* **2009**, *378*, 701-705.
(78) Low, S. Y.; Hill, J. E.; Peccia, J. *Biochemical and Biophysical Research Communications* **2009**, *386*, 544-548.
(79) Ogawa, A.; Tomita, N.; Kikuchi, N.; Sando, S.; Aoyama, Y. *Bioorganic & Medicinal Chemistry Letters* **2004**, *14*, 4001-4004.
(80) Liu, D. In *Handbook of nucleic acid purification*
Boca Raton: CRC Press, 2009.
(81) Heller, M.; Guttman, A. In *Integrated microfabricated biodevices*; Ramanujam, R., Sacks, W., Kang, J., Eds.; New York: Marcel Dekker, Inc., 2002, pp 71-84.
(82) Little, J. W. *Journal of Biological Chemistry* **1967**, *242*, 679-686.
(83) Marimuthu, C.; Tang, T.-H.; Tominaga, J.; Tan, S.-C.; Gopinath, S. C. B. *Analyst* **2012**, *137*, 1307-1315.
(84) Hayashi, K. *Genome Res.* **1991**, *1991*, 34-38.
(85) Nakabayashi, Y.; Nishigaki, K. *Journal of Biochemistry* **1996**, *120*, 320-325.
(86) Mallikaratchy, P.; Tang, Z.; Kwame, S.; Meng, L.; Shangguan, D.; Tan, W. *Molecular & Cellular Proteomics* **2007**, *6*, 2230-2238.
(87) Tang, J.; Yu, T.; Guo, L.; Xie, J.; Shao, N.; He, Z. *Biosensors and Bioelectronics* **2007**, *22*, 2456-2463.
(88) Jing, M.; Bowser, M. T. *Lab on a Chip* **2011**, *11*, 3703-3709.
(89) Dwivedi, H.; Smiley, R.; Jaykus, L.-A. *Applied Microbiology and Biotechnology* **2010**, *87*, 2323-2334.
(90) Manz, A. *Bioanalytical Chemistry*; London : Imperial College Press, 2004.
(91) Mikkelsen, S. R. *Bioanalytical Chemistry*; Hoboken, N.J. : John Wiley & Sons, 2004.
(92) Gonzalez, M.; Bagatolli, L. A.; Echabe, I.; Arrondo, J. L. R.; Argarana, C. E.; Cantor, C. R.; Fidelio, G. D. *Journal of Biological Chemistry* **1997**, *272*, 11288-11294.
(93) Chaiet, L.; Wolf, F. J. *Archives of Biochemistry and Biophysics* **1964**, *106*, 1-5.
(94) Zempleni, J.; Wijeratne, S. S. K.; Hassan, Y. I. *BioFactors* **2009**, *35*, 36-46.
(95) Weber, P.; Ohlendorf, D.; Wendoloski, J.; Salemme, F. *Science* **1989**, *243*, 85-88.
(96) Hendrickson, W. A.; Pahler, A.; Smith, J. L.; Satow, Y.; Merritt, E. A.; Phizackerley, R. P. *Proceedings of the National Academy of Sciences* **1989**, *86*, 2190-2194.
(97) Reznik, G. O.; Vajda, S.; Smith, C. L.; Cantor, C. R.; Sano, T. *Nat Biotech* **1996**, *14*, 1007-1011.
(98) Holmberg, A.; Blomstergren, A.; Nord, O.; Lukacs, M.; Lundeberg, J.; Uhlén, M. *Electrophoresis* **2005**, *26*, 501-510.
(99) Green, N. M.; C.B. Anfinsen, J. T. E.; Frederic, M. R. In *Advances in Protein Chemistry*; Academic Press, 1975; Vol. Volume 29, pp 85-133.
(100) Laitinen, O.; Hytönen, V.; Nordlund, H.; Kulomaa, M. *Cellular and Molecular Life Sciences* **2006**, *63*, 2992-3017.
(101) Green, N. M. *Method Enzymol.* **1990**, *184*, 51-67.
(102) Gonzalez, M.; Argarana, C. E.; Fidelio, G. D. *Biomolecular Engineering* **1999**, *16*, 67-72.
(103) Bulmus, V.; Ding, Z.; Long, C. J.; Stayton, P. S.; Hoffman, A. S. *Bioconjugate Chemistry* **1999**, *11*, 78-83.
(104) Swift, J. L.; Heuff, R.; Cramb, D. T. *Biophysical journal* **2006**, *90*, 1396-1410.
(105) Buranda, T.; Lopez, G. P.; Keij, J.; Harris, R.; Sklar, L. A. *Cytometry* **1999**, *37*, 21-31.

(106) Hirsch, J. D.; Eslamizar, L.; Filanoski, B. J.; Malekzadeh, N.; Haugland, R. P.; Beechem, J. M.; Haugland, R. P. *Analytical Biochemistry* **2002**, *308*, 343-357.
(107) Marttila, A. T.; Hytonen, V. P.; Laitinen, O. H.; Bayer, E. A.; Wilchek, M.; Kulomaa, M. S. *Biochemical Journal Structure* **2003**, *369*, 249-254.
(108) Morag, E.; Bayer, E. A.; Wilchek, M. *Biochemical Journal* **1996**, *316*, 193-199.
(109) Yoon, H. C.; Hong, M.-Y.; Kim, H.-S. *Langmuir* **2001**, *17*, 1234-1239.
(110) Ding, Z.; Long, C. J.; Hayashi, Y.; Bulmus, E. V.; Hoffman, A. S.; Stayton, P. S. *Bioconjugate Chemistry* **1999**, *10*, 395-400.
(111) Bulmus, V.; Ding, Z.; Long, C. J.; Stayton, P. S.; Hoffman, A. S. *Bioconjugate Chemistry* **1999**, *11*, 78-83.
(112) Terry, S. C.; Jerman, J. H.; Angell, J. B. *Electron Devices, IEEE Transactions on* **1979**, *26*, 1880-1886.
(113) Kopp, M. U.; Mello, A. J. d.; Manz, A. *Science* **1998**, *280*, 1046-1048.
(114) Seiler, K.; Harrison, D. J.; Manz, A. *Analytical Chemistry* **1993**, *65*, 1481-1488.
(115) Harrison, D. J.; Fluri, K.; Seiler, K.; Fan, Z.; Effenhauser, C. S.; Manz, A. *Science* **1993**, *261*, 895-897.
(116) Khandurina, J.; Jacobson, S. C.; Waters, L. C.; Foote, R. S.; Ramsey, J. M. *Analytical Chemistry* **1999**, *71*, 1815-1819.
(117) Simpson, P. C.; Roach, D.; Woolley, A. T.; Thorsen, T.; Johnston, R.; Sensabaugh, G. F.; Mathies, R. A. *Proceedings of the National Academy of Sciences* **1998**, *95*, 2256-2261.
(118) McDonald, J. C.; Duffy, D. C.; Anderson, J. R.; Chiu, D. T.; Wu, H.; Schueller, O. J. A.; Whitesides, G. M. *Electrophoresis* **2000**, *21*, 27-40.
(119) http://www.cellectricon.se/sites/home/home.php; Cellectricon.
(120) http://www.fluidigm.com/ *fluidigm*.
(121) http://www.biacore.com/lifesciences/index.html *GE Healthcare*.
(122) Becker, H.; Gärtner, C. *Analytical and Bioanalytical Chemistry* **2008**, *390*, 89-111.
(123) Becker, H.; Locascio, L. E. *Talanta* **2002**, *56*, 267-287.
(124) Maluf, N. *An Introduction to Microelectromechanical Systems Engineering*; Artech House, Boston, 2000.
(125) Yuan, S.; Zhou, Z.; Wang, G.; Liu, C. *Microelectronic Engineering* **2003**, *66*, 767-772.
(126) Weck, M.; Fischer, S.; Vos, M. *Nanotechnology* **1997**, *8*, 145-148.
(127) Liu, K. K.; Du, Z. H.; Tseng, F. G.; Chou, M.-C.; Fang, J. Y.; Chieng, C. C. *Proc. SPIE* **2001**, *4236*, 44-48.
(128) McDonald, J. C.; Chabinyc, M. L.; Metallo, S. J.; Anderson, J. R.; Stroock, A. D.; Whitesides, G. M. *Analytical Chemistry* **2002**, *74*, 1537-1545.
(129) Henry, A. C.; Tutt, T. J.; Galloway, M.; Davidson, Y. Y.; McWhorter, C. S.; Soper, S. A.; McCarley, R. L. *Analytical Chemistry* **2000**, *72*, 5331-5337.
(130) Shaw, J. M.; Gelorme, J. D.; LaBianca, N. C.; Conley, W. E.; Holmes, S. J. *IBM Journal of Research and Development* **1997**, *41*, 81-94.
(131) Duffy, D. C.; McDonald, J. C.; Schueller, O. J. A.; Whitesides, G. M. *Analytical Chemistry* **1998**, *70*, 4974-4984.
(132) Oosterbroek, R. E.; Berg, A. v. d. A. *Lab-on-a-chip : miniaturized systems for (bio)chemical analysis and synthesis*, 1st ed. ed.; Amsterdam ; Boston : Elsevier, 2003.
(133) Saliterman, S. *Fundamentals of bioMEMS and medical microdevices*; Bellingham, Wash. : SPIE Press, 2006.
(134) Martynova, L.; Locascio, L. E.; Gaitan, M.; Kramer, G. W.; Christensen, R. G.; MacCrehan, W. A. *Analytical Chemistry* **1997**, *69*, 4783-4789.
(135) Locascio, L. E.; Perso, C. E.; Lee, C. S. *Journal of Chromatography A* **1999**, *857*, 275-284.
(136) Becker, H.; Heim, U. *Sensors and Actuators A: Physical* **2000**, *83*, 130-135.
(137) Anderson, J. R.; Chiu, D. T.; Jackman, R. J.; Cherniavskaya, O.; McDonald, J. C.; Wu, H.; Whitesides, S. H.; Whitesides, G. M. *Analytical Chemistry* **2000**, *72*, 3158-3164.
(138) Sheng, Y.; Bowser, M. T. *Analyst* **2012**, *137*, 1144-1151.

(139) Sassi, A. P.; Paulus, A.; Cruzado, I. D.; Bjornson, T.; Hooper, H. H. *Journal of Chromatography A* **2000**, *894*, 203-217.
(140) Piotter, V.; Mueller, K.; Plewa, K.; Ruprecht, R.; Hausselt, J. *Microsystem Technologies* **2002**, *8*, 387-390.
(141) Sun, Y.; Kwok, Y. C. *Analytica Chimica Acta* **2006**, *556*, 80-96.
(142) Pethig, R.; Burt, J.; Parton, A.; Rizvi, N.; Talary, M.; Tame, J. *Journal of Micromechanics and Microengineering* **1998**, *8*, 57-63.
(143) Roberts, M. A.; Rossier, J. S.; Bercier, P.; Girault, H. *Analytical Chemistry* **1997**, *69*, 2035-2042.
(144) Vulto, P.; Glade, N.; Altomare, L.; Bablet, J.; Tin, L. D.; Medoro, G.; Chartier, I.; Manaresi, N.; Tartagni, M.; Guerrieri, R. *Lab on a Chip* **2005**, *5*, 158-162.
(145) Lorenz, H.; Despont, M.; Fahrni, N.; Brugger, J.; Vettiger, P.; Renaud, P. *Sensors and Actuators, A: Physical* **1998**, *64*, 33-39.
(146) Li, B.; Yu, H.; Sharon, A.; Zhang, X. *Applied Physics Letters* **2004**, *85*, 2426-2428.
(147) Tse, L. A.; Hesketh, P. J.; Rosen, D. W.; Gole, J. L. *Microsystem Technologies* **2003**, *9*, 319-323.
(148) Morimoto, Y.; Tan, W.-H.; Takeuchi, S. *Biomedical Microdevices* **2009**, *11*, 369-377.
(149) Chan, C. M.; Ko, T. M.; Hiraoka, H. *Surface Science Reports* **1996**, *24*, 1-54.
(150) Wang, P.-C.; DeVoe, D. L.; Lee, C. S. *Electrophoresis* **2001**, *22*, 3857-3867.
(151) Brennan, W. J.; Feast, W. J.; Munro, H. S.; Walker, S. A. *Polymer* **1991**, *32*, 1527-1530.
(152) Whitesides, G. M.; Ostuni, E.; Takayama, S.; Jiang, X.; Ingber, D. E. *Annual Review of Biomedical Engineering* **2001**, *3*, 335-373.
(153) McDonald, J. C.; Whitesides, G. M. *Accounts of Chemical Research* **2002**, *35*, 491-499.
(154) Lisensky, G. C.; Campbell, D. J.; Beckman, K. J.; Calderon, C. E.; Doolan, P. W.; Rebecca, M. O.; Ellis, A. B. *Journal of Chemical Education* **1999**, *76*, 537.
(155) *Information About High Technology Silicone Materials*; Dow Corning Corporation:Midland,MI, 1991.
(156) Xia, Y.; Whitesides, G. M. *Annual Review of Materials Science* **1998**, *28*, 153-184.
(157) Mukhopadhyay, R. *Analytical Chemistry* **2007**, *79*, 3248-3253.
(158) Toepke, M. W.; Beebe, D. J. *Lab on a Chip* **2006**, *6*, 1484-1486.
(159) Lee, J. N.; Park, C.; Whitesides, G. M. *Analytical Chemistry* **2003**, *75*, 6544-6554.
(160) Sia, S. K.; Whitesides, G. M. *Electrophoresis* **2003**, *24*, 3563-3576.
(161) Xia, Y.; Whitesides, G. M. *Angewandte Chemie International Edition* **1998**, *37*, 550-575.
(162) Qin, D.; Xia, Y.; Whitesides, G. M. *Advanced Materials* **1996**, *8*, 917-919.
(163) Unger, M. A.; Chou, H.-P.; Thorsen, T.; Scherer, A.; Quake, S. R. *Science* **2000**, *288*, 113-116.
(164) Wu, H.; Huang, B.; Zare, R. N. *Lab on a Chip* **2005**, *5*, 1393-1398.
(165) Ho, W. S. W.; Sirkar, K. K. *Membrane handbook*; New York : Van Nostrand Reinhold 1992.
(166) Mulder, M. *Basic principles of membrane technology*; Dordrecht, Netherlands ; Boston : Kluwer Academic 1991.
(167) Geankoplis, C. J. *Transport processes and separation process principles : (includes unit operations)*; Upper Saddle River, NJ : Prentice Hall Professional Technical Reference 2003.
(168) Kusakabe, K.; Ichiki, K.; Hayashi, J.-i.; Maeda, H.; Morooka, S. *Journal of Membrane Science* **1996**, *115*, 65-75.
(169) Smaihi, M.; Schrotter, J.-C.; Lesimple, C.; Prevost, I.; Guizard, C. *Journal of Membrane Science* **1999**, *161*, 157-170.
(170) Blume, I.; Wijmans, J. G.; Baker, R. W. *Journal of Membrane Science* **1990**, *49*, 253-286.
(171) Feng, X.; Huang, R. Y. M. *Industrial & Engineering Chemistry Research* **1997**, *36*, 1048-1066.
(172) Morigami, Y.; Kondo, M.; Abe, J.; Kita, H.; Okamoto, K. *Separation and Purification Technology* **2001**, *25*, 251-260.
(173) Chung, T.-S.; Kafchinski, E. R.; Foley, P. *Journal of Membrane Science* **1992**, *75*, 181-195.
(174) Boom, R. M.; van den Boomgaard, T.; Smolders, C. a. *Journal of Membrane Science* **1994**, *90*, 231-249.
(175) Robeson, L. M. *Journal of Membrane Science* **1991**, *62*, 165-185.
(176) Ferain, E.; Legras, R. *Nuclear Instruments and Methods in Physics Research Section B: Beam Interactions with Materials and Atoms* **1994**, *84*, 331-336.

(177) Kros, A.; Nolte, R. J. M.; Sommerdijk, N. A. J. M. *Advanced Materials* **2002**, *14*, 1779-1782.
(178) Jones, S. E.; Ditner, S. A.; Freeman, C.; Whitaker, C. J.; Lock, M. A. *Applied and Environmental Microbiology* **1989**, *55*, 529-530.
(179) Brumlik, C. J.; Martin, C. R. *Journal of the American Chemical Society* **1991**, *113*, 3174-3175.
(180) Yamaguchi, A.; Uejo, F.; Yoda, T.; Uchida, T.; Tanamura, Y.; Yamashita, T.; Teramae, N. *Nat Mater* **2004**, *3*, 337-341.
(181) Martin, C. R. *Science* **1994**, *266*, 1961-1966.
(182) Crawfor, G. P.; Steele, L. M.; Crawford, R. O.; Inannacchione, G. S.; Yeager, C. J.; Doane, J. W.; Finotello, D. *Journal of Chemical Physics* **1992**, *96*, 7788-7796.
(183) Broyles, B. S.; Jacobson, S. C.; Ramsey, J. M. *Analytical Chemistry* **2003**, *75*, 2761-2767.
(184) Xu, N.; Lin, Y.; Hofstadler, S. A.; Matson, D.; Call, C. J.; Smith, R. D. *Analytical Chemistry* **1998**, *70*, 3553-3556.
(185) Long, Z.; Liu, D.; Ye, N.; Qin, J.; Lin, B. *Electrophoresis* **2006**, *27*, 4927-4934.
(186) Jiang, Y.; Wang, P.; Locascio, L.; Lee, C. *Analytical Chemistry* **2001**, *73*, 2048-2053.
(187) Gong, M.; Kim, B.; Flachsbart, B.; Shannon, M.; Bohn, P.; Sweedler, J. *IEEE Sensors Journal* **2008**, *8*, 601-607.
(188) Ismagilov, R. F.; Ng, J. M. K.; Kenis, P. J. A.; Whitesides, G. M. *Analytical Chemistry* **2001**, *73*, 5207-5213.
(189) Yao, S.; Anex, D. S.; Caldwell, W. B.; Arnold, D. W.; Smith, K. B.; Schultz, P. G. *Proceedings of the National Academy of Sciences* **1999**, *96*, 5372-5377.
(190) Li, H.; Yanan, Z.; Akin, D.; Bashir, R. *Microelectromechanical Systems, Journal of* **2005**, *14*, 103-112.
(191) Dürr, M.; Kentsch, J.; Müller, T.; Schnelle, T.; Stelzle, M. *Electrophoresis* **2003**, *24*, 722-731.
(192) Deng, T.; Prentiss, M.; Whitesides, G. M. *Applied Physics Letters* **2002**, *80*, 461-463.
(193) Ng, J. M. K.; Gitlin, I.; Stroock, A. D.; Whitesides, G. M. *Electrophoresis* **2002**, *23*, 3461-3473.
(194) West, J.; Becker, M.; Tombrink, S.; Manz, A. *Analytical Chemistry* **2008**, *80*, 4403-4419.
(195) Kovarik, M. L.; Jacobson, S. C. *Analytical Chemistry* **2009**, *81*, 7133-7140.
(196) Di Ventra, M.; Evoy, S.; Heflin, J. R. *Introduction to nanoscale science and technology*; Kluwer Academic Boston, 2004.
(197) Schoch, R.; Han, J.; Renaud, P. *Reviews of Modern Physics* **2008**, *80*, 839-883.
(198) Craighead, H. *Nature* **2006**, *442*, 387-393.
(199) Jong, J.; Lammertink, R.; Wessling, M. *Lab on a Chip* **2006**, *6*, 1125-1139.
(200) Lee, C. *Electrophoresis* **2001**, *22*, 3857-3867.
(201) Piruska, A.; Branagan, S.; Cropek, D.; Sweedler, J.; Bohn, P. *Lab on a Chip* **2008**, *8*, 1625-1631.
(202) Kim, B.; Yang, J.; Gong, M.; Flachsbart, B.; Shannon, M.; Bohn, P.; Sweedler, J. *Analytical Chemistry* **2009**, *81*, 2715-2722.
(203) Gong, M.; Flachsbart, B.; Shannon, M.; Bohn, P.; Sweedler, J. *Electrophoresis* **2008**, *29*, 1237-1244.
(204) Noblitt, S.; Kraly, J.; VanBuren, J.; Hering, S.; CollettJr, J.; Henry, C. *Analytical Chemistry* **2007**, *79*, 6249-6254.
(205) Kim, B.; Swearingen, C.; Ja-an, A.; Romanova, E.; Bohn, P.; Sweedler, J. *J. Am. Chem. Soc* **2007**, *129*, 7620-7626.
(206) Lamoree, M.; Van der Hoeven, R.; Tjaden, U.; Van der Greef, J. *Journal of Mass Spectrometry* **1998**, *33*, 453-460.
(207) Tokuyama, T.; Fujii, S.; Sato, K.; Abo, M.; Okubo, A. *Analytical Chemistry* **2005**, *77*, 3309-3314.
(208) Kurita, R.; Yabumoto, N.; Niwa, O. *Biosensors and Bioelectronics* **2006**, *21*, 1649-1653.
(209) Kim, M.; Kim, Y.; Kim, B. *Electrophoresis* **2003**, *24*, 200-206.
(210) Cooper, J.; Chen, J.; Li, Y.; Lee, C. *Analytical Chemistry* **2003**, *75*, 1067-1074.
(211) Jong, J.; Ankone, B.; Lammertink, R.; Wessling, M. *Lab on a Chip* **2005**, *5*, 1240-1247.
(212) Moskvin, L.; Nikitina, T. *Journal of Analytical Chemistry* **2004**, *59*, 2-16.
(213) Tulock, J.; Shannon, M.; Bohn, P.; Sweedler, J. *Analytical Chemistry* **2004**, *76*, 6419-6425.
(214) Kuo, T.; Sloan, L.; Sweedler, J.; Bohn, P. *Langmuir* **2001**, *17*, 6298-6303.
(215) Song, S.; Singh, A. K.; Shepodd, T. J.; Kirby, B. J. *Analytical Chemistry* **2004**, *76*, 2367-2373.

(216) Kirby, B. J. *Micro- and nanoscale fluid mechanics transport in microfluidic devices*; Cambridge, U.K. ; New York : Cambridge University Press 2010.
(217) Truskey, G.; Yuan, F.; Katz, D. In *Transport Phenomena in Biological Systems*; Upper Saddle River, N.J. : Pearson Prentice Hall 2004.
(218) Probstein, R. *Physicochemical Hydrodynamics*; Boston:Butterworths, 1989.
(219) Beebe, D. J.; Mensing, G. A.; Walker, G. M. *Annual Review of Biomedical Engineering* **2002**, *4*, 261-286.
(220) Kemery, P. J.; Steehler, J. K.; Bohn, P. W. *Langmuir* **1998**, *14*, 2884-2889.
(221) Gasparac, R.; Mitchell, D. T.; Martin, C. R. *Electrochimica Acta* **2004**, *49*, 847-850.
(222) Bluhm, E. A.; Bauer, E.; Chamberlin, R. M.; Abney, K. D.; Young, J. S.; Jarvinen, G. D. *Langmuir* **1999**, *15*, 8668-8672.
(223) Delamarche, E.; Bernard, A.; Schmid, H.; Michel, B.; Biebuyck, H. *Science* **1997**, *276*, 779-781.
(224) Duffy, D. C.; Gillis, H. L.; Lin, J.; Sheppard, N. F.; Kellogg, G. J. *Analytical Chemistry* **1999**, *71*, 4669-4678.
(225) Gallardo, B. S.; Gupta, V. K.; Eagerton, F. D.; Jong, L. I.; Craig, V. S.; Shah, R. R.; Abbott, N. L. *Science* **1999**, *283*, 57-60.
(226) Kataoka, D. E.; Troian, S. M. *Nature* **1999**, *402*, 794-797.
(227) Zhao, B.; Moore, J. S.; Beebe, D. J. *Langmuir* **2002**, *19*, 1873-1879.
(228) Juncker, D.; Schmid, H.; Drechsler, U.; Wolf, H.; Wolf, M.; Michel, B.; de Rooij, N.; Delamarche, E. *Analytical Chemistry* **2002**, *74*, 6139-6144.
(229) Tinland, B.; Pluen, A.; Sturm, J.; Weill, G. *Macromolecules* **1997**, *30*, 5763-5765.
(230) Stellwagen, E.; Stellwagen, N. C. *Electrophoresis* **2002**, *23*, 2794-2803.
(231) Rant, U.; Arinaga, K.; Fujiwara, T.; Fujita, S.; Tornow, M.; Yokoyama, N.; Abstreiter, G. *Biophysical journal* **2003**, *85*, 3858-3864.
(232) Langowski, J. *Biophysical Chemistry* **1987**, *27*, 263-271.
(233) Stellwagen, E.; Lu; Stellwagen, N. C. *Biochemistry* **2003**, *42*, 11745-11750.
(234) Ferrari, M. E.; Bloomfield, V. A. *Macromolecules* **1992**, *25*, 5266-5276.
(235) Dwyer, J. D.; Bloomfield, V. A. *Biophysical Journal* **1993**, *65*, 1810-1816.
(236) Record, M. T.; Anderson, C. F.; Lohman, T. M. *Quarterly Reviews of Biophysics* **1978**, *2*, 103-178.
(237) Fulmer, A. W.; Benbasat, J. A.; Bloomfield, V. A. *Biopolymers* **1981**, *20*, 1147-1159.
(238) Porschke, D. *Biophysical Chemistry* **1991**, *40*, 169-179.
(239) Pappaert, K.; Biesemans, J.; Clicq, D.; Vankrunkelsven, S.; Desmet, G. *Lab on a Chip* **2005**, *5*, 1104-1110.
(240) Nishizawa, M.; Menon, V.; Martin, C. *Science* **1995**, *268*, 700-702.
(241) Zhou, K.; Kovarik, M.; Jacobson, S. *J. Am. Chem. Soc* **2008**, *130*, 8614-8616.
(242) Hou, Z.; Abbott, N.; Stroeve, P. *Langmuir* **2000**, *16*, 2401-2404.
(243) Kovarik, M.; Jacobson, S. *Analytical Chemistry* **2008**, *80*, 657-664.
(244) Kuo, T.; Cannon, D.; Shannon, M.; Bohn, P.; Sweedler, J. *Sensors & Actuators: A. Physical* **2003**, *102*, 223-233.
(245) Cannon Jr, D.; Kuo, T.; Bohn, P.; Sweedler, J. *Analytical Chemistry* **2003**, *75*, 2224-2230.
(246) Kuo, T.; Cannon Jr, D.; Chen, Y.; Tulock, J.; Shannon, M.; Sweedler, J.; Bohn, P. *Analytical Chemistry* **2003**, *75*, 1861-1867.
(247) Hulteen, J.; Jirage, K.; Martin, C. *J. Am. Chem. Soc* **1998**, *120*, 6603-6604.
(248) Gatimu, E.; Sweedler, J.; Bohn, P. *The Analyst* **2006**, *131*, 705-709.
(249) Jirage, K.; Hulteen, J.; Martin, C. *Science* **1997**, *278*, 655-658.
(250) Schmuhl, R.; van den Berg, A.; Blank, D.; ten Elshof, J. *Angewandte Chemie International Edition* **2006**, *45*, 3341-3345.
(251) Osborn, J. L.; Lutz, B.; Fu, E.; Kauffman, P.; Stevens, D. Y.; Yager, P. *Lab on a Chip* **2010**, *10*, 2659-2665.
(252) Weigl, B. H.; Yager, P. *Science* **1999**, *283*, 346-347.
(253) Helton, K. L.; Yager, P. *Lab on a Chip* **2007**, *7*, 1581-1588.
(254) Brody, J. P.; Yager, P. *Sensors and Actuators A: Physical* **1997**, *58*, 13-18.

(255) Brody, J. P.; Yager, P.; Goldstein, R. E.; Austin, R. H. *Biophysical journal* **1996**, *71*, 3430-3441.
(256) McDonald, J.; Duffy, D.; Anderson, J.; Chiu, D.; Wu, H.; Schueller, O.; Whitesides, G. *Electrophoresis* **2000**, *21*, 27-40.
(257) Jo, B.; Van Lerberghe, L.; Motsegood, K.; Beebe, D. *Journal of microelectromechanical systems* **2000**, *9*, 76-81.
(258) Truskey, G.; Yuan, F.; Katz, D. In *Transport Phenomena in Biological Systems*; Upper Saddle River, N.J. : Pearson Prentice Hall 2004, pp 375-384.
(259) Skogestad, S. In *Chemical and energy process engineering*
Boca Raton, FL: CRC Press, 2009.
(260) Baehr, H. D. In *Heat and mass transfer*; Berlin, New York: Springer, 1998.
(261) Frost, N.; Bowser, M. *Lab Chip* **2010**.
(262) Kratky, O.; Porod, G. *Rec Trav Chim Pays-Bas* **1949**, *68*, 1106-1122.
(263) Teraoka, I. *Polymer solutions : an introduction to physical properties*; New York: Wiley, 2002.
(264) Record Jr, M.; Anderson, C.; Lohman, T. *Quarterly reviews of Biophysics* **1978**, *11*, 103-178.
(265) Salieb-Beugelaar, G. B.; Dorfman, K. D.; Vvan den Berg, A.; Eijkel, J. C. T. *Lab on a Chip* **2009**, *9*, 2508-2523.
(266) Lettmann, C.; Mockel, D.; Staude, E. *Journal of Membrane Science* **1999**, *159*, 243-251.
(267) Huisman, I. H.; Pradanos, P.; Calvo, J. I.; Hernandez, A. *Journal of Membrane Science* **2000**, *178*, 79-92.
(268) Bard, A. J. In *Electrochemical methods: fundamentals and applications*, 2nd ed. ed.; New York: Wiley, 2001.
(269) Martin, C. R.; Nishizawa, M.; Jirage, K.; Kang, M.; Lee, S. B. *Advanced Materials* **2001**, *13*, 1351-1362.
(270) Schmuhl, R.; Sekulic, J.; Roy Chowdhury, S.; van Rijn, C. J. M.; Keizer, K.; van den Berg, A.; ten Elshof, J. E.; Blank, D. H. A. *Advanced Materials* **2004**, *16*, 900-904.
(271) Plecis, A.; Schoch, R. B.; Renaud, P. *Nano Letters* **2005**, *5*, 1147-1155.
(272) Markin, V. S.; Volkov, A. G. *Electrochimica Acta* **1989**, *34*, 93-107.
(273) Mao, H.; Yang, T.; Cremer, P. S. *Analytical Chemistry* **2001**, *74*, 379-385.
(274) Desmarets, J.; Gresser, O.; Guedin, D.; Frelin, C. *Biochemistry* **1996**, *35*, 14868-14875.
(275) De Meyts, P.; Whittaker, J. *Nat Rev Drug Discov* **2002**, *1*, 769-783.
(276) Bell, G. *Science* **1978**, *200*, 618-627.
(277) West, G. B.; Brown, J. H.; Enquist, B. J. *Science* **1999**, *284*, 1677-1679.
(278) Humes, H. D.; Buffington, D. A.; MacKay, S. M.; Funke, A. J.; Weitzel, W. F. *Nat Biotech* **1999**, *17*, 451-455.
(279) Deen, W. M.; Lazzara, M. J.; Myers, B. D. *American Journal of Physiology - Renal Physiology* **2001**, *281*, F579-F596.
(280) Strain, A. J.; Neuberger, J. M. *Science* **2002**, *295*, 1005-1009.
(281) McLamore, E.; Jackson, W. A.; Morse, A. *Journal of Membrane Science* **2007**, *298*, 110-116.
(282) Netti, P. A.; Hamberg, L. M.; Babich, J. W.; Kierstead, D.; Graham, W.; Hunter, G. J.; Wolf, G. L.; Fischman, A.; Boucher, Y.; Jain, R. K. *Proc natl Acad Sci USA* **1999**, *96*, 3137-3142.
(283) Yuan, F. *Seminars in Radiation Oncology* **1998**, *8*, 164-175.
(284) Jain, R. K. *Journal of Controlled Release* **1998**, *53*, 49-67.
(285) Miranti, C. K.; Brugge, J. S. *Nat Cell Biol* **2002**, *4*, E83-E90.
(286) Koshland, D.; Goldbeter, A.; Stock, J. *Science* **1982**, *217*, 220-225.
(287) Griffith, L. G.; Naughton, G. *Science* **2002**, *295*, 1009-1014.
(288) Williams, K. A.; Saini, S.; Wick, T. M. *Biotechnology Progress* **2002**, *18*, 951-963.
(289) Kedem, O.; Katchalsky, A. *BBA - Biochimica et Biophysica Acta* **1958**, *27*, 229-246.
(290) Spiegler, K. S.; Kedem, O. *Desalination* **1966**, *1*, 311-326.
(291) Deen, W. M. *AIChE Journal* **1987**, *33*, 1409-1425.
(292) Bowen, W. R.; Mukhtar, H. *Journal of Membrane Science* **1996**, *112*, 263-274.
(293) Jakob, M. *Heat transfer*; New York, Wiley, 1964.
(294) Michaels, A. *Trans Am Soc Artif Intern Organs* **1966**, *12*, 387-392.
(295) Yeh, H. M.; Huang, C. M. *Journal of Membrane Science* **1995**, *103*, 135-150.

(296) Yeh, H. M.; Peng, Y. Y.; Chen, Y. K. *Journal of Membrane Science* **1999**, *163*, 177-192.
(297) Noordman, T. R.; Wesselingh, J. A. *Journal of Membrane Science* **2002**, *210*, 227-243.
(298) Jung Oh, S.; Moon, S.-H.; Davis, T. *Journal of Membrane Science* **2000**, *169*, 95-105.
(299) Palaty, Z.; Zakova, A. *Journal of Membrane Science* **1996**, *119*, 183-190.
(300) Palaty, Z.; Zakova, A.; Dolecek, P. *Journal of Membrane Science* **2000**, *165*, 237-249.
(301) Hsieh, Y.-C.; Zahn, J. D. *Sensors and Actuators B: Chemical* **2005**, *107*, 649-656.
(302) Noda, I.; Gryte, C. C. *AIChE Journal* **1979**, *25*, 113-122.
(303) Gill, W. N.; Bansal, B. *AIChE Journal* **1973**, *19*, 823-831.
(304) Happel, J. *AIChE Journal* **1959**, *5*, 174-177.
(305) Klein, E.; Holland, F.; Lebeouf, A.; Donnaud, A.; Smith, J. K. *Journal of Membrane Science* **1976**, *1*, 371-396.
(306) Jagannathan, R.; Shettigar, U. *Medical and Biological Engineering and Computing* **1977**, *15*, 500-512.
(307) Walker, G.; Davies, T. *AIChE Journal* **1974**, *20*, 881-889.
(308) Cooney, D. O.; Kim, S.-S.; James Davis, E. *Chemical Engineering Science* **1974**, *29*, 1731-1738.
(309) Loney, N.; Huang, C.; Simon, L. *World Journal of Microbiology and Biotechnology* **2005**, *21*, 791-796.
(310) Yeh, H. M. *Computers and Chemical Engineering* **2009**, *33*, 815-821.
(311) Yeh, H. M.; Chang, Y. H. *Journal of Membrane Science* **2005**, *260*, 1-9.
(312) Mason, E. A.; Viehland, L. A. *Journal of Chemical Physicas* **1978**, *68*, 3562-3573.
(313) Mason, E. A.; Lonsdale, H. K. *Journal of Membrane Science* **1990**, *51*, 1-81.
(314) Xu, J.; Heys, J.; Barocas, V.; Randolph, T. *Pharmaceutical Research* **2000**, *17*, 664-669.
(315) Bird, B. R.; Stewart, W. E.; Lightfoot, E. N. *Transport phenomena*, Rev. 2nd ed ed.; New York : J. Wiley, 2007.
(316) Wang, P.; Yang, Y.; Hong, H.; Zhang, Y.; Cai, W.; Fang, D. *Current Medicinal Chemistry* **2011**, *18*, 4169-4174.
(317) Nimjee, S. M.; Rusconi, C. P.; Sullenger, B. A. *Annual Review of Medicine* **2005**, *56*, 555-583.
(318) Lee, J.-H.; Canny, M. D.; De Erkenez, A.; Krilleke, D.; Ng, Y.-S.; Shima, D. T.; Pardi, A.; Jucker, F. *Proceedings of the National Academy of Sciences of the United States of America* **2005**, *102*, 18902-18907.
(319) Chu, T. C.; Shieh, F.; Lavery, L. A.; Levy, M.; Richards-Kortum, R.; Korgel, B. A.; Ellington, A. D. *Biosensors and Bioelectronics* **2006**, *21*, 1859-1866.
(320) Collett, J. R.; Cho, E. J.; Lee, J. F.; Levy, M.; Hood, A. J.; Wan, C.; Ellington, A. D. *Analytical Biochemistry* **2005**, *338*, 113-123.
(321) Hesselberth, J.; Robertson, M. P.; Jhaveri, S.; Ellington, A. D. *Reviews in Molecular Biotechnology* **2000**, *74*, 15-25.
(322) Brody, E. N.; Willis, M. C.; Smith, J. D.; Jayasena, S.; Zichi, D.; Gold, L. *Molecular Diagnosis* **1999**, *4*, 381-388.
(323) Kong, R.-M.; Zhang, X.-B.; Chen, Z.; Tan, W. *Small* **2011**, *7*, 2428-2436.
(324) Odenthal, K. J.; Gooding, J. J. *Analyst* **2007**, *132*, 603-610.
(325) Jhaveri, S.; Rajendran, M.; Ellington, A. D. *Nat Biotech* **2000**, *18*, 1293-1297.
(326) Wang, H.; Yang, R.; Yang, L.; Tan, W. *ACS Nano* **2009**, *3*, 2451-2460.
(327) Shiddiky, M. J. A.; Torriero, A. A. J.; Zeng, Z.; Spiccia, L.; Bond, A. M. *Journal of the American Chemical Society* **2010**, *132*, 10053-10063.
(328) Peng, Y.; Wang, X.; Xiao, Y.; Feng, L.; Zhao, C.; Ren, J.; Qu, X. *Journal of the American Chemical Society* **2009**, *131*, 13813-13818.
(329) Katz, E.; Willner, I. *Angewandte Chemie International Edition* **2004**, *43*, 6042-6108.
(330) Stahl, S.; Hultman, T.; Olsson, A.; Moks, T.; Uhlen, M. *Nucleic Acids Res.* **1988**, *16*, 3025-3038.
(331) Park, S.-m.; Ahn, J.-Y.; Jo, M.; Lee, D.-k.; Lis, J. T.; Craighead, H. G.; Kim, S. *Lab on a Chip* **2009**, *9*, 1206-1212.
(332) Lou, X.; Qian, J.; Xiao, Y.; Viel, L.; Gerdon, A. E.; Lagally, E. T.; Atzberger, P.; Tarasow, T. M.; Heeger, A. J.; Soh, H. T. *Proceedings of the National Academy of Sciences* **2009**, *106*, 2989-2994.
(333) Qian, J.; Lou, X.; Zhang, Y.; Xiao, Y.; Soh, H. T. *Analytical Chemistry* **2009**, *81*, 5490-5495.

(334) Huang, C.-J.; Lin, H.-I.; Shiesh, S.-C.; Lee, G.-B. *Biosensors and Bioelectronics* **2012**.
(335) Ferguson, B. S.; Buchsbaum, S. F.; Swensen, J. S.; Hsieh, K.; Lou, X.; Soh, H. T. *Analytical Chemistry* **2009**, *81*, 6503-6508.
(336) Ferguson, B. S.; Buchsbaum, S. F.; Wu, T.-T.; Hsieh, K.; Xiao, Y.; Sun, R.; Soh, H. T. *Journal of the American Chemical Society* **2011**, *133*, 9129-9135.
(337) Liu, P.; Li, X.; Greenspoon, S. A.; Scherer, J. R.; Mathies, R. A. *Lab on a Chip* **2011**, *11*, 1041-1048.
(338) Zhang, H.; Mitrovski, S. M.; Nuzzo, R. G. *Analytical Chemistry* **2007**, *79*, 9014-9021.
(339) Paul, A.; Avci-Adali, M.; Ziemer, G.; Wendel, H. P. *Oligonucleotides* **2009**, *19*, 243-254.
(340) Avci-Adali, M.; Paul, A.; Wilhelm, N.; Ziemer, G.; Wendel, H. P. *Molecules* **2010**, *15*, 1-11.
(341) Boissinot, K.; Huletsky, A.; Peytavi, R.; Turcotte, S.; Veillette, V.; Boissinot, M.; Picard, F. J.; Martel, E. A.; Bergeron, M. G. *Clinical Chemistry* **2007**, *53*, 2020-2023.
(342) Iki, N.; Yeung, E. S. *Journal of Chromatography A* **1996**, *731*, 273-282.
(343) Hestekin, C. N.; Lin, J. S.; Senderowicz, L.; Jakupciak, J. P.; O'Connell, C.; Rademaker, A.; Barron, A. E. *Electrophoresis* **2011**, *32*, 2921-2929.
(344) Kourkine, I. V.; Hestekin, C. N.; Buchholz, B. A.; Barron, A. E. *Analytical Chemistry* **2002**, *74*, 2565-2572.
(345) Albarghouthi, M. N.; Buchholz, B. A.; Huiberts, P. J.; Stein, T. M.; Barron, A. E. *Electrophoresis* **2002**, *23*, 1429-1440.
(346) O'Connell, C. D.; Atha, D. H.; Oldenburg, M. C.; Tian, J.; Siebert, M.; Handrow, R.; Grooms, K.; Heisler, L.; de Arruda, M. *Electrophoresis* **1999**, *20*, 1211-1223.
(347) Steinour, H. H. *Industrial & Engineering Chemistry* **1944**, *36*, 618-624.
(348) Lamb, H. *Hydrodynamics (6th edition ed.)*; Cambridge University Press, 1994.
(349) Buscall, R.; White, L. R. *Journal of the Chemical Society, Faraday Transactions 1: Physical Chemistry in Condensed Phases* **1987**, *83*, 873-891.
(350) Richardson, J. F.; Zaki, W. N. *Chemical Engineering Science* **1954**, *3*, 65-73.
(351) Dressman, D.; Yan, H.; Traverso, G.; Kinzler, K. W.; Vogelstein, B. *Proceedings of the National Academy of Sciences* **2003**, *100*, 8817-8822.
(352) Ageno, M.; Dore, E.; Frontali, C. *Biophysical journal* **1969**, *9*, 1281-1311.
(353) Bimboim, H. C.; Doly, J. *Nucleic Acids Research* **1979**, *7*, 1513-1523.
(354) Luck, G.; Zimmer, C.; Snatzke, G.; Söndgerath, G. *European Journal of Biochemistry* **1970**, *17*, 514-522.
(355) Barber, R. *Biochimica et Biophysica Acta (BBA) - Nucleic Acids and Protein Synthesis* **1971**, *238*, 60-66.
(356) Fonslow, B. R.; Bowser, M. T. *Analytical Chemistry* **2005**, *77*, 5706-5710.
(357) Fonslow, B. R.; Barocas, V. H.; Bowser, M. T. *Analytical Chemistry* **2006**, *78*, 5369-5374.
(358) Brumlik, C. J.; Martin, C. R.; Tokuda, K. *Analytical Chemistry* **1992**, *64*, 1201-1203.
(359) Wootters, A. H.; Lilly, M. P.; Hallock, R. B. *Journal of Low Temperature Physics* **1998**, *110*, 561-566.
(360) Crawford, G.; Steele, L.; Crawford, R. O.; Iannacchione, G.; Yeager, C.; Doane, J.; Finotello, D. *Journal of Chemical Physicas* **1992**, *96*, 7788-7796.
(361) Nuxoll, E. E.; Hillmyer, M. A.; Wang, R.; Leighton, C.; Siegel, R. A. *ACS Applied Materials & Interfaces* **2009**, *1*, 888-893.